NANOSCALE ENERGY STORAGE ELECTRODES BY TEMPLATE-SYNTHESIS

By

CHARLES ROBERT SIDES

A DISSERTATION PRESENTED TO THE GRADUATE SCHOOL
OF THE UNIVERSITY OF FLORIDA IN PARTIAL FULFILLMENT
OF THE REQUIREMENTS FOR THE DEGREE OF
DOCTOR OF PHILOSOPHY

UNIVERSITY OF FLORIDA

2005

This document is dedicated to my beloved wife and family.

ACKNOWLEDGMENTS

I would like to use this platform to expression sincere appreciation to my research advisor, Charles R. Martin, for his guidance through my graduate career. I believe that I leave with us equally pleased with our accomplishments.

I would like to thank my parents, Charles R. Sides and Martha C. Sides; my sister Anna Dobbins, her husband Clint, and their two new children Bella and Chase; my younger brother Matthew and his wife Kelly; my youngest brother William, unmarried as of yet; my grandparents, Evelyn and Raymond Sides and Evelyn Campbell; and the most recent addition, my new wife, the former Alison S. Knefely. Each of these family members has motivated and encouraged me during each turn in this winding road.

I had the distinct pleasure of working with Stephen E. Creager (undergraduate research advisor), Bruno Scrosati, and Fausto Croce (hosts during collaboration visit to Rome and Chieti, Italy). I enjoyed both the professional and personal interactions. I also thank the following members of the Martin group who advised me on experimental design, presentation style, and my golf swing: Dr. Naichao Li, Dr. Lane Baker, Dr. Punit Kohli, and Dr. C. Chad Harrell.

There are a number of other individuals that I want to acknowledge for helping me to enjoy my nine years in college – Wist, Riles, Grant, Wil, Baker, Buck, Elizabeth, Scott, Heather, Bruce and Butler.

TABLE OF CONTENTS

LIST OF TABLES

LIST OF FIGURES

Abstract of Dissertation Presented to the Graduate School
of the University of Florida in Partial Fulfillment of the
Requirements for the Degree of Doctor of Philosophy

NANOSCALE ENERGY STORAGE ELECTRODES BY TEMPLATE-SYNTHESIS

By

Charles Robert Sides

December 2005

Chair: Charles R. Martin
Major Department: Chemistry

Lithium-ion batteries powered the recent boom of personal electronic devices, such as cell phones, laptops and digital cameras. This success spawned a global research initiative to adapt this technology to more demanding applications, such as low-temperature systems or those relying on pulse-power. The electrodes of these batteries store charge by reversibly intercalating Li-ions. The facile insertion flux of Li-ions into the electrode and sluggish solid-state diffusion from surface to non-surface intercalation sites causes a polarization of charge. Therefore, under demanding conditions, the electrode discharges without fully accessing all charge-storage sites.

The electrode used in these studies is created by *template-synthesis*. Template-synthesis is a general nanofabrication method capable of creating structures of known geometry. Nanomaterial-based electrodes mitigate the rate-limiting effects of sluggish electron-kinetics and mass-transport. The large surface-area of this design serves to distribute the current density, improving electron-kinetics, while the small size ensures

that intercalation sites reside close to the surface, minimizing the distance Li-ions must diffuse in the solid-state.

The intent of this dissertation is to highlight the success of nanomaterials in the study and design of energy-storage systems. It begins with a discussion of the low-temperature performance of Li-ion battery electrodes. Charge-storage characteristics and reproducible electrode geometries identify the fundamental breakdown of Li-ion batteries at low-temperature as the decrease in solid-state diffusion coefficient of the Li-ion (D_{Li+}). This study then quantifies the value of D_{Li+} as a function of both intercalation-level and temperature. Next, it describes a variation of the previous template-synthesis method, in which the polymeric template is pyrolyzed to create a $LiFePO_4$/carbon composite electrode. This composite improves upon the poor electron-conductivity of the otherwise attractive $LiFePO_4$ cathode. Finally, preliminary results from polyvalent-ion (Mg^{2+}) intercalation into the V_2O_5 electrode are presented. Polyvalent-ions allow for more charge to be stored than is stoichiometrically possible by singly charged ions.

The advantage of incorporating nanomaterials into the design of energy-storage devices is the recurring theme of this document. While the studies are approached from a fundamental view, conclusions such as those reported here will undoubtedly have profound commercial impact on the increasingly portable world.

CHAPTER 1
INTRODUCTION AND TEMPLATE-SYNTHESIS

Introduction

Batteries provide power to an incredible number of devices that we rely on daily such as automotives, electronics, and hearing aids and pacemakers. In addition to being portable, batteries operate more efficiently than solar power, cleaner than fossil fuels, and safer than nuclear power. Andrew Volta is credited for the first battery device in 1799 and sixty years passed until Gaston Plante discovered the first practical rechargeable battery (the lead-acid battery still used in cars today.) Now there are several classes of rechargeable batteries, which include Plante's lead acid battery, nickel-based systems (nickel-metal hydride and nickel cadmium) and the Li-ion battery.

The introduction of Li-ion batteries by T. Nagaura and K. Tozawa of SonyTec Inc. in 1990 marked a major advance in battery technology.[1] Li-ion batteries have generated great interest as lightweight, portable, rechargeable power sources over the last decade. Li-ion batteries are now the power source of choice for laptops, cell phones, digital cameras, and camcorders. Table 1-1 compares several of the rechargeable batteries currently on the market.[2] Note that the Li-ion battery has unparalleled energy density, but is comparatively expensive. Li-ion batteries are popular because of their high cell potential, large cycle life, high energy (Wh L^{-1}, Wh kg^{-1},) and power density (W L^{-1}, W kg^{-1}.) For many applications these advantages outweigh the expense of these batteries.

Table 1-1: Comparison of commercial rechargeable batteries.

		Energy Density	
Battery Type	Nominal Voltage (V)	By Weight (Wh kg^{-1})	By Volume (Wh L^{-1})
Pb-acid	2	25	80
Ni-Cd	1.2	50	150
Ni-MH	1.2	75	200
Li-ion	3.6	150	325

The public has quickly embraced this technology, which accounts for an approximately 3 billion dollar annual market.[3] Despite the commercial success of these batteries, a global research initiative exists to improve the existing design. The goal of this research is to apply this technology to more demanding applications, such as those relying on pulse-power or improved low-temperature performance. A specific example is for use as the electric component of hybrid vehicles, which is currently a NiMH based system. However, the current Li-ion battery design cannot adequately satisfy the power requirements of such systems due to the inability to deliver a sufficient quantity of charge at high discharge currents[4] combined with concerns of safety and capital expenses.

The emergence of the burgeoning field of nanotechology has already tremendously impacted the field of scientific research. The fields of biotechnology and electronics have revolutionized. This dissertation details my efforts to incorporate the field of nanomaterials to improve the design of Li-ion batteries.

Background on Li-ion Batteries

The three primary components of any battery are the cathode, the electrolyte, and the anode. Li-ion batteries operate by reversibly intercalating charge in each of the two electrodes. *Intercalation* is the process by which a specific quantity of guest species (Li^+) is able to reversibly enter/exit a host structure (*e.g.*, V_2O_5, carbon), causing little or no difference to the host. These electrodes are separated by an ion-conductive electrolyte. Upon discharge, the Li-ions deintercalate from the low-potential electrode, migrate through the electrolyte, and insert into the high-potential electrode. The ions then must rely on solid-state diffusion to fill the non-surface intercalation sites. A corresponding quantity of charge travels the circuit and provides power to the load. This process is detailed in Figure 1-1.

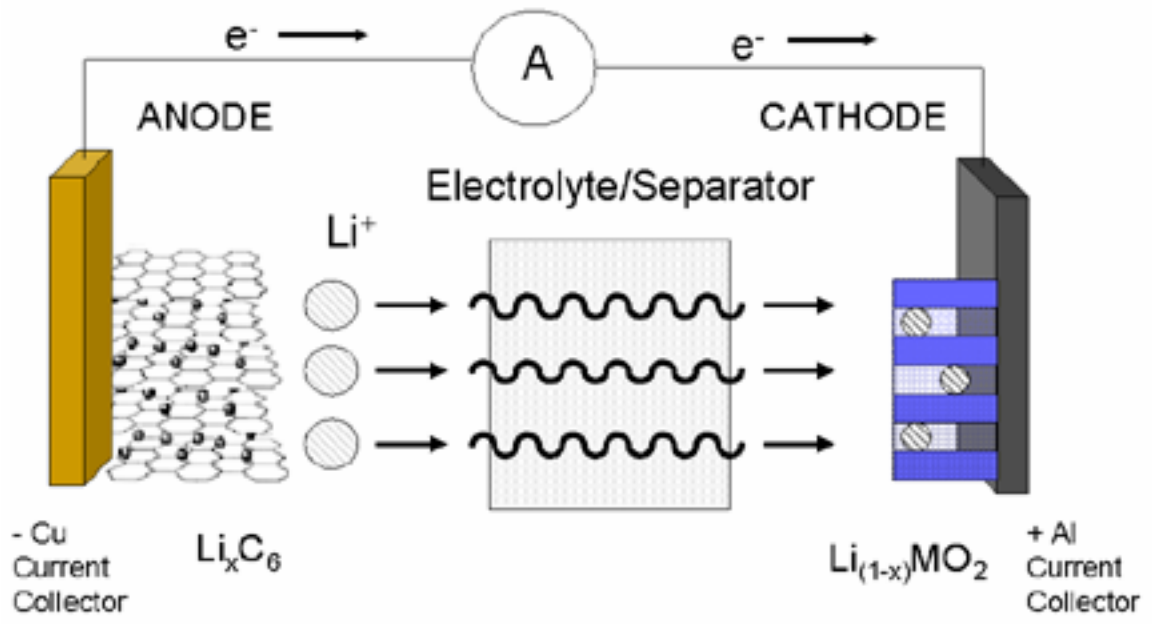

Figure 1-1: Schematic of discharge process of Li-ion battery. Charge moves from anode to cathode during discharge. Adapted from van Schalkwijk. [5].

If current flow is reversed (from cathode to anode), Li-ions insert into the low-potential electrode and the system is charged. The low-potential electrode is the *anode*

and the high-potential electrode is the *cathode*. This convention (adopted from the discharge process) is obeyed regardless of the direction of current flow. As in a traditional electrochemical process, the reaction is limited by either mass-transfer (diffusion of ionic species) or electron-kinetics. It does differ though, because it is the host, not the diffusing species, which oxides/reduces. General forms of the charge/discharge reactions for a Li-ion battery cathode and anode are shown in Equation 1-1 and 1-2, respectively.

$$\text{Cathode}: \quad MO_2 + xLi^+ + xe^- \underset{\text{charge}}{\overset{\text{discharge}}{\rightleftharpoons}} Li_xMO_2 \qquad 1\text{-}1$$

$$\text{Anode}: \quad 6\,C + xLi^+ + xe^- \underset{\text{discharge}}{\overset{\text{charge}}{\rightleftharpoons}} Li_xC_6 \qquad 1\text{-}2$$

For the cathode material shown in Equation 1-1 M = transition metal or a mixture of transition metals. The most popular choices are Co, Mn, Ni, and V. These are the constituents of the complex that undergo the redox reaction.

The anode material is shown in Equation 1-2 as carbon. Development of the carbon-based anode was an engineering improvement to mitigate the early safety issues of lithium-metal anodes. Replacing the Li metal anode with the carbonaceous material obviated the short-circuit issues caused by dendritic growth during the Li-deposition process. Graphite has a layered structure and is a popular alternative to lithium because it can store a large amount of charge (~370 mAh g^{-1}) and has a reduction potential just positive of lithium metal (~ 100 mV). The cell voltage delivered by a battery is the

difference in the operating potential of the two electrodes, so a significantly negative anodic potential is necessary to maintain the large cell voltage.

Nanomaterials by Template-Synthesis

The Martin research group has pioneered the nanofabrication strategy of template synthesis.[6] This general method has been used to synthesize nanostructures of a variety of materials such as gold,[7-10] carbon, [11-13]semiconductors,[14,15] polymers,[6,16] and Li-ion battery electrodes,[12,14,17-26] our focus here. This method involves deposition of a material precursor into a micro- or nanoporous template. This template can be a variety of porous materials, such as commercially available track-etch polymer filters, anodized alumina, or even colloidal crystals. Depending on both the pore-diameter and the specific chemical interactions between the pore wall and the precursor, the resulting structures may be tubes (hollow) or wires (solid). The template is functional by restricting particle-growth. It may remain intact to impart directionality or increased mechanical strength during the experiments.

For battery materials, the template is a commercially-available polycarbonate filter. The pores of this filter are monodisperse, nanoscopic in diameter, nominally cylindrical in shape, and traverse the entire length of the membrane. Electrode precursor is deposited into the pores of the organic template. The template is then preferentially etched by oxygen plasma, leaving structures of identical geometry as the pores. A sintering process imparts crystallinity to the structures to ensure that the host-structure is maintained during the intercalation/deintercalation process. These structures are referred to as “nano” if one or more of their dimensions are on the nanoscale (< 100 nm). However, the aspect ratio (length / width) is often on the order of 10.

Templates

Track-etch Membranes

Micro- and nanoporous polymeric filtration membranes prepared via the "track-etch" method are available from commercial sources (*e.g.*, GE Osmonics) in a variety of materials and pore geometries.[27] Polycarbonate is perhaps the most common example of a track-etch filter material. Other options of materials include polyester, Teflon®, and polyethersulfone. An electron micrograph of the surface of a polycarbonate template membrane is shown in Figure 1-2.

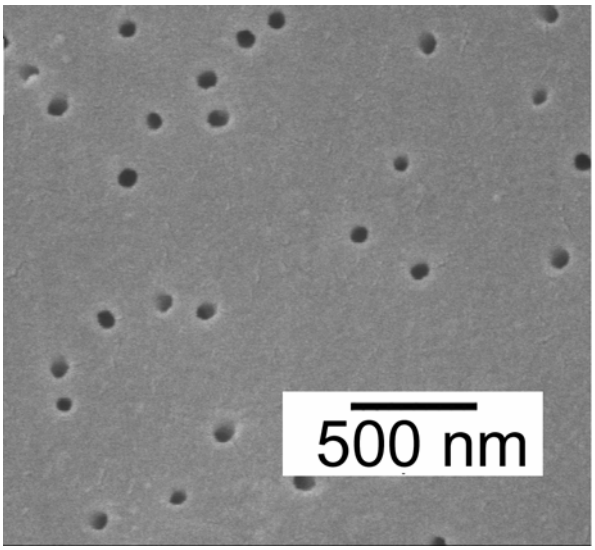

Figure 1-2: Scanning electron micrograph of the surface of a commercial nanoscale polycarbonate track-etch template membrane.

The term *track-etch* refers to the pore-production process.[28,29] Pores of the filters are created by exposing the solid material film to nuclear fission fragments, which leave randomly-dispersed damage-tracks in the film. The high energy (on the order of 2 GeV) of the fragments ensures that the tracks span the entire length of the membrane (typically from 6 to 10 μm). These reactive chains end at the damage-tracks in the polycarbonate film and are then etched with a basic chemical solution, and they become pores. One ion

creates one track, which in turn becomes one pore. During production the pore density is controlled by the duration of time that the polycarbonate film is exposed to the charged particles. Typical track-etch membrane pore-densities are 10^4 to 10^8 pores cm^{-2}.[30]

Varying parameters of this etching solution such as temperature, strength and exposure time dictate the pore diameter. Commercial membranes are available with pore diameters ranging from 10 nm to 20 μm. The microporous material etches to form uniform cylindrical pores, but as the pore diameter is reduced to the smaller nanoscopic dimensions the shape of the pore becomes like a cigar, slightly tapered at the ends. Microscopic investigations of template-synthesized nanostructures prepared within the pores of such nanoporous membranes have shown that the diameter of the pore in the center of the membrane is larger than the diameter at the membrane surface.[22,31] This pore geometry may arise from the fission fragment that creates the damage track and also generates secondary electrons, which contribute to the damage along the track. The number of secondary electrons generated at the faces of the membrane is less than in the central region of the membrane. An alternate theory is that the surfactant protective layer adsorbed to the surface of the membrane retards the local etching process.[29] Either suggested mechanism leads to "bottleneck" pores.

In the production of template-synthesized nanostructured battery materials, polymeric (specifically polycarbonate) track-etch membranes are the current template of choice. These templates may be easily removed in conditions that do not adversely affect the nanostructures themselves. The wide variety of commercially available pore diameters and densities can generate comparative structures of differing geometries that are key tools for fundamental investigations. The disadvantage that is associated with

these types of membranes and their application to electrode materials is their low porosity. These values are typically between 2 – 10%. This decreases the ratio of active material to a given footprint area or volume region on the current collector surface. It is important to remember, however, that these electrodes will serve as tools for fundamental studies, not a viable approach for commercial synthesis.

Anodized alumina

Another template membrane used in our laboratory is anodized alumina. Anodization of aluminum metal in an acidic environment causes the metal to etch in a fashion that leaves a porous structure.[32] These pores are extremely regular, having monodisperse diameters and cylindrical shapes in a hexagonal array. Unlike the track-etch process, this process is systematic and generates an isolated, non-connected pore structure. The pore densities of these alumina filters can be on the order of 10^{11} pores cm^{-2}, which is about 1000 times the density available in the track-etch polycarbonate membranes. The porosities can be as high as 50%. Also, alumina filters have much greater mechanical stability and chemical resistivity than polycarbonate. However, there is an extremely limited selection of commercially available pore sizes, and the smaller pores are branched. These membranes can be very thick (10 -100 μm). It is also notable that this alumina structure is electronically insulating.

There are advantages of alumina templates, but, to date, the application to Li-ion battery research has been limited. The high porosity (template pore volume becomes material volume) would dramatically increase the volumetric capacity (mAh L^{-1}) available for a template-synthesized electrode. However, the chemical resistivity of the membrane dictates that more harsh dissolution methods be employed. There are few Li-

ion battery intercalation electrodes that survive such exposure. Recently though another research group has shown reversible Li-ion intercalation into MnO_2 wires electrochemically deposited in alumina template[33].

Colloidal-crystals

In the previous examples of templates, the pore-structure is cylindrical in general shape. An alternative to this configuration is a nanosphere template (see Stein's recent review).[34] In this method, spherical particles with diameters of nano- to microscale dimensions (typically ~ 100s of nm) are deposited in a close-packed array. This is commonly accomplished by a solvent evaporation technique. If a solvent evaporates at a slow, controlled rate, it imparts an order to the particles. These particles are typically made of polymers (latex, polysterene) or silica. Since they are spherical in shape, void-volume exists in the interstitial sites, even when close-packed. These interstitial sites serve as the porous network and the nanosphere array act as the template. These close-packed spheres have a theoretical packing efficiency (defined as [volume of space occupied by the spheres/total volume]) depending on specific arrangements of between 68 – 74%. Therefore, the theoretical void volume is approximately 30% in a close-packed array and increases to 48% in a monolayer of spheres.

Again by physically restricting particle growth (as opposed to a chemical technique), the deposition strategy becomes general. The requirements of size, shape, and uniformity are transferred from the material to the template. This is demonstrated with examples from the literature of synthesis of a variety of materials such as metal salts,[34,35] metal particles,[36] polymeric materials,[37,38] and evaporated or electroplated metal films.[39] Though the spherical shape is the most common, it is possible that the sphere can be distorted to other shapes, such as an ellipsoid or even a "doughnut"-shape.[38]

Material Deposition Strategies

There are a number of differing structures of templates used for template-synthesis. There are just as many material-deposition strategies. It is the combination of templates and deposition-methods that provide a multiplicative number of solutions to a given challenge. In our laboratory alone we have shown examples of sol-gel deposition, electrochemical deposition (metals and polymers), electroless deposition, and chemical vapor deposition.

Sol-gel

Sol-gel chemistry has recently evolved as a powerful approach for preparing inorganic materials such as glasses and ceramics. This method for the synthesis of inorganic materials has a number of advantages over more conventional synthetic procedures. For example, high-purity materials can be synthesized at a lower temperature. In addition, homogeneous multi-component systems can be obtained by mixing precursor solutions; this allows for easy chemical doping of the materials prepared.[40] Such a versatile deposition technique partners well with the template-synthesis nanofabrication method.

The sol-gel process typically involves hydrolysis of a solution of the precursor molecule to obtain first a suspension of colloidal particles (the sol) and then a gel composed of aggregated sol particles. The amorphous gel may then be thermally treated to yield a more crystalline product. We have recently conducted various sol-gel syntheses within the pores of the alumina and polycarbonate membranes to create both tubes and wires of a variety of inorganic oxide materials, including semiconductors[14,15] and Li-ion battery intercalation materials.[20,22,24,25] First, the template membrane is immersed into a sol for a given period of time, and the sol deposits on the pore walls.

After hydrolysis, either a tube or wire of the gelled material is formed within the pores. As with other template synthesis techniques, longer immersion times yield wires, while brief immersion times produce tubes.

The formation of tubes after short immersion times indicates that the sol particles adsorb to the template membrane's pore walls. It has also been found that the rate of gelation is faster within the pore than in bulk solution. This is most likely due to the enhancement in the local concentration of the sol particles owing to adsorption on the pore walls. An electrostatic interaction may also pull charged sol particles to the walls of the template membrane.[14]

Previously, our group has demonstrated the formation of TiO_2 semiconductor nanostructures via template-synthesis.[15] The mechanism of formation of TiO_2 from acidified titanium alkoxide solutions is well documented. In the early stages of the synthesis, sol particles are held together by a network of -Ti-O- bonds. These particles ultimately coalesce to form a three-dimensional infinite network, the gel. The fact that tubes are initially obtained when this process is done in the alumina membrane indicates that the sol particles adsorb to the pore walls. It is well-known that at the acidic pH values, the sol particles are weakly positively charged. Tubes are formed because these positively charged particles interact with anionic sites on the alumina pore wall.[14] Several other inorganic oxides, specifically MnO_2, Co_3O_4, ZnO, WO_3, and SiO_2, have been synthesized in a similar fashion. Since transition-metal oxides are typical choices for Li-ion battery cathodes, it can easily be seen how this method partners well with research of this field.

Other deposition strategies of template-synthesis

Electrochemical deposition is a based on electroplating metal from a solution into the pores of the template. The structures plate axially from a current collector. By controlling the charge (current and time) passed, the length of the structure can be controlled. This method typically produces wires, but tubes are possible when a molecular anchor is employed. We have made electrochemical plated structures of gold, silver, nickel, platinum and even polymers.

Conversely, the electroless plating method relies on the electrochemical series for metals to replace ones more noble than themselves. A polymer (nonconductive) template is "sensitized" by Sn-ions, which are replaced by Ag particles, which are replaced by Au particles. These gold particles coalesce to form a continuous structure. This method plates metals from the walls of the template (radially); therefore, they plate as tubes with a controllable inner diameter down to when they become solid-wires. The plating occurs indiscriminately onto all faces of the membrane exposed to the solution. The most common example is the electroless deposition of gold into a track-etch polymeric template.

Vapor deposition is useful because of the conformal coating that it can create by depositing materials in the vapor phase. It is commonly applied for making carbon nanotubes from ethylene gas; however, there are examples of conducting, semi-conducting and insulating materials. The difficulty with this method is the selection of suitable precursors. Anodized alumina templates are ideal selections to accompany this method, because of the ruggedness of that template. We deposit carbon by this method at greater than 600 ^{o}C. Another advantage to this method is that tubes of thin wall

diameters are possible. The Martin laboratory has shown that vapor-deposited carbon nanotubes are ideal tools for fundamental studies of electroosmotic flow investigations.[11]

Impact of Template-Synthesis to Nanoelectrochemsitry

Fundamental Electrochemical Investigations

Gold nanoelectrode ensemble

One of the first fields where these template-synthesized nanomaterials demonstrated superior functional capabilities is as an array of gold nanoelectrodes elements.[10] Our group has created an array of gold nanoelectrodes by electroless deposition of Au to form solid wires in a track-etch polycarbonate template. Nanoelectrodes offer opportunities to perform electrochemical experiments to investigate the kinetics of redox processes that are too fast to measure at conventional macroscopic electrodes.[41,42] Also, they have the ability to serve as useful electrodes even in highly resistive media.[43] Depending on the spacing (pore density) and timescale of the experiment (voltammetric scan rate), we were able to demonstrate by "radial" and "total overlap" diffusional and voltammetric responses. The radial case refers to when the diffusion layer of each element is independent, whereas the total overlap refers to when the layers merge to act as a single diffusion layer. Template-synthesized gold nanowires operating in the "total overlap" regime are able to measure electrochemical response of redox molecules at trace concentrations (less than 2 nM for $TMAFc^{+}$).[10,44] This is a result of the faradaic response being a function of geometric gold surface area, and the background double-layer charging current being a function of active Au area. Gold nanoelectrodes were shown to provide advantageous electrochemical results, due to their unique template-synthesized geometry.

Carbon nanotube membrane

Carbon nanotubes are of great interest in both fundamental and applied science. Our group has created template-synthesized carbon nanotubes by chemical vapor deposition of ethylene gas onto a home-grown alumina membrane. This carbon nanotube membrane (CNM) is used for fundamental electrochemical investigations, specifically as tools to monitor and control electroosmotic flow (EOF).[11,45] EOF refers to the movement of solution past a stationary surface due to an externally applied electric field and is a consequence of the way ions are distributed near surfaces.[46] The Martin laboratory has shown the ability to measure EOF through carbon nanotube membranes. This work was further developed into the ability to control the rate and direction of EOF inside a CNM by depositing a thin-layer of PVFc. By applying a potential, the sign and magnitude of surface-charge, and thus EOF, can be effectively modulated.

Li-ion Battery Nanoelectrodes

Polymeric track-etch templates

Nanomaterials are advantageous in regards to both ionic and electronic conductivity. Decreasing particle-size decreases the solid-state diffusion distance for Li^+ and increases the specific surface area, thus distributing the current and decreasing the effective current-density. This serves to increase the electron-transfer kinetics of the system. Solid-state diffusion coefficients are dependent on material and state-of-charge, but are extremely small, in the range of 10^{-11} to 10^{-15} cm^2 s^{-1}. This is an intrinsic property. Therefore, our strategy is to use nanoparticles and minimize the distance the Li-ion must diffuse. This creates a situation in which the intercalation sites are as close to the electrode surface as possible.

The Martin laboratory published its preliminary data of Li-ion batteries in 1997.[12,14] This was not long after these batteries were introduced to the marketplace. Patrissi[22] and Li[19] were the first of the Martin laboratory to demonstrate the structural and electrochemical characterization of template-synthesized Li-ion batteries electrodes, V_2O_5 cathodes and Sn-based anodes, respectively. The work detailed here builds upon the preliminary findings of these scientists. They built the foundations for a number of the experiments discussed below.

A tremendous number of laboratories across the world are involved in this research. Several premier journals devote sections of every issue to featuring advances in energy storage (specifically, Li-ion based technology). Current major goals in this research are to 1) create high-rate pulse-power compatible structures, 2) identify alternative electrode materials (specifically more energetic, less expensive, and less hazardous cathodes), 3) fabricate solid-electrolytes with viable ionic conductivity at room temperature. Energy storage and production are topics of conversation at every corner of the industrialized world.

The focus of research in the field of Li-ions batteries is to create systems of the highest energy and power densities, both on a gravimetric and volumetric basis. Essentially the goal is to get more power from a smaller, lighter device. Template-synthesis as applied to the field of Li-ion batteries creates ideal tools for the fundamental studies of factors that limit both rate and power. Previously, we have focused on using constant-current to discharge template-synthesized electrodes and comparing that to the response of thin-film control electrodes. During the discharge process, Li-ions deintercalate from the anode, migrate through a Li-ion conducting electrolyte, and then

intercalate into the cathode. When these Li-ions intercalate into an electrode, they are not able to solid-state diffuse rapidly enough to compensate for the facile nature of the insertion-flux ($D \sim 10^{-8}$ to 10^{-11} cm^2 s^{-1}). This results in concentration-polarization of Li-ions at the surface during intercalation; conversely, the polarization is in the core during the deintercalation process.[47]

This is a practical limitation to the stoichiometric quantity of charge-storage (mAh g^{-1}) that is theoretically possible. The discharge-rate (current) determines this rate of insertion-flux; therefore at the high currents of a demanding application, this concentration-polarization problem is exacerbated. Since the diffusion coefficient is an intrinsic property of the electrode material, we work with the strategy of decreasing the size of the electrode-particles. This allows the intercalation sites to be closer to the surface, shortening the distance over which the sluggish solid-state diffusion process must propagate.[20,22,24,25]

This plan of using smaller particles has another attribute. The increased surface-area per total-volume fraction serves to decrease the effective current density at any given rate. This works to offset any sluggish electron-kinetics of the system. Since the electrodes must exhibit both good electronic and ionic conductivity, a structure comprised of electronically addressable small particles is extremely favorable. This has been demonstrated by template-synthesis of both cathodic[20,22,24,25] and anodic materials.[20,48] In every case, the nanostructured material was able to deliver higher specific capacity (mAh g^{-1}) at any given discharge rate (C, $C = h^{-1}$) than the microstructured control electrode.

For an electrode to function in a rechargeable system, it must be able to maintain its ability to be charged and discharged for many cycles. This cycle-life parameter is measured as the charge-discharge cycle is repeated at the same rate. Our nanostructured electrodes has been cycled for greater than 1400 times at the high-rate of 58 C, without diminishing the quantity of charge delivered per cycle.[20]

As demonstrated in the above discussion, electrodes comprised of small particles are advantageous. Void-volume is used to keep these particles small. While this has no effect on the gravimetric capacity (mAh g^{-1}), it does on volumetric capacity (mAh L^{-1}). Volumetric restrictions of an application may be just as stringent as gravimetric restrictions. Our lab has shown the ability to "refill" a portion of this void-volume with more active material to increase the charge stored per liter.[23] In that investigation, the volumetric charge delivered by the template-synthesized nanostructured electrode at high-rates of discharge actually surpassed that delivered by the thin-film control.

Nanosphere-templated structures

Laboratories throughout the world are employing template-synthesis methods. Other groups (most notably from the University of Minnesota) have worked with a template method that uses nanospheres to create similar short-diffusion-distance materials.[49] An array of monodisperse PMMA spheres of diameter of 300 nm serves as the template. Approximately 10 layers of these spheres construct an array. The void-volume of these close-packed spheres hosts a Sn-based precursor solution. After processing the precursor into a state capable of reversible Li-ion intercalation, the PMMA-template spheres were removed via calcination. The electrode structure shrinks as a result of this heating. Average solid-state diffusion distance for Li-ions is about 170 nm. This electrode showed good order to an area of 100 μm^2. The resulting electrode

was characterized electrochemically and was able to reversibly store and deliver charge under conditions similar to those previously described.[49]

Li-ion Battery Electrode Fabrication Strategies

Commercial Process Method

This synthetic method can be contrasted to a general method for commercial Li-ion battery systems.[47] There are many types of commercial batteries, such as prismatic cells, coin cells, and "jelly-roll" cylindrical cells. The assembly and application of each are different; however, the synthesis and components are general. The commercial battery cathode is created in a high-temperature procedure that gives particles of the active transition-metal-oxide. This process generates particles that range in diameter from approximately 2 to 20 microns. These discrete particles are then mixed into slurry with polymeric binder (PVDf) and a conductive element (carbon) and pressed into a metal mesh current collector. The conductive element is necessary to improve the electronic conductivity of the system, which is very low in this system because the particles are only point-connected. The polymer is necessary to simply ensure that the slurry physically contacts the current collector. In our template-synthesis approach, these inactive (not capable of Li-ion intercalation) components are not necessary and are excluded so as not to decrease volumetric and gravimetric energy densities or complicate analysis.[50] Notice that competing technologies use the mass of only the active material when determining charge-per-gram.

Template-Synthesis Method

In this embodiment of Li-ion electrodes a precursor-impregnated polycarbonate template membrane is attached to a section of metal foil. The foil has dual-functionality as it serves as a substrate during synthesis and as a common current collector during

electrochemical characterization. Template-synthesis methods yield a fiber-based electrode that consists of structures that mirror the geometry (length, diameter, and number density) of the pores of the template. Typical values are 100-nm in diameter, 6 microns in length, and 10^8 elements per cm^2. These structures extend from the surface of the current collector like the bristles of a brush. There are only two components of the electrode – active material and current collector. Each electrode is then electrochemically characterized as a half-cell.

Because of the parallel electronic-conduction mechanism of our template-synthesized nanostructrued electrodes, carbon is not required.[25] No binder is necessary because the structures are directly attached to the metal foil that serves as both a physical substrate and a common current collector. The absence of non-active components in our electrodes also assists in increasing volumetric energy densities.

An Electrochemical Primer

Comparing Electrochemical Methods

A standard electrochemical experiment could be envisioned as a planar metal electrode (working electrode) and a facile redox couple such as ferrocene/ferrocenium. The ferrocene would be dissolved in water, along with a supporting electrolytic salt. This other salt is composed of nonelectroactive ions and serves to decrease the contribution to migration to the mass transfer, as well as decreasing the cell resistance. A reference electrode is in the system as well. The purpose of this electrode is to provide a comparative value for the applied potential. If the ionic conductivity (S cm^{-1}) of the electrolyte is comparatively low, a Luggin capillary may be employed to minimize the effective distance between the working and reference electrodes. This decreases the cell resistance, minimizes iR drop, and ensures that the potential measured is accurate. A

counter electrode is inert in the system conditions and serves to pass current through the system. A potentiostat is connected to the electrodes. Envision a potentiostat as the instrument that sets the working electrode to the appropriate potential compared to the reference electrode and measures the flow of current between the working and counter electrodes.

For a reduction-oxidation (redox) reaction to occur, an electron and ion must unite. Figure 1-3 illustrates this from thermodynamics. Electron-kinetics describes the ability for electrons to be transferred at a certain rate constant. Ion transport (mass transfer) is accomplished by one of three mechanisms: diffusion, migration, and convection. Commonly systems eliminate convection by not stirring the system. The effect of migration, movement of ions in an electric field, is minimized by the supporting electrolyte. This leaves diffusion as the predominant mass-transfer mechanism. Diffusion is a result of a concentration gradient. This concentration gradient is related to flux of the species by a proportionality constant, its diffusion coefficient (D). This parameter has units of area per time. A small molecule in water has $D \sim 1 \times 10^{-5}$ cm^2 s^{-1}. While the diffusive movements of species are random in nature, the bulk movement serves to smooth concentration gradients.

Electrochemical measurements on Li-ion batteries are similar, but not identical. We test our electrodes in a half-cell setup, meaning that the cathode and anode are individually characterized. Li-ions are solvated in a non-aqueous electrolyte. This setup is inside of an argon glovebox, to protect the dry electrolyte and the lithium metal. The diffusive movement is associated with the Li-ions, but Li-ions are stored and the host material is subject to the redox reactions.

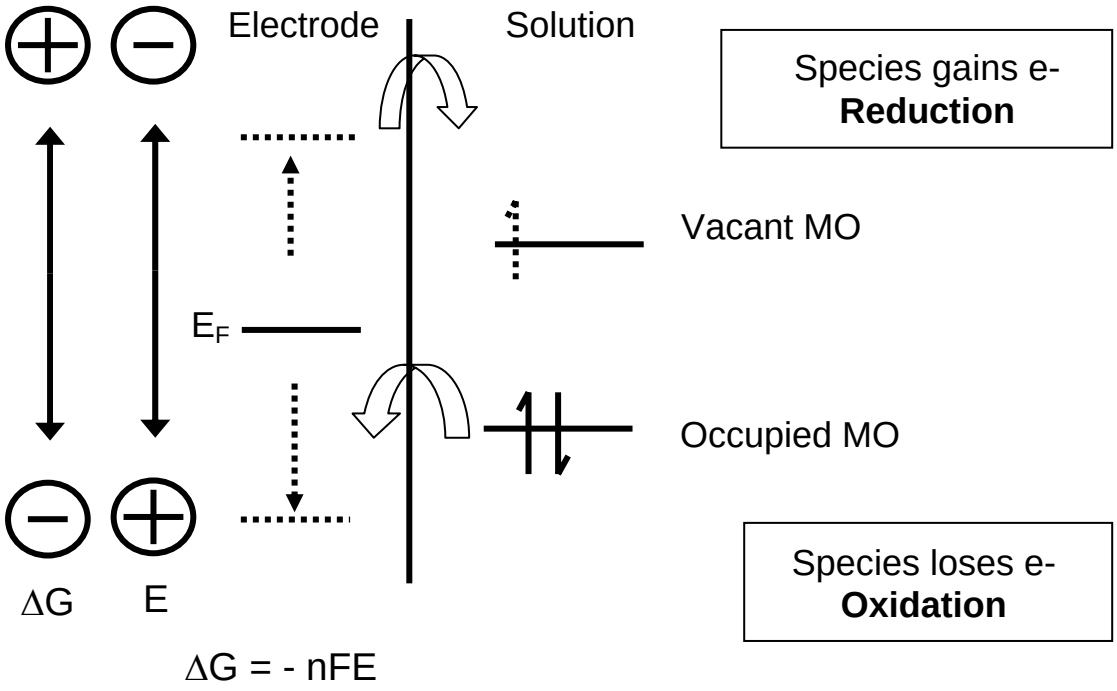

Figure1-3: Fundamentals of electrochemical reactions comparing oxidation and reduction reactions. E_F is the Fermi level, the average energy of the electrons of the current collector.

The host material is electronically conductive and injects electrons by contact with a metal current collector. This intermediary between the ions and the current collector serves to slow electron transfer. In addition, though Li-ions are small, they must diffuse through solid-material as opposed to only liquid in a traditional system. The diffusion coefficient for this process is about 6 orders of magnitude lower than for a liquid-phase system. Therefore, the rates of the experiments must be several orders of magnitude less than those used to typical experiments. Again, the rate of the reaction is either limited by mass-transfer or electron-transfer.

Comparison of Diffusion Regimes

This leads us to a discussion of two regimes of diffusion that are discussed in this dissertation – semi-infinite and finite. Semi-infinite diffusion refers to the situation when

movement of ions is unrestricted. Ions may freely diffuse without boundary constraints, so during the timescale of the experiment effects of the cell walls are not felt on the system. Therefore, at some value away from the electrode there is no concentration gradient. The direct opposite is the case for finite diffusion when the movement of ions is constrained. This is often the case in thin-layer experiments where propagation of the diffusion layer is truncated at some distance, the thickness of the thin-layer.

A colleague once compared these diffusion regimes to me as an analogy of two people each holding one end of a rope. The first causes the rope to oscillate by moving his hand up and down. This movement represents the diffusion process. If the rope is sufficiently long enough, the second person cannot feel the response (semi-infinite diffusion). However, if the rope is short enough, the perturbation is felt by the second person and it is stopped by his hand (finite diffusion). There is no infinite diffusion regime, because the diffusing species is confined by the walls of the cell, and as t approaches infinity it will eventually encounter this system constraint.

Electrochemical Methods for Li-ion Battery Electrodes

We will use several standard electrochemical methods to characterize the Li-ion battery electrodes – cyclic voltammetry, chronopotentiometry, and small potential-steps. Cyclic voltammetry will be used to confirm the activity of the electrode, identify the potential region of electroactivity, and comment on the electron-kinetics and diffusion regimes of the process. This is accomplished by sweeping an applied potential, while monitoring the current response. Chronopotentiometry uses constant applied currents to charge and discharge the electrode, while monitoring the change in potential. By applying a known current to a known electrode mass, the time is easily converted to charge stored and thus quantity of Li^+. Larger currents (faster rates) decrease the time

regime for the intercalation process. Therefore, the solid-state diffusion process can access less of the intercalation sites at larger currents. Measurement of the *rate-capability* is a useful way to compare electrodes. The final method uses small applied potential steps and monitors the current-response over time. Data from these small potential steps are interpreted via the Cottrell relationship to identify the solid-state diffusion coefficient of the Li-ion and identify the activation energy of the diffusion process via an Arrenhenius relationship.

Since the quantity of charge stored in a Li-ion battery electrode is dependent on the mass of the electrode, the molecular weight of the host species, as well as the stiochiometric theoretical maximum, a normalized parameter is necessary when discussing charge-discharge experiments. This parameter is C-Rate, 1 C = 1 h^{-1}, described in Equation 1-3.

$$C - Rate = \frac{i}{C_s\ m} \qquad 1\text{-}3$$

Here, i represents the applied current, C_s represents the theoretical specific capacity (mAh g^{-1}), and m represents the mass of the electrode. The rate of 1 C is the current necessary to incorporate the theoretical maximum charge in 1 h. For reference, if a laptop battery lasts for 2 h, it is discharged at an average rate of C/2 (though, the rate is actually a little higher, because this calculation assumes theoretical charge-storage.)

Figure 1-4 is a schematic of the result of the concentration polarization effect. This effect depends greatly on C-Rate. At small rates, there is enough time for Li-ions to occupy/vacate nearly all of the intercalation sites, even at the core of the electrode particle. At high rates, there is much less time for these Li-ions to diffuse in the solid-

state, creating this large number of inaccessible intercalation sites, resulting in poor charge-storage characteristics.

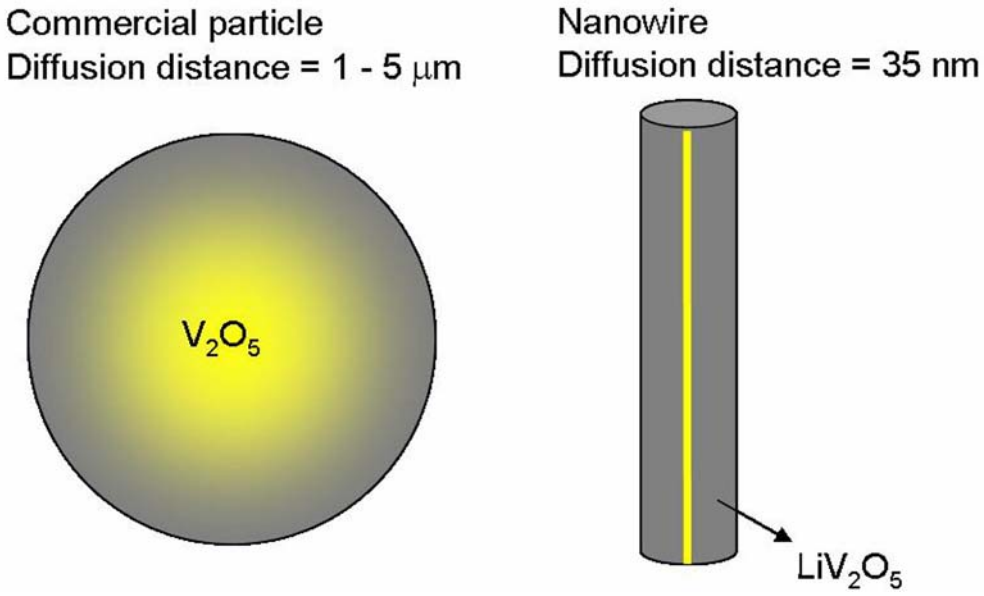

Figure 1-4: Concentration polarization of intercalating Li-ions. Ions are non-uniformly distributed and are concentrated at the electrode surface. Gray represents LiV_2O_5; whereas, yellow represents V_2O_5.

Chapter Summary

The intent of this dissertation is to demonstrate how nanoscale Li-ion battery design succeeds where conventional technology fails. It will begin with a discussion of the improved low-temperature performance of these electrodes. This will then be extended to quantify the solid-state diffusion coefficient of the Li-ion as a function of intercalation-level and temperature. Next, it describes a variation of the general synthetic method, in which the polymer template is pyrolzed to create a $LiFePO_4$/carbon composite electrode. Finally, this is followed by a demonstration of polyvalent-ion (Mg^{2+}) intercalation into V_2O_5.

CHAPTER 2
NANOSTRUCTURED ELECTRODES AND THE LOW-TEMPERATURE PERFORMANCE OF LI-ION BATTERIES

Introduction

Li-ion batteries have become the power source of choice for consumer electronic devices such as cell phones and laptop computers.[2,51-58] This is because these batteries have good rechargeability (1000+ cycles) and offer higher energy density (stored charge per unit volume or mass of the battery) than competing battery technologies.[2,51] However, it is well documented that Li-ion batteries show poor performance at low temperature or under the extreme currents necessary for pulse-power.[59-63] Specifically, the amount of charge delivered from the battery at temperatures below 0 ^{o}C is substantially lower than the amount of charge delivered at room temperature.[59,60,62] This precludes the utilization of these batteries in a number of defense, space and even terrestrial applications.[64] Figure 2-1 is generated from data published by Nagasubramainan[60] on the effect of temperature on the performance of a commercial Li-ion battery cell. Note that the C-Rates are very low; however, still there is a dramatic decrease in the charge-storage ability of the cell as temperature is decreased.

We have been investigating the application of nanotechnology to Li-ion battery electrode design.[17,20-22,24] Previously, the Martin laboratory has shown that template-synthesized Li-ion battery electrodes are capable of delivering more charge-per-gram at the same normalized discharge-rate (C-Rate) than control film electrodes. Based on these studies it seemed likely that Li-ion battery electrodes composed of nanoscopic particles

of the electrode material could mitigate this low-temperature performance problem. We prove this case here by showing that nanofibers (diameter = 70 nm) of the electrode material V_2O_5 deliver dramatically higher specific discharge capacities at low temperatures than V_2O_5 fibers with micro-sized diameters.

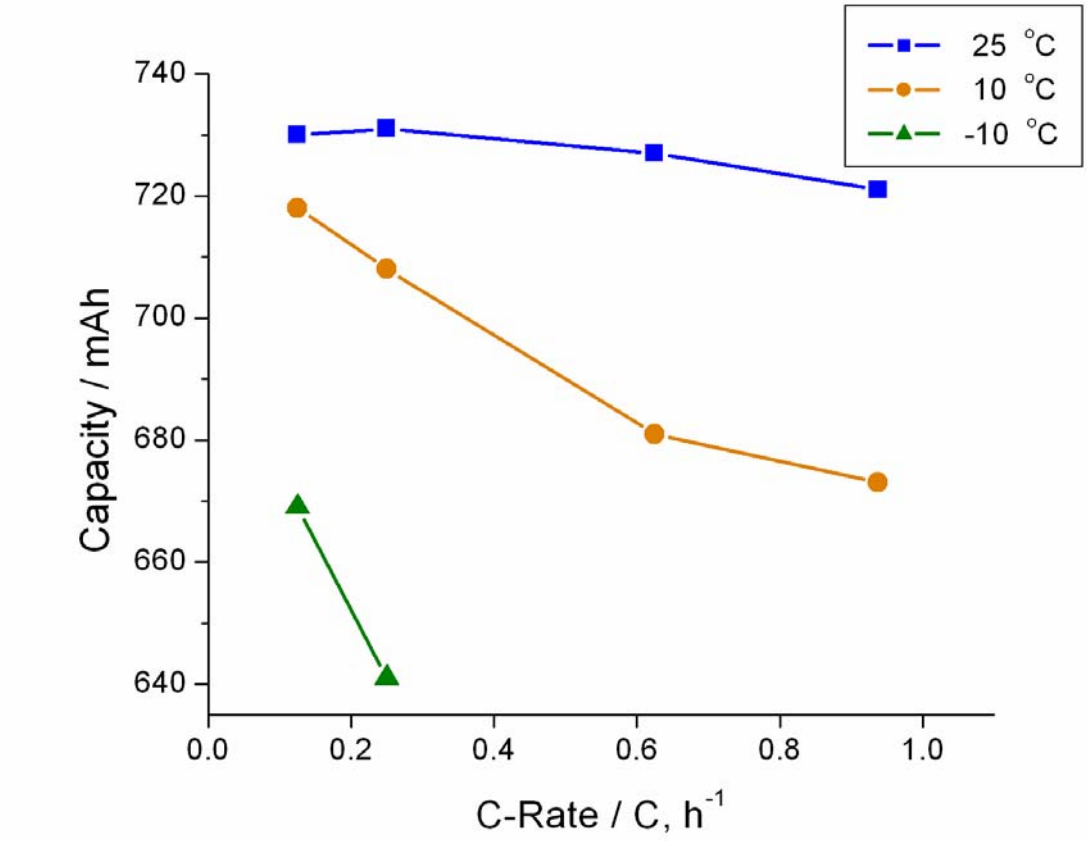

Figure 2-1: Discharge proprieties of a commercial Li-ion battery (AT&T Cylindrical 17500) at low temperature. This cell has a rated capacity of 800 mAh.

Li-ion batteries store charge by intercalating Li^+ from a contacting solution phase, along with an equivalent number of electrons, into the battery's anode material.[2] During discharge the Li^+ must diffuse out of the anode material, through the electrolyte, and intercalate into the cathode material. This process can be seen in Figure 1-1.

For the cathode material V_2O_5, investigated here, the reversible charging and discharging reactions can be written as Equation 2-1.

$$V_2O_5 + xLi^+ + xe^- \underset{\text{charge}}{\overset{\text{discharge}}{\rightleftharpoons}} Li_xV_2O_5 \qquad 2\text{-}1$$

Other laboratories have concluded that the cathode, anode, and electrolyte were the source of the fundamental breakdown that occurs at low temperature. While there is controversy in the scientific literature,[59,60,62,63] the most likely causes of the poor low-temperature performance are either - 1.) Diminution in the rates of these electrochemical charge/discharge reactions at low temperature. 2.) Diminution in the rate at which Li^+ diffuses within the particles which constitute the electrode at low temperature. We hypothesized that in either case, an electrode composed of nanoscopic particles (diameter less than 100 nm) would provide better low temperature performance than the ~10-μm - sized particles[65] used in commercial battery electrodes. This is because an electrode composed of nanoscopic particles would, in general, have higher surface area than an electrode composed of large particles, and this would mitigate the slow electrochemical kinetics problem. Furthermore, the distance that Li^+ must diffuse within the particle would be decreased for nanoscopic particles, and this would mitigate the slow solid-state diffusion problem.

Electrode Synthesis

To prove this point we have used the template-synthesis method[6] to prepare cathodes composed of monodisperse V_2O_5 nanofibers (diameter = 70 nm) that protrude from a current collector surface like the bristles of a brush (Figure 2-2A). We compare the low-temperature charge/discharge performance of these nanofiber cathodes with

cathodes composed of V_2O_5 fibers with diameters of 0.8 μm (Figure 2-2C), as well as with cathodes composed of 0.45 μm-diameter fibers (Figure 2-2B). If our hypothesis is correct, the low-temperature performance of the cathode composed of the 70 nm-diameter nanofibers (designated the 70-nm electrode) should be dramatically better than that of the cathode composed of the 0.8 μm-diameter fibers (0.8-μm electrode), and the low-temperature performance of the cathode composed of the 0.45 μm-diameter fibers (0.45-μm electrode) should be between these two extremes. This experimental design exploits the power of the template-synthesis method for preparing monodisperse fibers having any desired diameter,[6] and builds on our prior work on the electrochemistry of nanostructured Li-ion battery electrodes.[17,20-22,24]

The template-synthesis method entails using the pores in a synthetic membrane or other solid to form nanofibers, nanowires or nanotubes of a desired material.[6] Commercially-available (Poretics, Inc) polycarbonate filtration membranes (figure 2-2D) were used as the templates for these studies. These filters have monodisperse cylindrical pores that run through the complete thickness (6 - 10 μm) of the membrane and are available with a wide range of pore diameters. The pore diameter of the template determines the diameter of the fibers synthesized within the pores.[6]

This method was described in detail previously.[22] Briefly, a 1.0 cm x 0.7 cm piece of the template membrane was placed on the surface of a Pt foil electrode, and 0.6 μL of the liquid V_2O_5 precursor triisopropoxyvanadium (TIVO) was applied to the membrane surface. TIVO fills the pores in the template, and hydrolysis in air converts this material to V_2O_5. This chemistry is straight-forward and it shown in Equation 2-2.

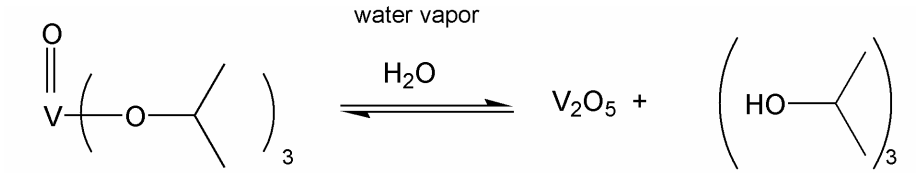

Vanadium (V) triisopropoxide Vanadium pentoxide isopropanol vapor 2-2

In fact, this reaction is so facile that the deposition must occur inside an argon-filled glovebox, so that the precursor may impregnate the pores in this low-viscosity state. It is then transferred to a low O_2 environment (antechamber of the glovebox), so that they hydrolysis can proceed slowly enough as to form continuous structures inside the pores. This was allowed to proceed at room temperature for 12 hours, followed by hydrolysis for 2 hours at 80 ^oC in air. The film of V_2O_5 that covered the upper face of the membrane was then removed by wiping with a damp cotton swab, and this procedure was repeated to ensure that the pores were completely filled with V_2O_5. Oxygen plasma (25 W, 15 Pa, 2 hours) was then used to remove the polycarbonate template. To ensure complete conversion to crystalline V_2O_5, the fibers were than heated at 400 ^oC for 10 hours in flowing O_2 gas. X-ray diffraction studies confirmed that the material obtained is orthorhombic V_2O_5 (experimental details discussed later).[66] A schematic of this process is shown in Figure 2-2.

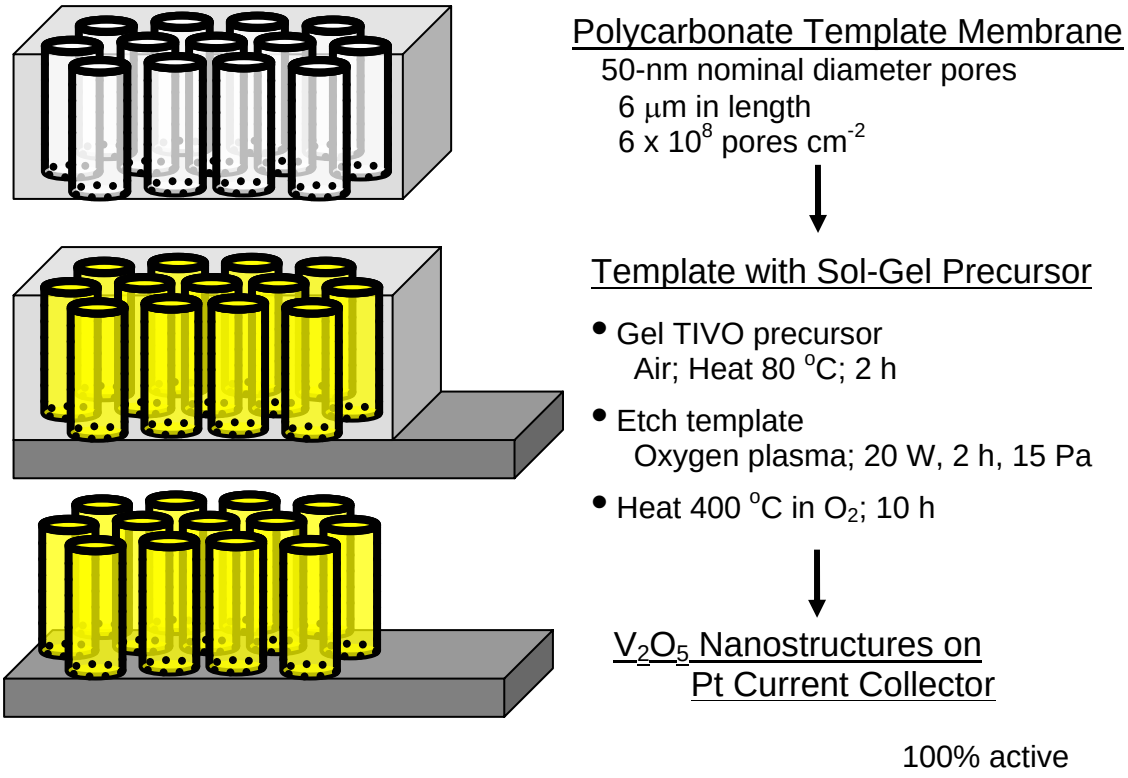

Figure 2-2: Schematic of the template-synthesis of a V_2O_5 electrode.

Scanning Electron Microscopy

Scanning electron micrographs of electrodes of created in various templates are shown Figure 2-3. These samples are attached to stubs by conductive copper tape prior to imaging. The electrodes were not sputtered with any conductive material. This demonstrates the sufficient electron conductivity of these samples. The polycarbonate template was sputtered with a thin layer of Au/Pd to prevent excessive charging during image acquisition.

These template-synthesized V_2O_5 nano and microfibers electrodes serve as useful tools in fundamental investigations, though the void-volume, that is responsible for the short diffusion distances, sacrifices volumetric capacity (mAh L^{-1}). Previously, we demonstrated a method that creates a compromise of these two interrelated parameters.[23]

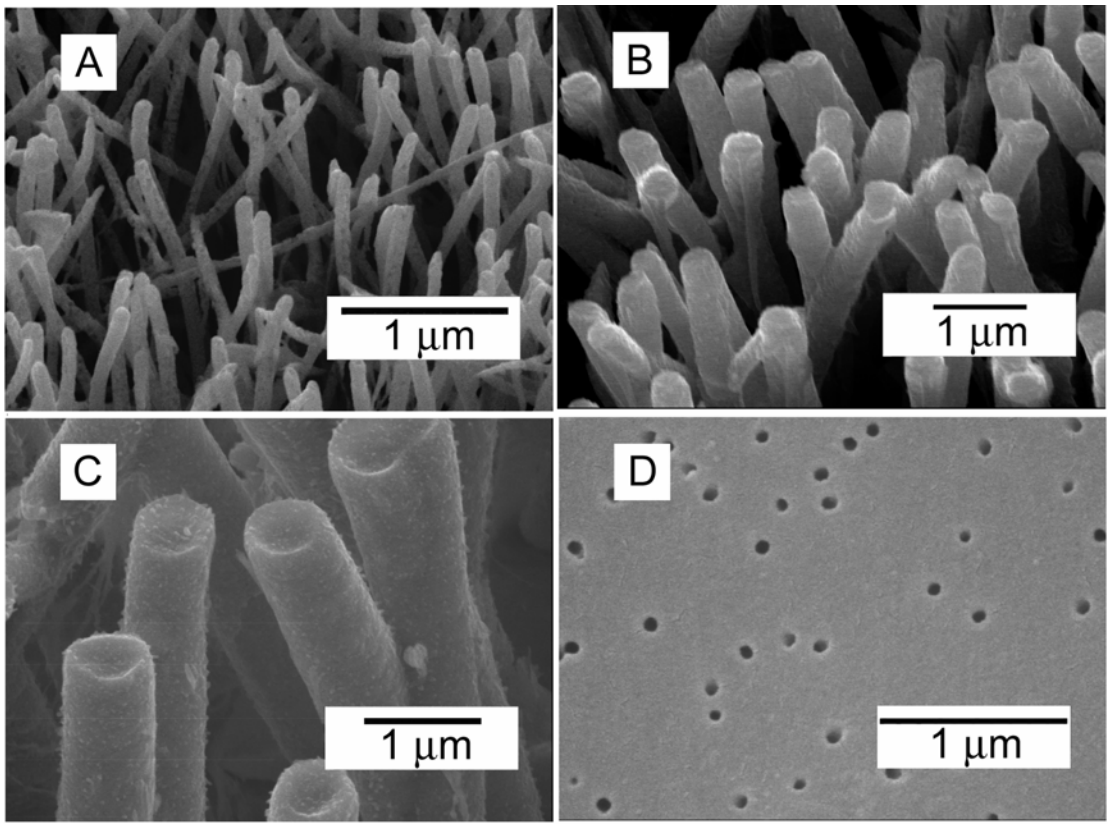

Figure 2-3: Scanning electron micrographs. A) 70-nm electrode. B) 0.45-µm electrode. C) 0.8-µm electrode. D) Polycarbonate template used to prepare the 70-nm electrode.

Electrode Electrochemical Investigations

Constant Current Discharge Experiments

The charge/discharge reactions for these nano and microfiber electrodes were investigated in an electrolyte solution that was 1 M in $LiClO_4$ dissolved in a 1:1:1 (by volume) mixture of ethylene carbonate, diethyl carbonate, and dimethyl carbonate.[67] Li metal ribbons served as the counter and reference electrodes. A schematic of this electrochemical cell can be seen in Figure 2-4.

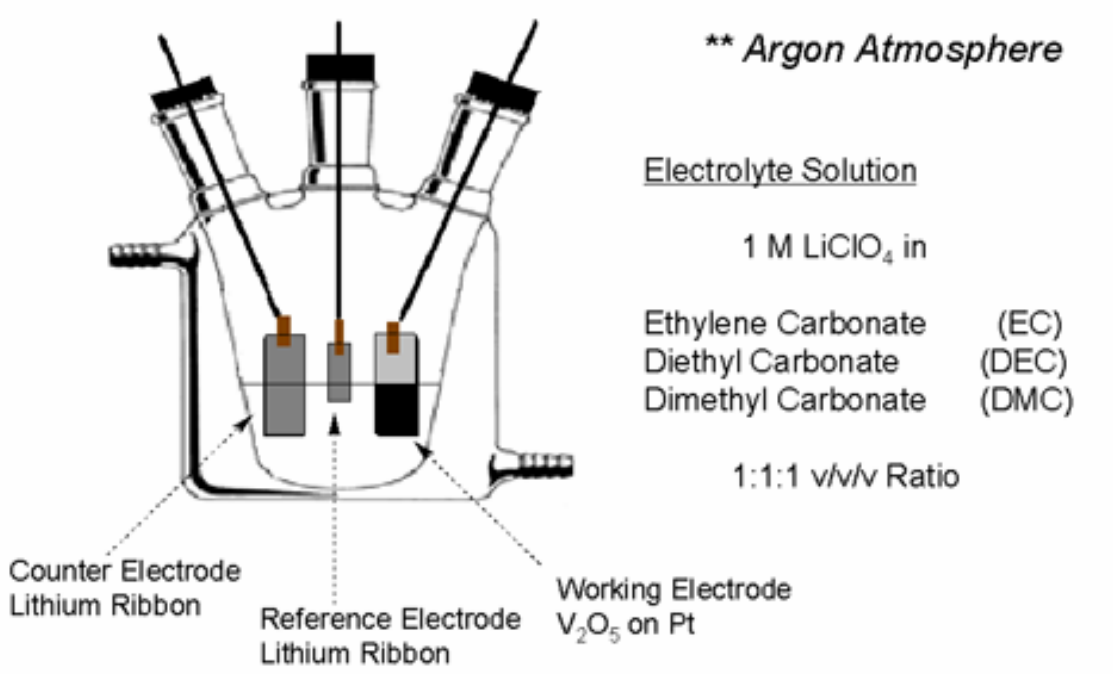

Figure 2-4: Electrochemical cell used for the characterization of V_2O_5 electrodes.

Temperature was set and maintained via a circulation bath of 80:20 ethylene glycol:water. All potentials are quoted here vs. the Li/Li^+ reference. A galvanostat was used to apply a constant current to sequentially discharge and charge the V_2O_5 (Equation 2-1), and monitor the change in potential of the V_2O_5 electrode as a function of time. The discharge reaction was continued until a potential of 2.8 V was achieved, and the charge reaction was terminated when the potential reached 3.8 V. Over this potential window 1 mol of V_2O_5 is known to reversibly intercalate 1 mol of Li^+, (*i.e.*, x = 1 in Equation 2-1).[68] This corresponds to a maximum specific (per g) charge-storage capacity of 148 mAh g^{-1}. The mass of V_2O_5 present in all of our electrodes was determined gravimetrically so that the specific capacities could be determined from the potential-vs.-discharge-time data.

A typical potential-vs.-time curve associated with constant-current discharge of a 70-nm electrode at 25 ^oC is shown in Figure 2-5. A specific capacity of 145 mAh g^{-1} (equivalent to x = 0.98) was obtained from these data.

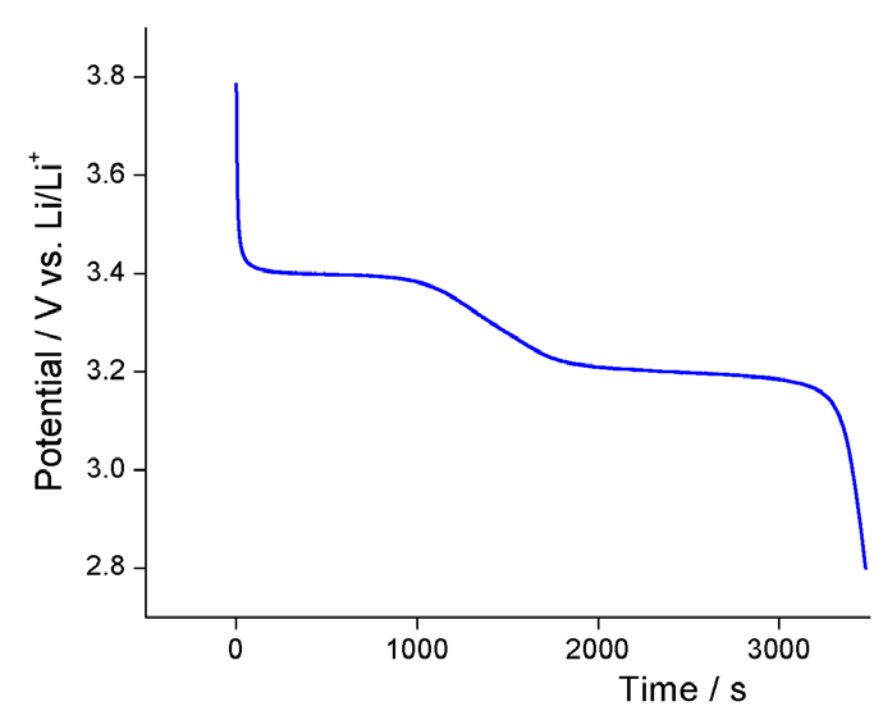

Figure 2-5: Slow-rate (C/3) constant current discharge of 70-nm V_2O_5 electrode using the cell pictured above.

This shows that at this temperature and current density, nearly 100% of the maximum specific capacity of the cathode is being delivered. The effect of discharge current or C-Rate and temperature on the specific capacity of the 70-nm electrode is shown in Table 2-1.

Table 2-1: The effect of discharge rate and temperature on the specific capacity of the 70-nm electrode.

C-Rate / h^{-1}	Specific Capacity / mAh g^{-1}		
	25 °C	0 °C	-20 °C
0.2			77.5
1	144.8	104.9	63.8
5	123.0	74.4	40.7
10	107.5	60.2	33.5
20	90.4	48.7	27.3
25			25.5
30		43.1	24.8
35			23.0
40	72.9	39.6	22.7

Comparison of Rate Capabilities

At all temperatures, we see the decrease in capacity with discharge rate, typical of Li-ion battery electrodes.[20,21,51,57] However, as expected,[60-62] this decrease in capacity becomes much more pronounced at low temperatures. Data of this type were obtained for all three of the V_2O_5 fiber electrodes. Again, our objective is to demonstrate that the 70-nm electrode is able to deliver greater specific capacity at low temperatures than the electrodes composed of the larger-diameter fibers. We define the specific capacity of the 70-nm electrode at a given discharge current, *I*, and temperature, *T* (Table 2-1), as $C_{s\text{-}70,I,T}$. We define the identical parameter (*i.e.*, same current and temperature) for the 0.8-μm electrode as $C_{s\text{-}0.8,I,T}$. Finally, we define a capacity ratio $R_{70/0.8} = C_{s\text{-}70,I,T} / C_{s\text{-}0.8,I,T}$. If $R_{70/0.8}$ is greater than unity, then at these particular values of *I* and *T*, the 70-nm electrode shows a capacity advantage relative to the 0.8-μm electrode.

Figure 2-6A shows plots of $R_{70/0.8}$ vs. the discharge rate for experiments done at temperatures of 25 ^{o}C, 0 ^{o}C and -20 ^{o}C. Looking at the 25 ^{o}C curve first, we see that at low discharge rates, $R_{70/0.8}$ is nearly unity, which means that at room temperature and low discharge rate, both electrodes are delivering nearly 100% of their maximum specific capacities; hence, at room temperature and low discharge rates, there is no capacity advantage for the 70-nm electrode relative to the0.8-μm electrode. At higher discharge rates $R_{70/0.8}$ increases above unity, indicating that there is now a capacity advantage for the nanofiber electrode; however, at room temperature this advantage is modest.

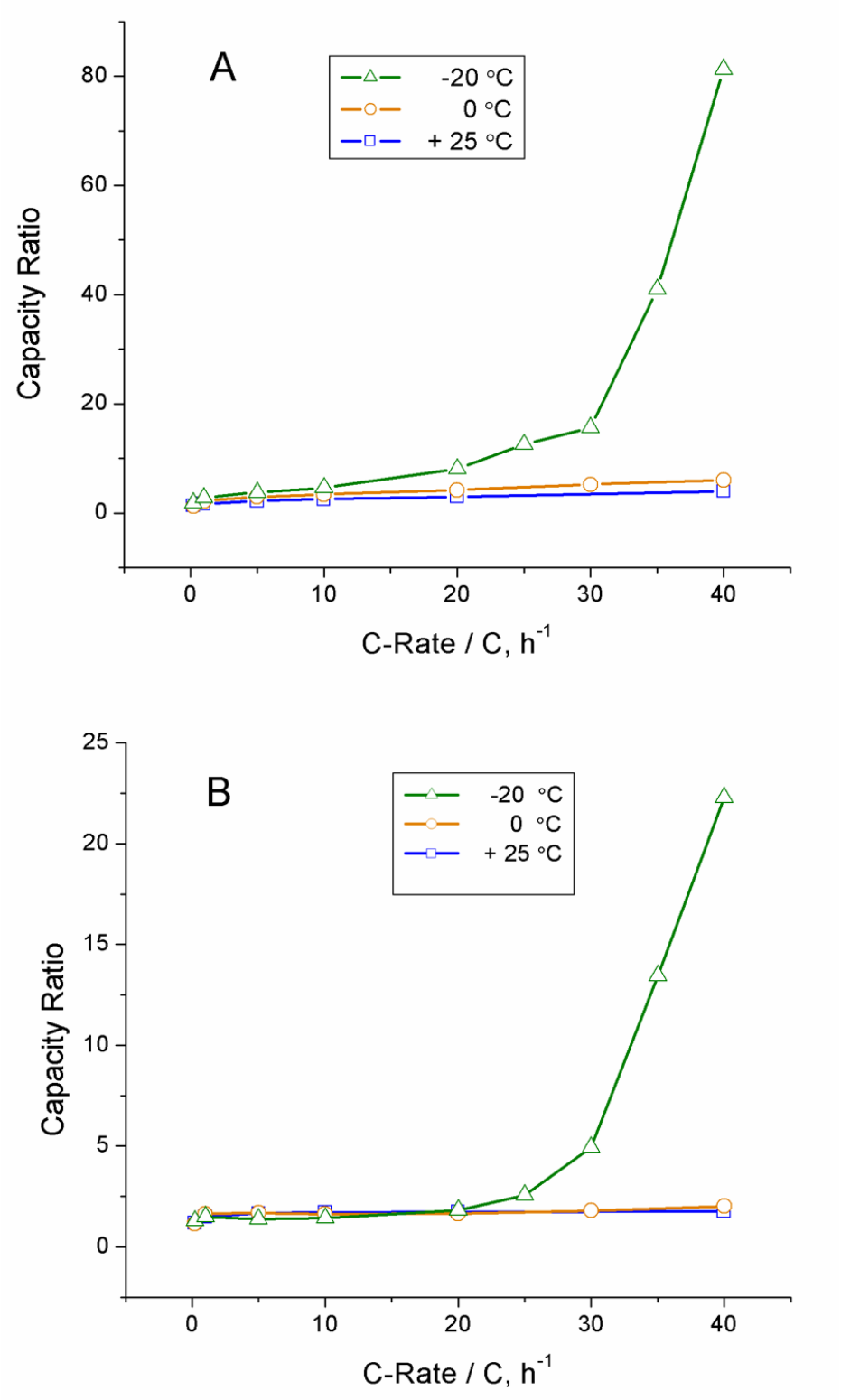

Figure 2-6: Capacity ratio (see text) versus discharge rate for experiments conducted at 25 °C (Blue), 0 °C (Orange), and -20 °C (Green). A) $R_{70/0.8}$ B) $R_{70/0.45}$.

Turning now to the -20 ^{o}C data, we find that at the lowest discharge rate the 70-nm electrode delivers twice the specific capacity of the 0.8-μm electrode. Furthermore, $R_{70/0.8}$ increases dramatically with discharge rate; indeed, at the highest rate studied, the specific capacity delivered by the 70-nm electrode is almost two-orders of magnitude greater than the specific capacity delivered by the 0.8-μm electrode. *These data prove our hypothesis – that an electrode composed of nanoscopic particles shows better (indeed, dramatically better) low-temperature performance than an electrode composed of micron-sized particles.* The 70-nm electrode also shows a capacity advantage at the intermediate temperature of 0 ^{o}C, but as would be expected, the advantage is not nearly as dramatic as at -20 ^{o}C. These data confirm the results obtained with commercial Li-ion batteries - that performance at room temperature and 0 ^{o}C are not so different but that performance becomes markedly worse at -20 ^{o}C.[62,67]

We obtained similar data for the 0.45-μm electrode and calculated the analogous specific capacity ratio $R_{70/0.45} = C_{s\text{-}70,I,T} / C_{s\text{-}0.45,I,T}$. If our hypothesis is correct, the 70-nm electrode should show better low-temperature performance than the 0.45-μm electrode ($R_{70/0.45} > 1$), but at any value of discharge current, $R_{70/0.45}$ should be less than $R_{70/0.8}$. A comparison of the curves in Figure 2-6A and B shows that this is indeed the case.

We have proven that a nanostructured Li-ion battery electrode shows better low-temperature performance than analogous electrodes composed of micron-sized particles. Two questions remain. 1.) How do these studies relate to practical battery-electrode design? 2.) From a fundamental viewpoint, what is the genesis of this improved low-T performance? With regard to question 1, our results suggest that to improve low-T performance, practical Li-ion battery electrodes should be prepared using smaller

particles of the active material than the ~10 μm-sized particles currently used. However, a practical Li-ion battery electrode contains other components in addition to the active material; these include a polymeric binder and graphitic particles to improve electronic conduction through the electrode.[50] The effect of amount and particle size of these ancillary components would also have to be evaluated. In this regard, our experimental design based on template-synthesized micro and nano particles has tremendous advantage for the fundamental studies performed here because these ancillary components are not needed and therefore do not complicate the analysis.

Our data also provide an answer to question 2. We suggested above that the poor low-temperature performance of Li-ion batteries is due to either a decrease in the diffusion coefficient within the electrode particles, or a decrease in the rate of the electrode reactions (Equation 2-1), with decreasing temperature. If the solid-state diffusion coefficient is the culprit then low-temperature performance should improve with decreasing particle diameter, and this is exactly what is observed here.

If electrode reaction rate is the culprit, then low-temperature performance should improve with a parameter we designate S_c, the electrode-particle surface area per cm^2 of current collector area. The beauty of the template method is that S_c can be easily calculated from the fiber diameter, the pore density of the template membrane, and the fiber length. Table 2-2 shows these parameters. These calculations show that because of the interplay between pore diameter and density in the template membranes, S_c is higher for the 0.45-μm electrode (S_c = 14.1) than for the 70-nm (S_c = 7.9) or the 0.8-μm (S_c = 6.8) electrodes. This indicates that if electrode reaction rate is the culprit, then the 0.45-μm electrode would show the best low-temperature performance, and this is not observed

experimentally. Hence, our data show that the temperature dependence of the solid-state diffusion coefficient determines the low-temperature performance of the electrodes studied here.

Evaluation of S_c

As discussed in the text of the paper, S_c is the electrode-particle surface area per cm^2 of current collector area. The parameters needed to calculate S_c are presented in Table 2-2.

Table 2-2: Parameters needed to calculate S_c.

Pore Diameter (nm)	Pore Density (cm^{-2})	Membrane thickness (μm)
70	$6x10^8$	6
450	$1x10^8$	10
800	$3x10^7$	9

To calculate S_c for the template-synthesized nano or microfiber electrode, one first calculates the circumference of an individual fiber. The surface area of the fiber is the product of the circumference and the length of the fiber. The length is given by the membrane thickness. The number of fibers per cm^2 of current collector surface area is equivalent to the pore density of the membrane. Therefore, the surface area per fiber multiplied by the pore density is S_c.

Effect of Cycle Life

The order of the series of experiments dictates that each test delivers less charge than the previous (*e.g.*, low to high C-rate of discharge and high to low temperature.) Therefore, it is helpful to examine any adverse effects on the cycle life on the system. After the entire set of experiments was completed, if the system was returned to room temperature (25 ^oC), the electrodes maintained 98+% of the capacity shown in the

original series of tests at that temperature. This is an important control experiment to help validate the data that are the basis for our conclusions.

Also, the cycle-life can easily be characterized by charging and discharging the electrode with a constant current. Figure 2-7 shows the cycle life of a V_2O_5 nanostructured electrode that is charged and discharged at the constant rate of 10 C. Since the same current is used to charge and discharge the electrode, the columbic efficiency (charge out / charge in) reduces to a ratio of discharge time / charge time. The columbic efficiency of this electrode was greater than 95%. The electrode stored and delivered virtually the same charge over nearly 400 cycles at a high rate of discharge.

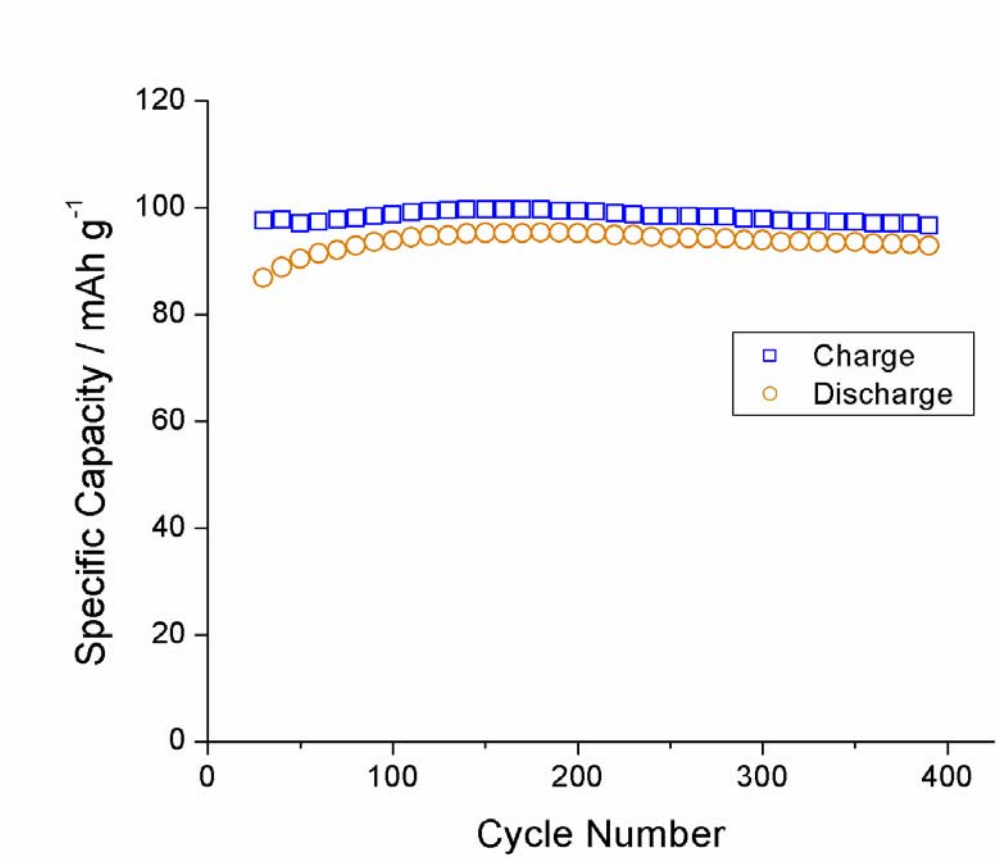

Figure 2-7: Cycle life of 70-nm V_2O_5 electrode charged and discharged at 10 C for 400 cycles. Columbic efficiency (Q_{out} / Q_{in}) over this range is greatly than 95%.

Effect of Electronic Conductivity

In commercial Li-ion battery cathodes, it is necessary to add an electronically conductive material, typically carbon particles, to improve electronic conductivity through the electrode. We have shown that this is not necessary with template synthesized electrodes.[20-22,24] This is because while the electronic resistance of a single fiber (R_f) making up the template-synthesized electrode might be high, the electrode is a parallel ensemble of such fibers. As such, the total resistance of the electrode (R_t) is given by $R_t = R_f/N$, where N is the number of fibers in the electrode.

That electronic conductivity does not dominate the rate capabilities of the electrodes studied here is easy to prove. Assuming the same length, it is easy to show that the electronic resistance of a 70 nm diameter fiber is 33 times higher than that of a 0.8 μm diameter fiber composed of the same material. If the rate capability was limited by electronic conductivity, the 70-nm electrode would show the worst rate capability and the 0.8-μm electrode would show the best. This is exactly the opposite of what is observed experimentally.

Chapter Summary

This chapter clearly demonstrates the advantages of template-synthesis as a method to create ideal electrodes for fundamental studies of Li-ion batteries. The electrode precursor was deposited into the pores of a commercially available polycarbonate template membrane. The template serves to restrict particle growth as the precursor is hydrolysized to V_2O_5, a known Li-battery cathode material. These V_2O_5 wires extend from the surface of a current collector like bristles of a brush. The geometry of the pores of the template is imparted onto these wires – a nanoporous template yields nanostructured wires and microporous template yields microstructured wires. We

demonstrated the ability to create structures of reproducible diameters by this template-synthesis method.

Three of these electrodes with different wire geometries were electrochemically charged and discharged by a constant-current. By creating particles of the shortest solid-state diffusion distance, we were able to demonstrate superior low-temperature rate-capabilities when compared to microstructured control electrodes. However, these superior discharge characteristics would be achieved with any competitive nanofabrication method. The ability of template-synthesis to create structures of reproducible solid-state diffusion distance and surface-area is what differentiates it from other nanofabrication methods. Analysis of these data identifies the decrease in solid-state diffusion coefficient of the Li-ion associated with the decrease in temperature to be the rate-limiting factor in Li-ion batteries. The conclusions presented in this chapter are a benchmark study in the field of low-temperature Li-ion battery research.

CHAPTER 3
EVALUATION OF SOLID-STATE DIFFUSION COEFFICIENT OF LI-IONS AT LOW TEMPERATURE

Introduction

Since their introduction in the early 1990s by Sony[1], Li-ion batteries have been the focus of intense research to adapt their design to more demanding systems, such as those operating on pulse-power and at low-temperature. It is widely known that these batteries can only provide limited capacity (mAh) at low temperatures.[25,60,61] The previous chapter identified the fundamental breakdown that occurs in these batteries at low temperature to be the decrease in solid-state diffusion coefficient of the Li-ion (D_{Li+}).[25] The critical step in this analysis was the ability to produce nanowire-based electrodes with controllable particle-diameter, length, and density. This was accomplished by *template-synthesis*.[69] *Template-synthesis* is a general nanofabrication method, pioneered in the Martin laboratory, capable of creating nanostructures of gold,[8,9] carbon,[12] semiconductors,[14] polymers,[6] and Li-ion battery electrodes.[20,22,24]

Since we identified the decrease in D_{Li+} as the rate-limiting factor in low-temperature environment,[25] the next logical progression is to quantify that decrease. Aurbach *et al.* [70,71] have demonstrated the ability of the potentiostatic intermittent titration technique (PITT) to measure the value D_{Li+} in Li-ion battery electrodes. This experimental method is based on a series of small potential steps and data analysis via the Cottrell-relationship. This was first described in this embodiment by Huggins and coworkers.[72] This method results in the systematic discharge (intercalation) of a Li-ion

battery cathode, such as V_2O_5. Lithium is known to reversibly intercalate 1 mol of charge into an equivalent of V_2O_5 host over the potential window 2.8 to 3.8 V vs Li/Li^+ as described by Delmas *et al.*[68] according to the reversible intercalation reactions of Equation 2-1.

One of the complications identified in prior studies is the ability to create structures of reproducible diffusion distance.[70] Template-synthesized nanostructured V_2O_5 electrodes are again an ideal tool for this analysis, due to the reproducibility of the nanowires solid-state diffusion distance (a factor closely related to the analysis) and their ability to equilibrate uniformly after an electrochemical perturbation. The electrochemical response of these template-synthesized electrodes is not as subject to the interferences of conventional systems, such as concentration-polarization of the Li-ion [25] and the effects of conductive carbon and polymeric binders [50] (absent in this system). This chapter reports our efforts to quantify this decrease in solid-state diffusion-coefficient of the Li-ion with decrease in system temperature.

Electrode Synthesis

Template-synthesis was used to fabricate V_2O_5 electrodes. This process has been detailed elsewhere.[25] A 3 cm^2 section of commercially-available polycarbonate template (Poretics) was placed atop a section of Pt foil. A 1 μL drop of triisopropoxide vanadium (TIVO) precursor impregnated the pores of the template from the top. This was performed in an argon environment to prevent hydrolysis of the precursor prior to complete filling the pores. This assembly is then transferred to a low humidity environment (antechamber of the glovebox) and hydrolysis proceeds slowly over 8 hours. The particle-growth is restricted by the pore wall of the template; therefore, a nanoporous

template yields an array of nanoscale diameter wires and microporous template yields microscale diameter wires. The templates used here are polycarbonate. The nanoporous template has nominally 50-nm diameter pores, 6 microns in length with a density of 6 x 10^8 pores cm^{-2}. The microporous template has nominally 0.8-μm diameter pores, 9 microns in length with a density of 3 x 10^7 pores cm^{-2}. In order to ensure the micropores are completely filled, the filling procedure is repeated.[25]

The assembly is then heated to 80 ^oC for 2 hours in air to ensure complete hydrolysis. Oxygen plasma (20 Pa, 25 W, 2 hours) preferentially etches the organic template, leaving structures that have the same geometry of the pores. These structures extend from the Pt current collector like the bristles of a brush. This assembly is then heated in flowing O_2 for 10 hours to convert the V_2O_5 into its crystalline form. Note there is no conductive carbon or polymeric binder used in this synthesis.

Electrolyte Synthesis

Li-ion battery electrolytes are based on non-aqueous solvents. The primary reason is that the available potential envelop is greatly extended in such solvents. Aqueous-based systems are limited to ~ 1.2 Volts as not to engage undesired reactions, *i.e.*, the splitting of water. The solvent system is a mixture of aprotic carbonates. Ethylene carbonate (EC) has a high dielectric constant; therefore, it ensures that the $LiClO_4$ dissociates. However, EC is a solid at room temperature and must be gently heated to melt prior to use. Therefore, diethyl carbonate (DEC) is added to decrease the viscosity of the system; which greatly improves ionic conductivity. Dimethyl carbonate (DMC) is added in proportion with diethyl carbonate in low temperature experiments, because of its ability to maintain ionic conductivity at low temperatures. These solvent systems are

relatively standard in Li-ion battery research. They are dry and it is imperative that they remain dry throughout the experiment.

The salt used for all of these experiments is $LiClO_4$. There are several examples in the literature of alternative counter-ions. Perhaps the most common seen in commercial-systems is $LiPF_6$. Others include $LiBF_4$ and $LiAsF_6$. We selected $LiClO_4$, because it is much easier to handle than the competing salts. $LiPF_6$, for example, is much more hydroscopic and hazardous than $LiClO_4$ and has only slightly improved conductivity. The $LiClO_4$ is heated on a hot plate in the argon glovebox to aid the electrolyte to remain dry.

Measurement of Diffusion Distance

As stated previously, a primary advantage of using template-synthesized Li-ion battery electrodes for this analysis is the ability to create structures of reproducible solid-state diffusion distance. We have used scanning electron microscopy (SEM) to verify the geometry of our structures. Figure 3-1A is a low-magnification image that demonstrates the uniformity of the structures. Figure 3-1B is a high-magnification image of these structures to identify the solid-state diffusion distance (ℓ), determined by the radius of the nanofiber. This is a valid assumption since these wires are equally accessible to radial Li-ion intercalation and their aspect ratio is high (*i.e.*, the surface area available for radial diffusion vastly exceeds that available for axial diffusion). This value is 50 nm. The uniformity of diffusion distance of the particles should provide a single characteristic diffusion time-regime, where all are subject to semi-infinite diffusion at the same times.

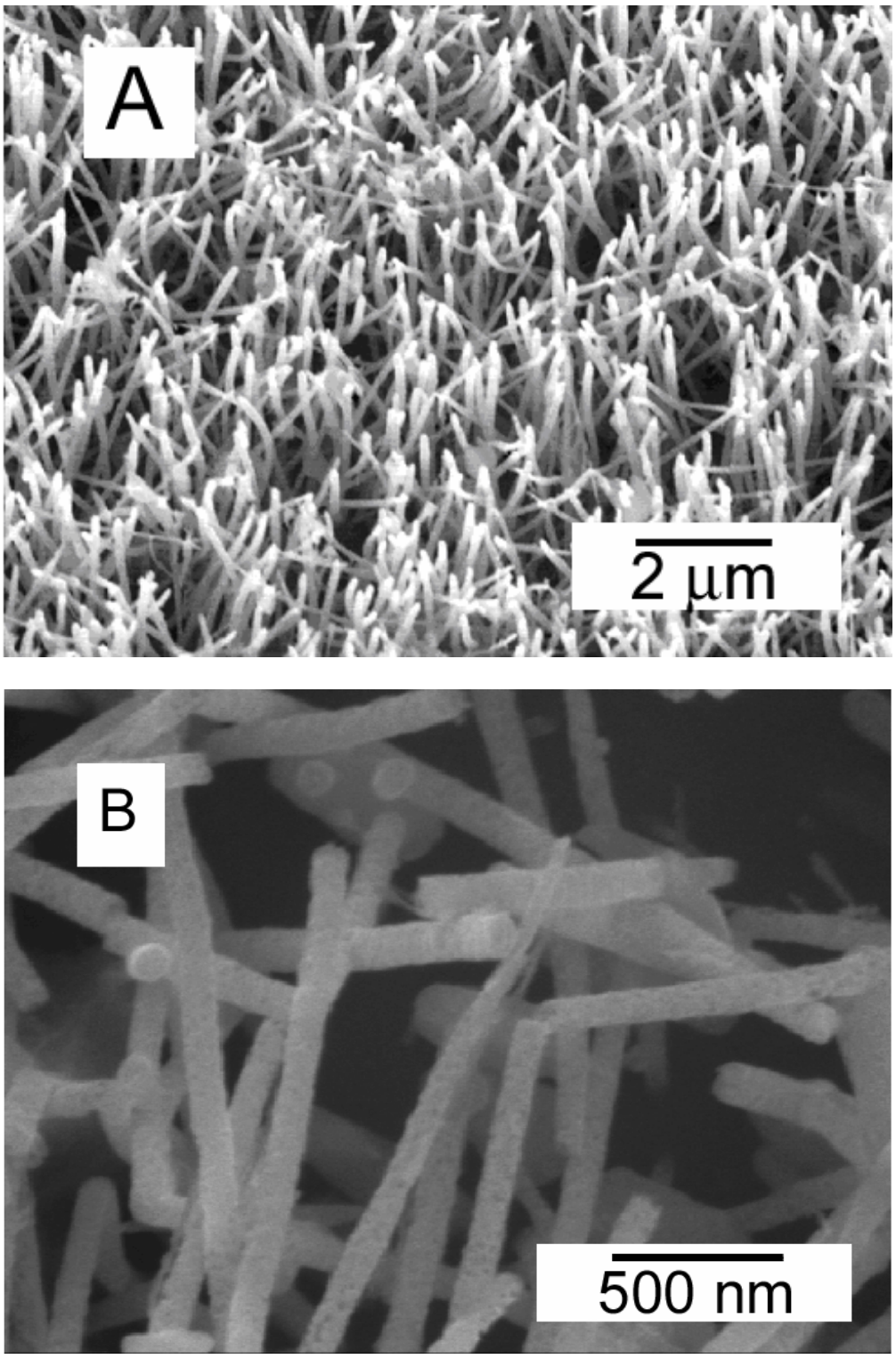

Figure 3-1: Scanning electron micrograph. A) This low magnification image shows the uniformity over the large number of wires that constitute the electrode. B) This high magnification image is used to identify the solid-state diffusion path-length (radius of a nanowire) to be 50 nm.

Electrochemical Investigations

Potentiostatic Intermittent Titration Technique (PITT)

Each electrode is characterized in a three-electrode jacketed cell. Temperature is set and maintained by a cooling circulation bath. Lithium ribbon is used as both the reference and counter electrodes. The electrolyte is 1 M $LiClO_4$ in an equivolume solvent mixture of ethylene carbonate, diethyl carbonate, and dimethyl carbonate (EC:DEC:DMC.) The PITT electrochemical experiments begin with the electrode completely in the charged (as synthesized) state. A -15 mV potential step polarized the electrode for the period of 45 minutes. This process was repeated over the entire range of 3.8 to 2.8 Volts versus Li/Li^+. The temperature is then reduced to the next level. A slow linear potential sweep (0.1 mV s^{-1}) is used to return the electrode to the charged-state after 3 hours has elapsed for temperature equilibration. The experimental potential-step series was repeated. The cyclic voltammetric experiments are performed in an identical system with a scan rate of 0.1 mV s^{-1}.

A typical electrochemical response (current peak and decay) after the negative potential step is shown in Figure 3-2A. Since the electrode material is synthesized in the delithiated (x = 0) charged state, the potential steps are negative (ΔE = -15 mV), so as to intercalate Li^+ with every step. Therefore, the currents are negative as well. Note that a disproportionate quantity of charge is intercalated at the potentials that correspond to the voltammetric peaks, as expected. After the 45 minute duration of the polarization, the currents have reached a small, but non-zero, steady state value. Preliminary analysis of these data follows the work of Aurbach *et al.*[70] In that experiment, they identified distinct kinetic regions during the charge reaction of anodic graphite by examining the $It^{1/2}$ versus log t plot.

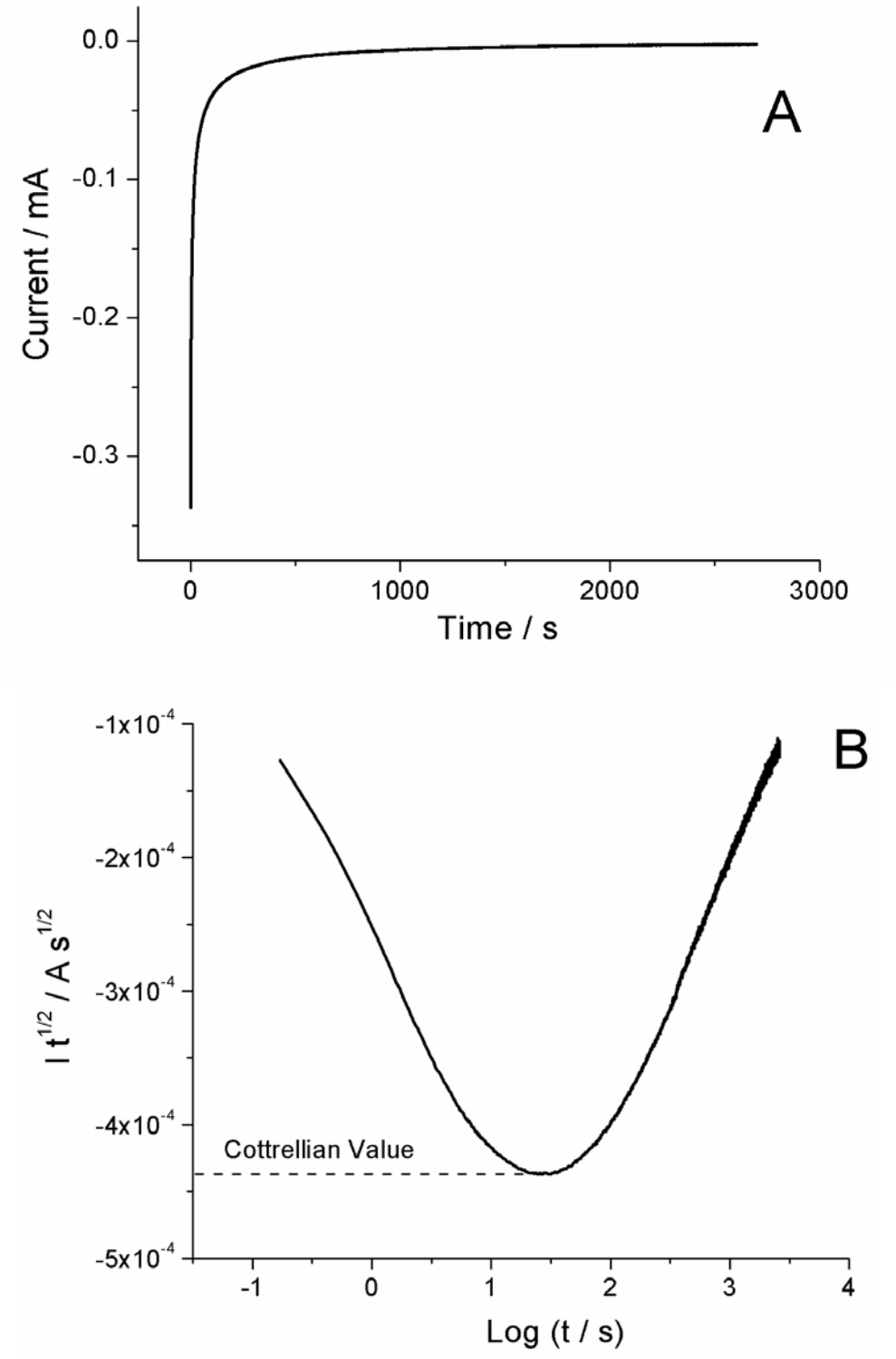

Figure 3-2: Electrochemical response of nanostructured V_2O_5 electrode to a ΔE = -15 mV potential step. A) Current-time transient recorded for 45 minutes as the current decayed to a steady-state value. B) Current-time transient shown in Cottrell-plot form. The plateau represents the Cottrellian value $It^{1/2}$.

Figure 3-2B represents the current-time transient (Fig. 3-2A) as a similar $It^{1/2}$ versus log t plot. This method conveniently identifies the solution to the Cottrell relationship[73] (*i.e.*, where semi-infinite linear diffusion plays a major role), as it is the plateau of the plot. This particular plateau (3.200 V) lasts approximately 20 s in duration and is identified on the figure. The kinetic regimes[70] are clearly seen and correlate to 1.) the time-constant associated with the double-layer capacitance and the charge-transfer resistance (the short-time linear region prior to the plateau) 2.) the solution to the Cottrell relationship, where the value of $It^{1/2}$ is independent of time (the plateau) and 3.) the transition into the finite diffusion regime, where enough time has elapsed that the diffusion layer has propagated to encompass the entire nanowire [$\ell < \sqrt{(2Dt)}$] (The long-time linear region post to the plateau.)

Figure 3-3 demonstrates the potential-dependency of the time-region associated with this plateau. As the potentials approach that of the voltammetric peaks the plateaus shift to longer times and more negative values. This data can be easily converted to the solid-state diffusion coefficient of the Li-ion by means of Equations 3-1 and 3-2. Equation 3-1 establishes tau (τ) as the characteristic diffusional time constant. Equation 3-2 expresses the simple relationship of this time constant to the solid-state diffusion coefficient of the Li-ion (D_{Li+}).

$$\tau = \frac{\Delta Q^2}{\left(It^{1/2}\right)^2 \pi} \tag{3-1}$$

$$D_{Li+} = \frac{\ell^2}{\tau} \tag{3-2}$$

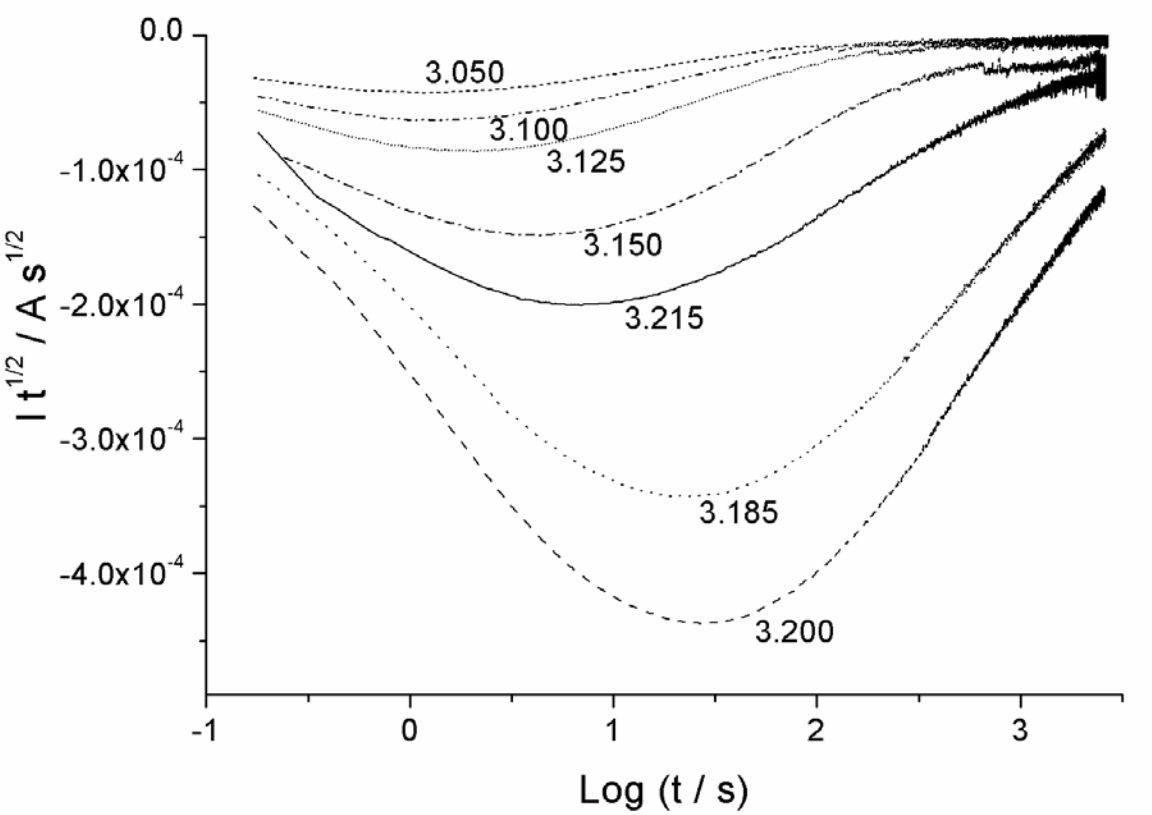

Figure 3-3: Cottrell-plots as a function of potential and thus level of intercalation. At the potentials corresponding to the voltammetric minima, the Cottrellian value $It^{1/2}$ is shifted to more negative values and occurs at longer times.

Again, $It^{1/2}$ is determined from the Cottrell-relationship plot (the ordinate value at plateau) (see Figure 3-2B); ΔQ represents the quantity of charge intercalated per step (this value is determined via a digital integration of the I-t response using the CorrView software package); ℓ is the characteristic diffusion path length (nanowire radius). The value for ΔQ is adjusted to account for the effect of background currents. Figure 3-4 shows this value of ΔQ at each E for the room temperature experiment.

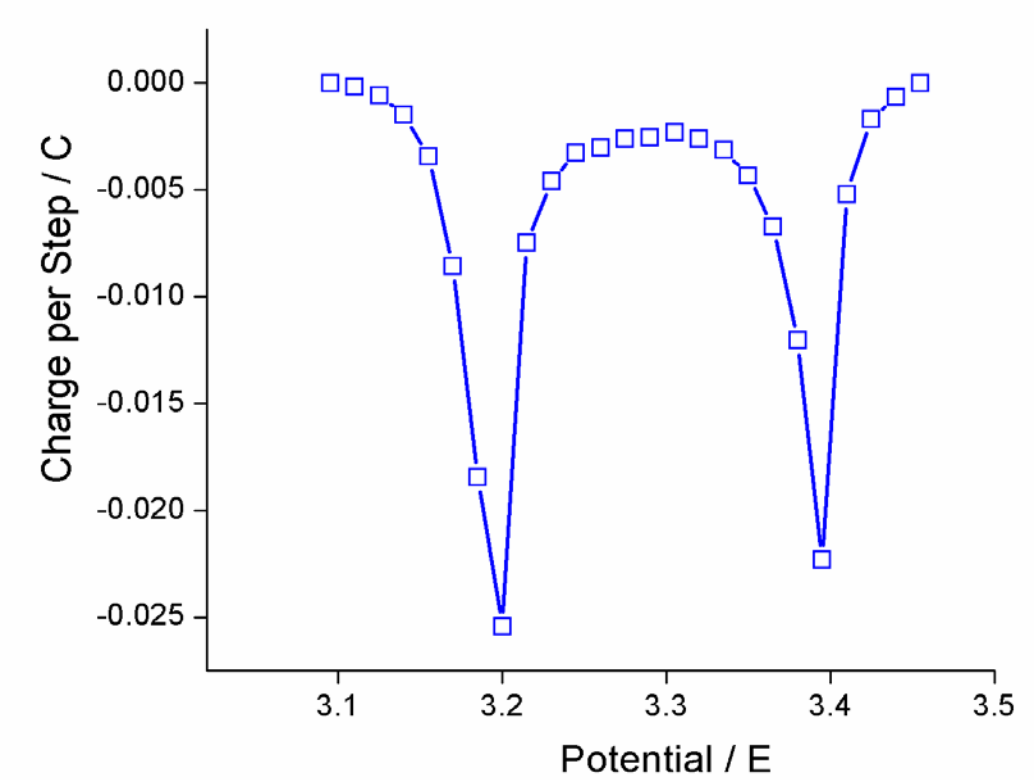

Figure 3-4: Charge intercalated per potential step. The majority of charge is intercalated at the potentials corresponding to voltammetric minima and galvanostatic plateaus.

Determining D_{Li+} (Data analysis)

Figure 3-5 clearly shows the dependency of D_{Li+} on T and E. Note that the y-axis (D_{Li+}) is plotted on a log scale. First, let us discuss the value of D_{Li+} at room temperature (blue curve.) This curve exhibits similar dependence of D versus E seen by several research groups.[71,74-77] Minima are observed at potentials of the voltammetric peaks and are attributed to the effects of ion-ion interaction on the energy of activation.[70,78] This is intuitive as the movement of ions between intercalation sites becomes retarded in the presence of more of these species. Also of note, the particular values are within the approximations made by other groups.[75,77]

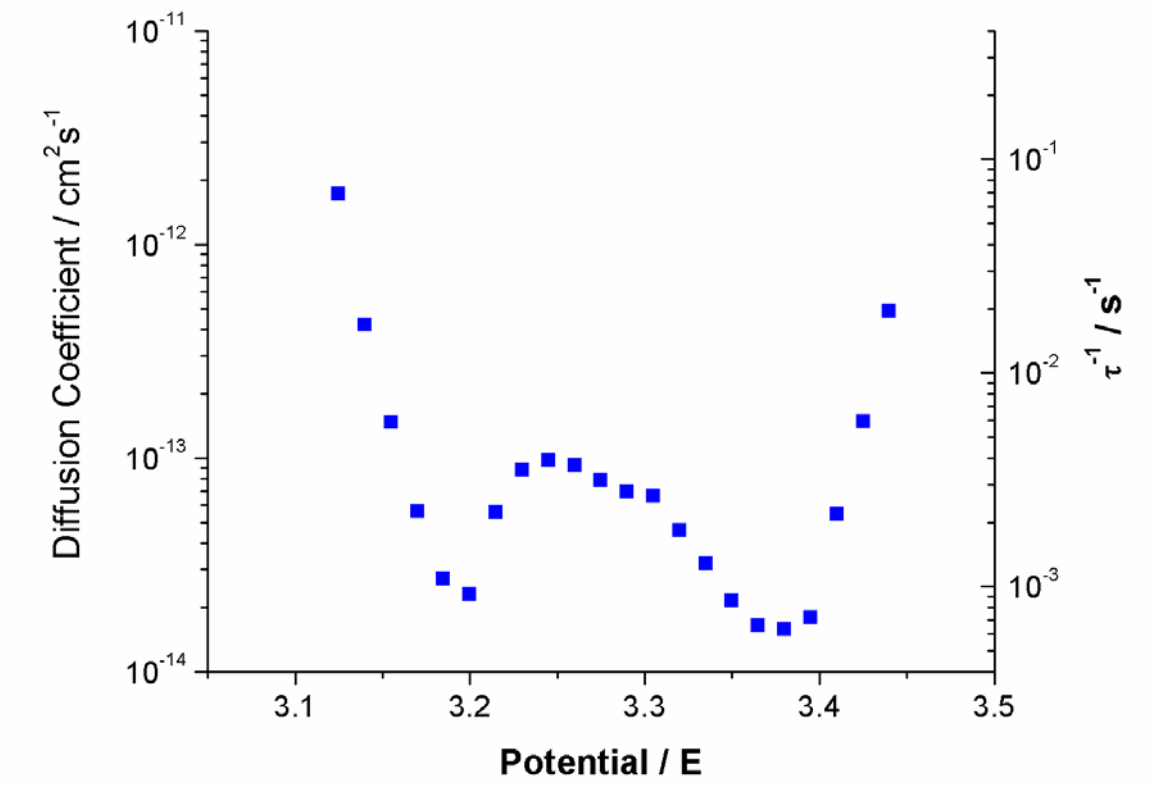

Figure 3-5: Solid-state diffusion coefficient as a function of potential. Y1-axis is the solid-state diffusion coefficient and the Y2-axis corresponds to characteristic diffusion time constant (τ) at room temperature. Note that both y-axes are plotted on a logarithmic scale.

Previously, we have seen less charge delivered from template-synthesized nanostructured electrodes as the temperature is decreased.[25] We attributed the decrease to a decrease in D_{Li+}. Comparing data collected at room temperature (blue) and those at 0 ^{o}C (orange), we see this is indeed the case. When comparing these curves, we notice the values of the orange curve are less than the blue curve in every instance. The minima are again observed and again correlate to the potentials of the voltammetric peaks. The minima of the low temperature curve are shifted slightly less positive of those observed with the room temperature curve. This is attributed to sluggish electrokinetics and is discussed in detail later.

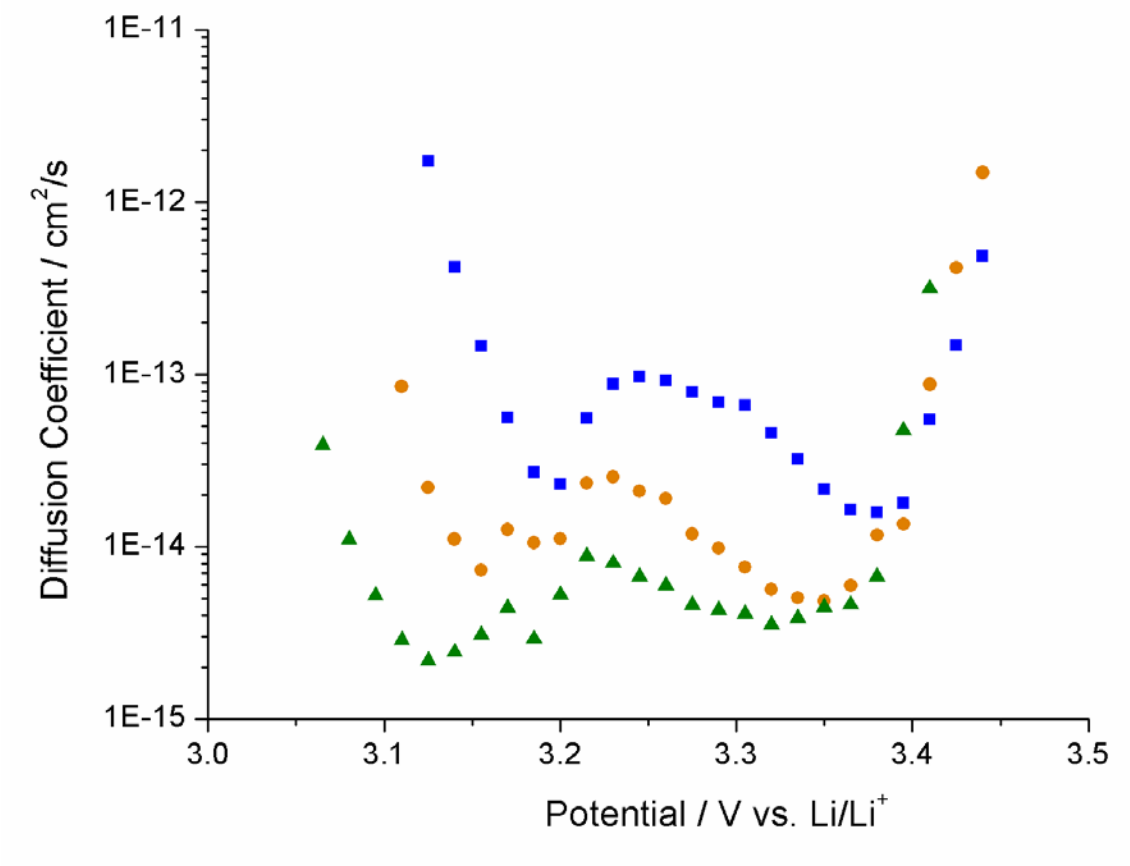

Figure 3-6: Dependence of D_{Li+} conducted at 25 °C (Blue squares), 0 °C (Orange circles), and -20 °C (Green triangles).

Figure 3-6 shows the trend continues in a comparison of the 0 °C curve to the -20 °C (green) curve. Again the decrease in D_{Li+} is seen, particularly at the low-potential region. The low-potential D_{Li+}-minimum at -20 °C (2.2×10^{-15} cm^2 s^{-1}) is an order of magnitude lower than the minima at 25 °C (2.3×10^{-14} cm^2 s^{-1}). These data confirm our previous conclusions that the rate-limiting factor of these electrodes at low-temperature is the decrease in solid-state diffusion coefficient. Again, the minima potentials are more negative than those at 0 °C.

Activation Energy of Diffusion Process

Energy of activation represents the thermal energy barrier that must be overcome for a process to proceed. Equation 3-3 is the general form of the Arrhenius equation that

describes the relationship between the rate constant *k* and the temperature *T*. Equation 3-3 is the form of the general Equation 3-4 and conveys the relationships of our data to E_A.

$$k = A\exp\left(-E_A / RT\right) \tag{3-3}$$

$$\ln D_{Li+} = \ln A \quad - \quad \left(E_A / R\right)\frac{1}{T} \tag{3-4}$$

As stated earlier and clearly observed in the figures above, the value of *D* is dependent on potential. We selected the *D* at potential of 3.24 V for this activation energy analysis, because it is between the two minima at every temperature, so the electrodes are in comparable states. The slope of this graph (Figure 3-7) is -5700 K and represents the $-E_A / R$ value shown in Equation 3-4. Therefore, we can assign E_A a value of 690 J. This represents the thermal energy barrier associated with the solid-state diffusion of the Li-ion.

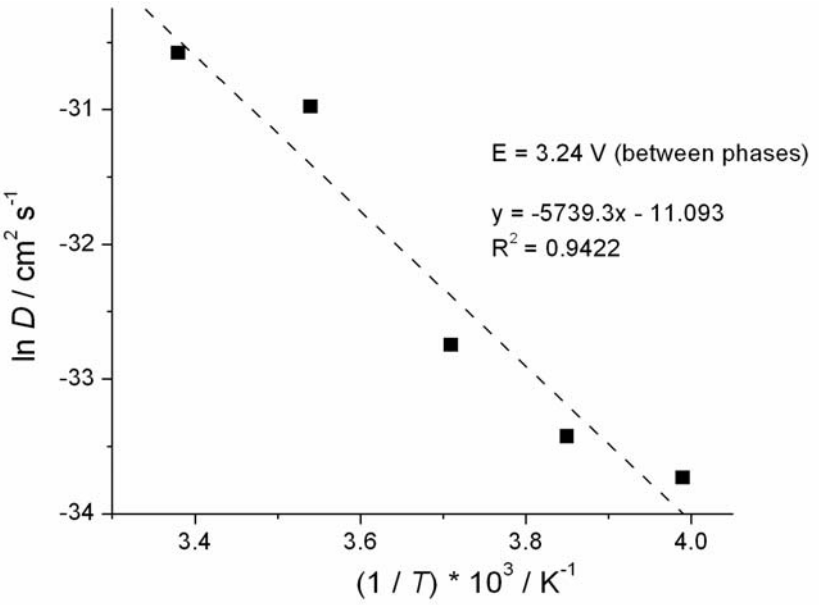

Figure 3-7: Arrhenius plot to solve for activation energy of diffusive process. The slope of this line represents $-E_A/R$. All values of D were taken at E = 3.24 V. At this potential the intercalation is between phases of intercalation (see text).

Cyclic Voltammetry

To further bolster this conclusion, we performed cyclic voltammetry (CV) experiments at all three temperatures with nanowires and microwires. In this experiment, the parameter ΔE_{pk} is the difference in the potentials at which the peak currents occur during the charging and discharging reactions. This parameter provides information concerning the electron-kinetics of the reaction (Equation 2-1). [79]

A typical CV of a 0.8-μm electrode is shown in Figure 3-8A. The data for the peak separation at the low-potential ($\Delta E_{pk}1$) for the nanowire and microwire electrode at the three different temperatures are presented in Figure 3-8B. These data show a correlation between the decrease in temperature and an increase in ΔE_{pk}. Also from these data, the ΔE_{pk} for the nanowire and microwire are very similar at each temperature. Therefore, we can state that the electron-kinetics of this process does decrease with temperature; however, it is not the dominant effect, as the decrease is virtually independent of these electrode geometries.

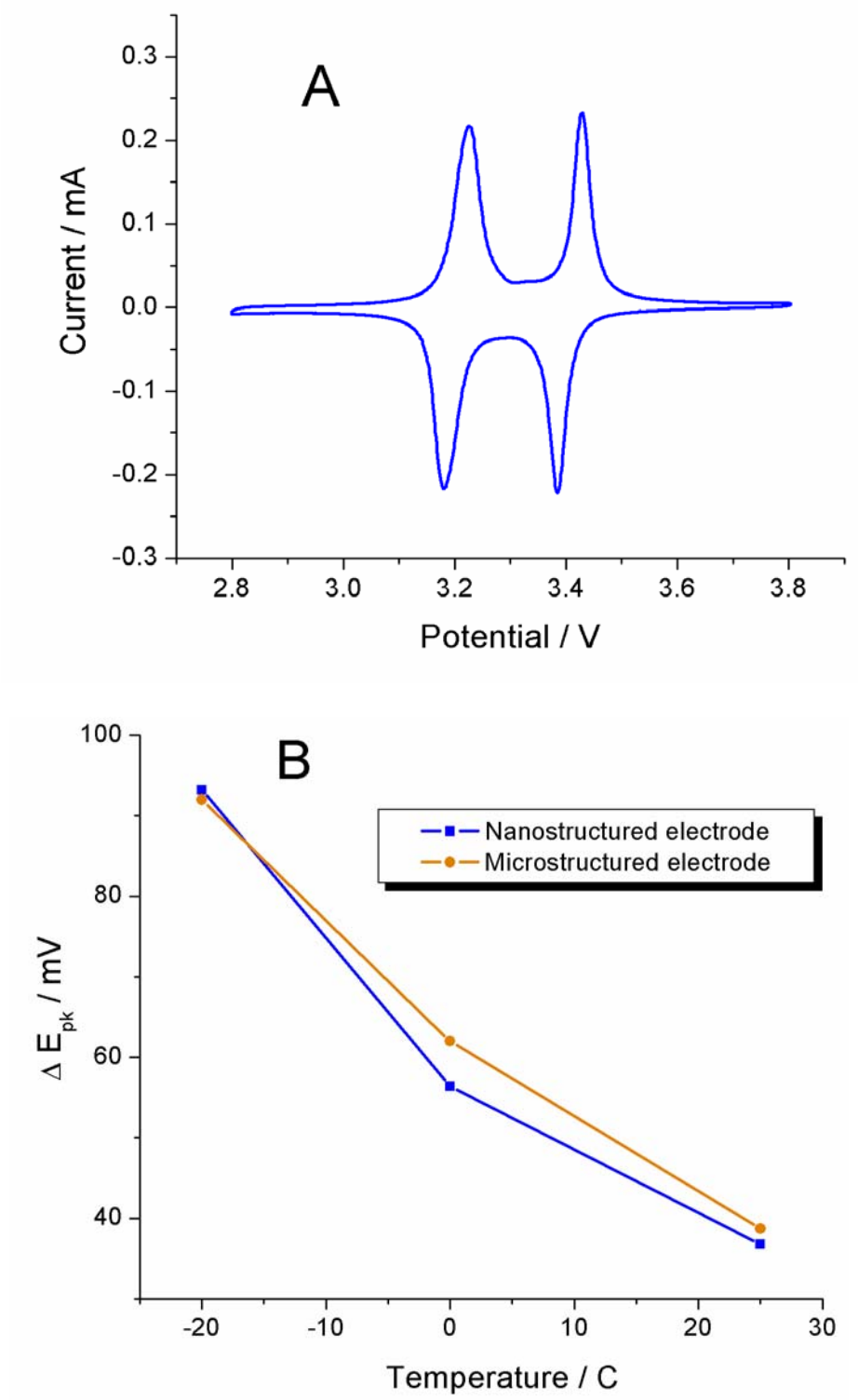

Figure 3-8: Cyclic voltammetric responses. A) Typical cyclic voltammetric response of 0.8-μm electrode at room temperature. Scan rate = 0.1 mV s^{-1}. B) Comparison of ΔE_{pk}1 from cyclic voltammograms of nano- and micro-structured electrodes at various temperatures.

Chapter Summary

In this chapter, we demonstrated the measurement of solid-state diffusion coefficient of Li-ions (D_{Li+}) as a function of potential and temperature. This is accomplished using the potential intermittent titration technique (PITT). PITT acquires data from small potential steps and analyzes data via the Cottrell relationship. Template-synthesis created electrode particles of reproducible and determinable solid-state diffusion distance. This method mitigates a critical data analysis issue identified by other research groups.

D_{Li+} was seen to vary greatly with potential. This potential represents various states of charge (Li-ion intercalation level) of the electrode. Minimas were observed in the potentials close to the voltammetric peaks. These peaks represent the potential at which the majority of charge is actively intercalating causing ion-ion interactions to decrease the diffusitivy of the ions. D_{Li+} decreases over the range of potentials with temperature. We performed these experiments at five different temperatures ranging from room temperature to -20 ^{o}C. This generates the data required to identify the activation energy for the diffusion process by an Arrenheius relationship.

We also report the results of cyclic voltammetric experiments where ΔE_{pk} is seen to be dependent on temperature, but independent of electrode-geometry (solid-state diffusion distance and electrode-particle area per template-area. Since ΔE_{pk} is a kinetic parameter, kinetics is again identified as a secondary contributor to the decrease in rate capabilities discussed in detail in the previous chapter.

In discussions on the research contained in this chapter, the validity of this PITT method has come under debate. The Cottrell equation is a globally accepted and

implemented method to determine the diffusion coefficient of small particles in aqueous systems diffusing in the semi-infinite regime to a planar electrode. The debate arises due to the uniqueness of this solid-state intercalation process. This method is analogous to ion diffusion through a polymer-coated electrode. Research of this type (e.g., Nafion-coated electrodes) gained popularity with the last generation of scientists. Collectively they describe this parameter as an "apparent" diffusion coefficient. Debate ensues on the spurious nature of the relationship of diffusion coefficient to voltammetric peak potentials. Many researchers believe this to be an artifact of the application of the Cottrell method to the battery intercalation mechanism.[80] It would be remiss to not mention this debate in a discussion of this method. At the time of publication of this dissertation, the debate continues.[80,81]

CHAPTER 4
A HIGH-RATE, NANOCOMPOSITE LIFEPO$_4$/CARBON CATHODE

Introduction

Lithium-ion batteries are the power source of choice for portable electronics, a multi-billion dollar market.[1] This outstanding commercial success has spawned great international interest in applying this technology to systems that demand higher power, such as the electric component of hybrid vehicles.[3] This would require new electrode materials that are less expensive, more energetic, and more environmentally friendly than the present ones. Of particular interest is the olivine-structured $LiFePO_4$ cathode developed by Goodenough and co-workers,[82] which offers several appealing features, such as a high, flat voltage profile and relatively high theoretical specific capacity (168 mAh g^{-1}), combined with low cost and low toxicity. However, the current designs of cells based on $LiFePO_4$ technology have not shown the ability to deliver high specific capacity at high discharge rates. For this reason, $LiFePO_4$ is currently not a promising electrode material for high-rate and pulse-power applications.

The discharge reaction for $LiFePO_4$ (Equation 4-1) entails intercalation of Li^+ (from the contacting electrolyte phase) along with an equivalent number of electrons into the electrode material. The rate capabilities of $LiFePO_4$ are limited primarily by its intrinsically poor electronic conductivity and by the low rate of Li^+ transport within the micron-sized particles used to prepare the battery electrode. A number of approaches have been proposed to improve this material's inherent poor electronic conductivity,

including carbon coating,[83] nano-fibril textures,[84] optimized synthesis procedures[85] and foreign metal doping.[86]

$$FePO_4 + x\ Li^+ + x\ e^- \underset{\text{charge}}{\overset{\text{discharge}}{\rightleftharpoons}} Li_xFePO_4 \qquad 4\text{-}1$$

We describe here a new approach for preparing high rate-capability $LiFePO_4$ electrodes. This approach builds on the application of the template synthesis method for preparing nanofiber Li-ion battery electrodes.[17,19,20,22,24] However, the method was modified such that the template-prepared $LiFePO_4$ nanofibers are mixed with carbon particles, and coated by thin carbon films, to yield a nanocomposite $LiFePO_4$/carbon matrix. As we have shown previously,[19,20,22] the nanofiber morphology mitigates the slow Li^+-transport problem, because the distance Li^+ must diffuse within the electrode material is minimized. The carbon matrix obtained with this new template-based method obviates the poor electronic conductivity problem. These nanocomposite $LiFePO_4$/carbon electrodes can deliver a capacity of 150 mAh g^{-1} at a rate of 5 C and maintains a substantial fraction of the theoretical capacity even at rates exceeding 50 C. To our knowledge, performance at this level has never been achieved by other types of $LiFePO_4$.

Electrode Synthesis

The sol-gel method developed by Croce *et al.* was employed for the synthesis of the electrode precursor solution.[87] Accordingly, LiOH monohydrate (Aldrich), ferric nitrate nonahydrate (Fisher), ascorbic acid (Fisher), phosphoric acid, and ammonium hydroxide were used to create the $LiFePO_4$ precursor solution. The template membranes were

commercially available polycarbonate filters (Poretics). Pt foil (2.5 x 1.5 x 0.025 cm, 99.99% purity, Aldrich) was used as the current collector. $LiClO_4$ (Aldrich), ethylene carbonate (Aldrich), diethyl carbonate (Aldrich) were used as received for preparing the electrolyte.

An approximately 1 cm^2 piece of the polycarbonate filter was immersed in a precursor solution of 1 M $LiFePO_4$ in water in 24 hours. This solution was synthesized with ferric nitrate, lithium hydroxide, and phosphoric acid in proportions for a 1:1:1 molar ratio. Ascorbic acid, in equimolar ratio to the total metal (Li^+ plus Fe^{2+}) content, aided the synthesis by forming a complex with the iron, and ammonium hydroxide was used to raise the pH to ~2. The impregnated template was then attached to a Pt current collector and dried in air at 80 ^oC for 10 minutes. A 10 μL drop of precursor solution was placed on top of the dried filter to increase the amount of active material in the sample. It was dried again under the same conditions. This assembly, template intact, was heated in a reducing atmosphere of flowing Ar/H_2 gas (95/5 %). The temperature was slowly taken over the course of 4 hours from 250 ^oC to 650 ^oC and held there for 12 hours. This procedure yields the Fe(II) oxidation state necessary for $LiFePO_4$ and decomposes the template into the carbon necessary for improved conductivity. A schematic of this process is shown in Figure 4-1.

In all of our previous examples of template-synthesized nanofiber electrodes[19,20,22] after synthesis of the nanofibers the template would be totally removed to yield the nanofibers protruding from an underlying current collector surface like the bristles of a brush. For the $LiFePO_4$ nanofibers prepared here we instead pyrolyzed the polycarbonate in a reducing Ar/H_2 environment at a temperature of 650 ^oC. This yields graphitic carbon

particles intimately mixed with the $LiFePO_4$ nanofibers, and thin carbon films that coat these fibers.

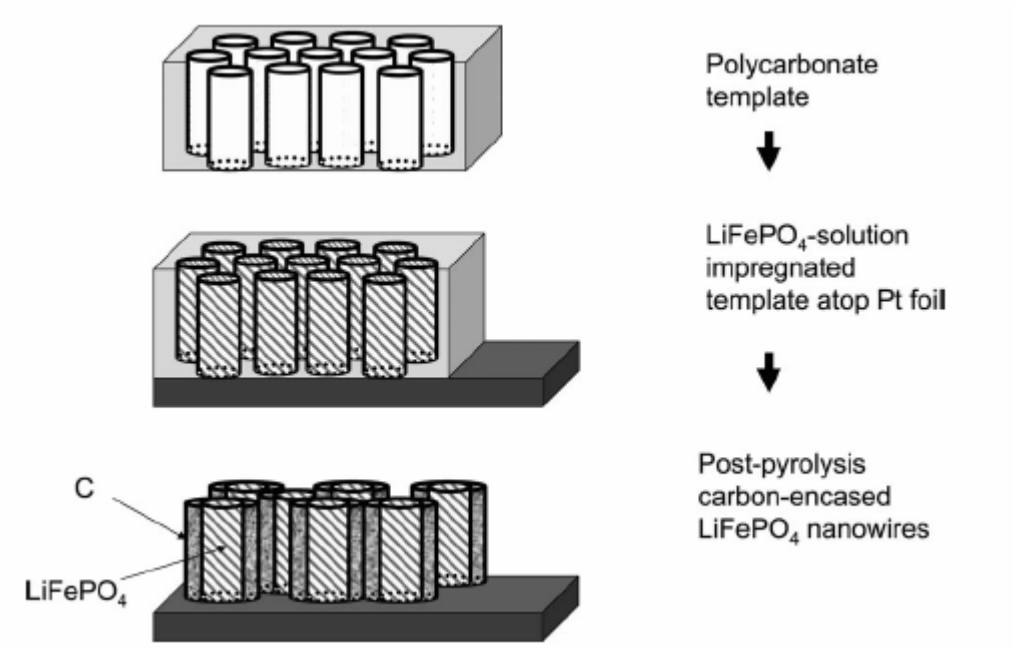

Figure 4-1: Schematic of template-synthesis of $LiFePO_4$/carbon nanocomposite electrode.

Two different templates were used. A template with a slightly larger pore-diameter of 100 nm is used for microscopy. A template of 50 nm pore-diameter is used for electrochemistry. The template being used for each experiment is clearly stated.

Structural Investigations

Scanning Electron Microscopy

A FEG - SEM JEOL JSM 6335F instrument was used to obtain SEM images of the electrode. The nanostructured electrodes on Pt foil were prepared for imaging by attaching them to a SEM stub by conductive copper tape. No conductive metal sputtering was required for the composite electrodes, but a thin Au/Pd sputtering was applied to the bare $LiFePO_4$ wires (Figure 4-2C) prior to imaging.

To obtain detailed images of the morphology of the nanocomposite structure we found it prudent to use a template with nominally 100 nm-diameter pores. The larger $LiFePO_4$ nanofibers obtained from this template are more easily imaged with scanning electron microscopy. This template was also 6 μm thick and had a pore density of $4x10^8$ pores per cm^2. A lower magnification scanning electron microscopic (SEM) image of the resulting $LiFePO_4$/carbon nanocomposite electrode is shown in Figure 4-2A. Because of the relatively low porosity of the template, there is substantial void volume, but in analogy to our prior nanofiber electrodes of this type, the $LiFePO_4$ nanofibers can be seen crossing through this void space.[19,20,22] Higher magnification images (Figure 4-2B) show that there are carbon particles dispersed through this matrix and that the $LiFePO_4$ nanofibers are coated with thin carbon films. To prove that these fibers are coated with carbon films, we prepared fibers in the same template, but instead of then pyrolyzing the template, we simply removed it quantitatively by burning it away in O_2 plasma. Hence, in this sample the fibers are not coated with carbon films.[19,20,22] An image of these fibers is shown in Figure 4-2C.

The fibers from the pyrolyzed membrane (Figures 4-2A and B) have a textured surface morphology and have a larger diameter than the fibers from the plasma-removed membrane (Figure 4-2C). Both the larger diameter and the textured surface are due to the carbon coating surrounding the fibers from the pyrolyzed membrane.

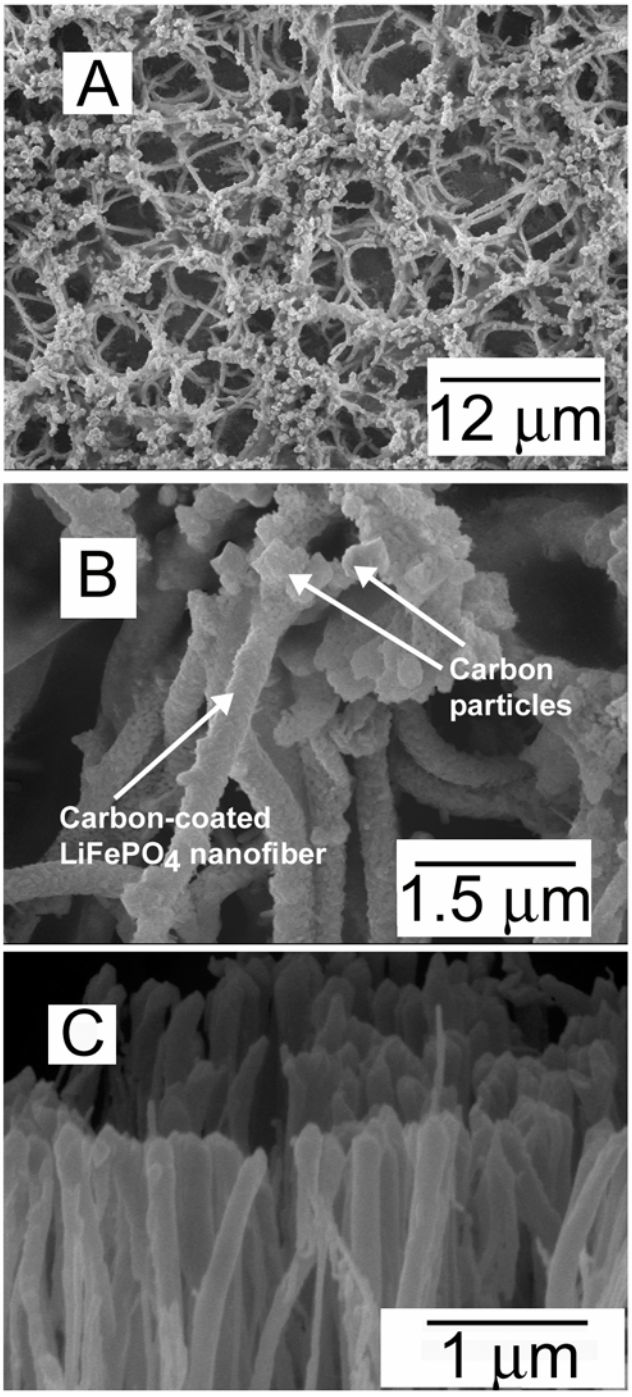

Figure 4-2: Scanning electron micrographs. A) Lower magnification image of the nanocomposite $LiFePO_4$/carbon electrode. B) Higher magnification image of the nanocomposite $LiFePO_4$/carbon electrode. Composite fiber diameter is 350 nm. C) Image of $LiFePO_4$ electrode synthesized by template dissolution method (absent of carbon). $LiFePO_4$ fiber diameter is 170 nm.

X-ray Diffraction Studies (XRD)

The X-ray diffraction data are presented in Figure 4-3. The pattern represents the diffraction of $LiFePO_4$/carbon on quartz. The quartz substrate was used because the Pt foil would give a large signal in this region. This signal would dwarf the relative signal from the $LiFePO_4$/nanocomposite. The lines below correspond to the accepted literature values for $LiFePO_4$, olivine group, triphylite subgroup, published as JCPDS 40-1499. The large amorphous wave ranging from 15 to 30 2Θ is characteristic of disordered carbon. Our group has seen similar diffraction patterns when working with disorderd carbons.

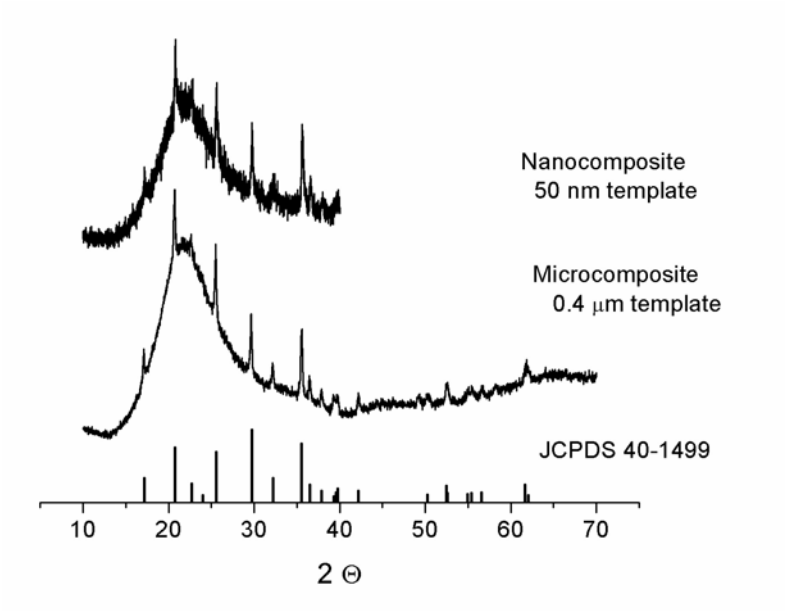

Figure 4-3: XRD pattern from nanocomposite, microcomposite, compared to accepted literature values for $LiFePO_4$. The substrate is quartz. Acquisition time is 10 s.

X-ray Photoelectron Spectroscopy

The XPS studies were performed on a Kratos XSAM 800 spectrometer with Al-Kα exitation (180W). The sample, mounted onto a stainless steel sample stub, was inserted into the sample analyzer chamber by means of a quick insertion probe, and spectral

acquisition commenced after the pressure decreased to $5x10^{-9}$ Torr. High resolution C1s spectra were recorded at a take-off angle of 75° relative to the sample surface. Data analysis was done by using the DS 800 software package. Peak positions were all referenced to 70.9 eV for the $Pt4f_{7/2}$ peak (literature value for metallic platinum used as sample support).

The presence of carbon was also confirmed by XPS analysis (Figure 4-4). The high resolution C1s spectrum may be fitted to three peaks with binding energies of 283.2 ± 0.5, 284.7 ± 0.3 and 286.0 ± 0.3 eV. According to previous work by the Martin laboratory[11], the lowest binding-energy peaks may be assigned to graphitic (283.2 eV) and amorphous (284.7 eV) carbon. The predominance of the 284.7 eV peak indicates that most of the carbon present is amorphous; this is confirmed by the X-ray diffraction data. The peak at the highest binding-energy (286.0 eV) is due to oxygen-containing surface functional groups. Oxygen functional groups are nearly always observed on carbon surfaces that have been exposed to air.[11]

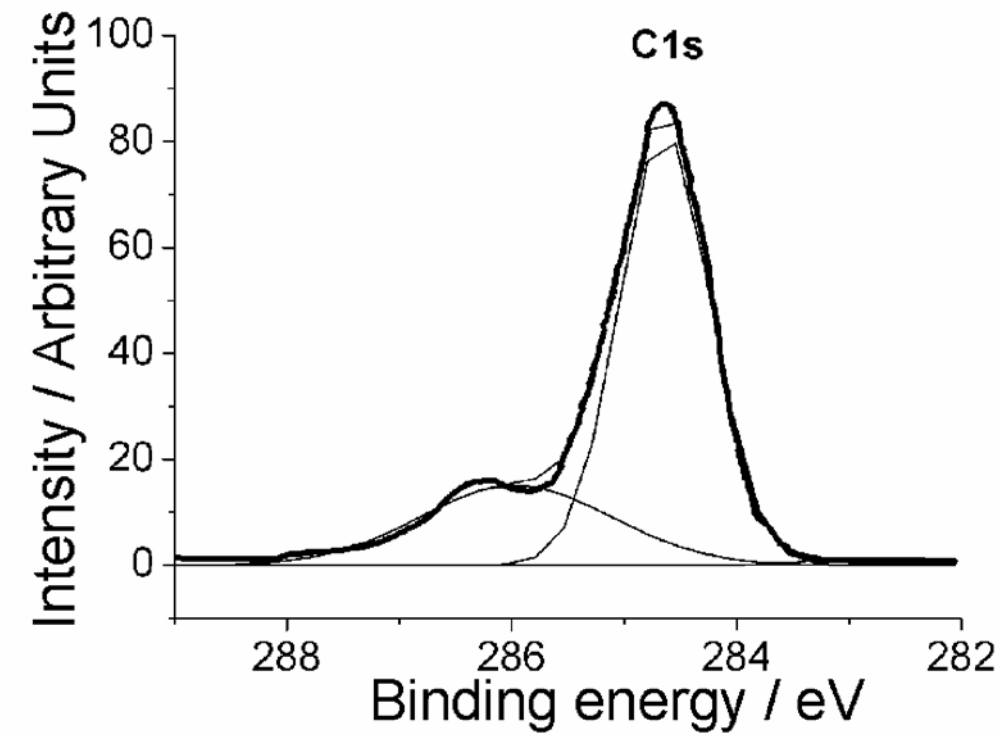

Figure 4-4: X-ray photoelectron spectroscopy data for C1s peak for the carbon in the nanocomposite electrode. Relative peak areas show amphorous form is dominant (~80%), but graphitic carbon is also present (~20%).

Analysis of Carbon Content

We estimated the weight percent of carbon in the composite electrode gravimetrically using an Ultra-Micro-Balance SC2 (Satorius). $LiFePO_4$ nanofibers were synthesized within the pores of the polycarbonate template on a Pt current collector, and the polymer was pyrolzyed as described previously. The mass of this composite, corresponding to the masses of the Pt current collector, the nanofibers and the carbon, was obtained. This composite was then heated in air at 600 ^{o}C for 30 minutes to burn off the carbon, and the mass was measured again. The difference between these two masses is the mass of carbon in the composite. Replicate analyses on four identically prepared samples gave a carbon content of 7 ± 4 % in the nanofiber/carbon composite.

The presence of carbon in this matrix was confirmed by X-ray diffraction analysis, Raman spectroscopy, and X-ray photoelectron spectroscopy (XPS). A Raman spectrum (data not shown) of the nanocomposite $LiFePO_4$/carbon electrode was also taken. The most intense peak (centered around 1000 cm^{-1}) and others at the lowest frequencies correspond to the PO_4 stretching modes of $LiFePO_4$. Bands at 1350 cm^{-1} and 1580 cm^{-1} are assigned to carbon.[88]

Electrochemical Investigations

For the electrochemical studies we wanted a template with small-diameter pores so that correspondingly small-diameter nanofibers of $LiFePO_4$ would be obtained. For this reason we used a template with nominally 50 nm-diameter pores for the electrochemical studies. This template was 6 μm thick and had a pore density of $6x10^8$ pores per cm^2 of surface area. Cyclic voltammetric and constant current charge/discharge experiments were performed in a three-electrode cell using a Solartron 1287 Potentiostat, driven by the CorrWare software package. The electrolyte for these experiments was 1 M $LiClO_4$ in ethylene carbonate:diethyl carbonate (3:7 v/v). The nanostructured $LiFePO_4$ was the working electrode and lithium ribbon was the reference electrode and counter electrode. Potentials are reported versus the Li/Li^+ reference. The experiments were performed in the inert atmosphere of a glovebox filled with argon gas.

This unique $LiFePO_4$/carbon nanocomposite electrode should be ideally suited for high rate applications because the distance that Li^+ must diffuse in the electrode material is limited to the radius of the nanofibers[19,20,22] and because the carbon matrix should provide for good electronic conductivity through the composite. This was confirmed experimentally via electrochemical characterization of these electrodes. Again, the

electrochemical studies were done on electrodes prepared in templates with 50 nm-diameter pores.

Cyclic Voltammetry

Cyclic voltammograms (CVs) for the nanocomposite electrode show reversible waves centered at 3.5 V associated with the reduction and re-oxidation of the $LiFePO_4$ (Figure 4-5A).[87,89] The difference in peak potentials (ΔE_{pk}) for this nanostructured electrode is 60 mV (Figure 4-5A). This may be contrast to CVs for conventional, non-nanostructured, $LiFePO_4$ electrodes, which at comparable scan rates and in comparable electrolyte solutions show $\Delta E_p > 200$ mV. [87,89] This clearly shows that our nanostructured $LiFePO_4$ electrodes lack a resistive component that is present in the conventional electrodes. *This verifies the major premise of this work – that the conductive carbon matrix overcomes the inherently poor electronic conductivity of $LiFePO_4$.*

Rate Capabilities

The constant-current discharge curve (lithium insertion, Equation 4-1) for the nanocomposite electrode shows the flat voltage plateau centered at 3.5 V, characteristic of $LiFePO_4$ (Figure 4-6A)[83,87,89]. At the lowest discharge rate used (3 C), the specific capacity for the composite is 165 mAh g^{-1}, essentially identical to the maximum theoretical capacity, 168 mAh g^{-1}. While capacity falls off with increasing discharge rate (Figure 4-6B) the electrode retains 36% of its theoretical capacity at discharge rates as high as 65 C. There are no other examples in the literature of $LiFePO_4$ being discharged at such enormous rates.

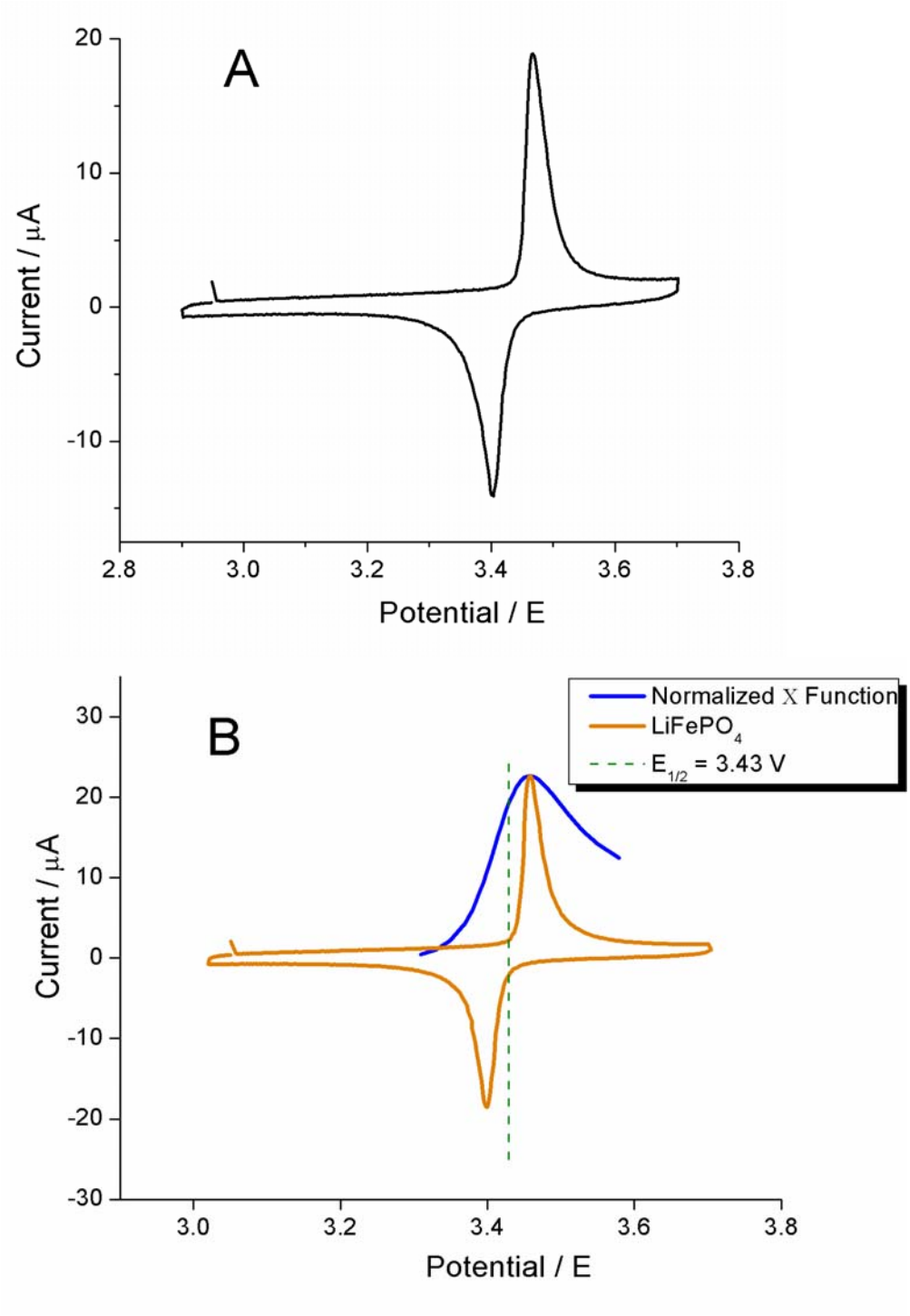

Figure 4-5: Cyclic voltammograms. A) Cyclic voltammogram for the nanocomposite $LiFePO_4$/carbon electrode prepared using a template with 50 nm-diameter pores. Scan rate = 0.1 mV s^{-1}. B) Comparison of voltammetric response to theoretical response exhibiting diffusional tailing. The diffusional wave was generated from the normalized X function.[79]

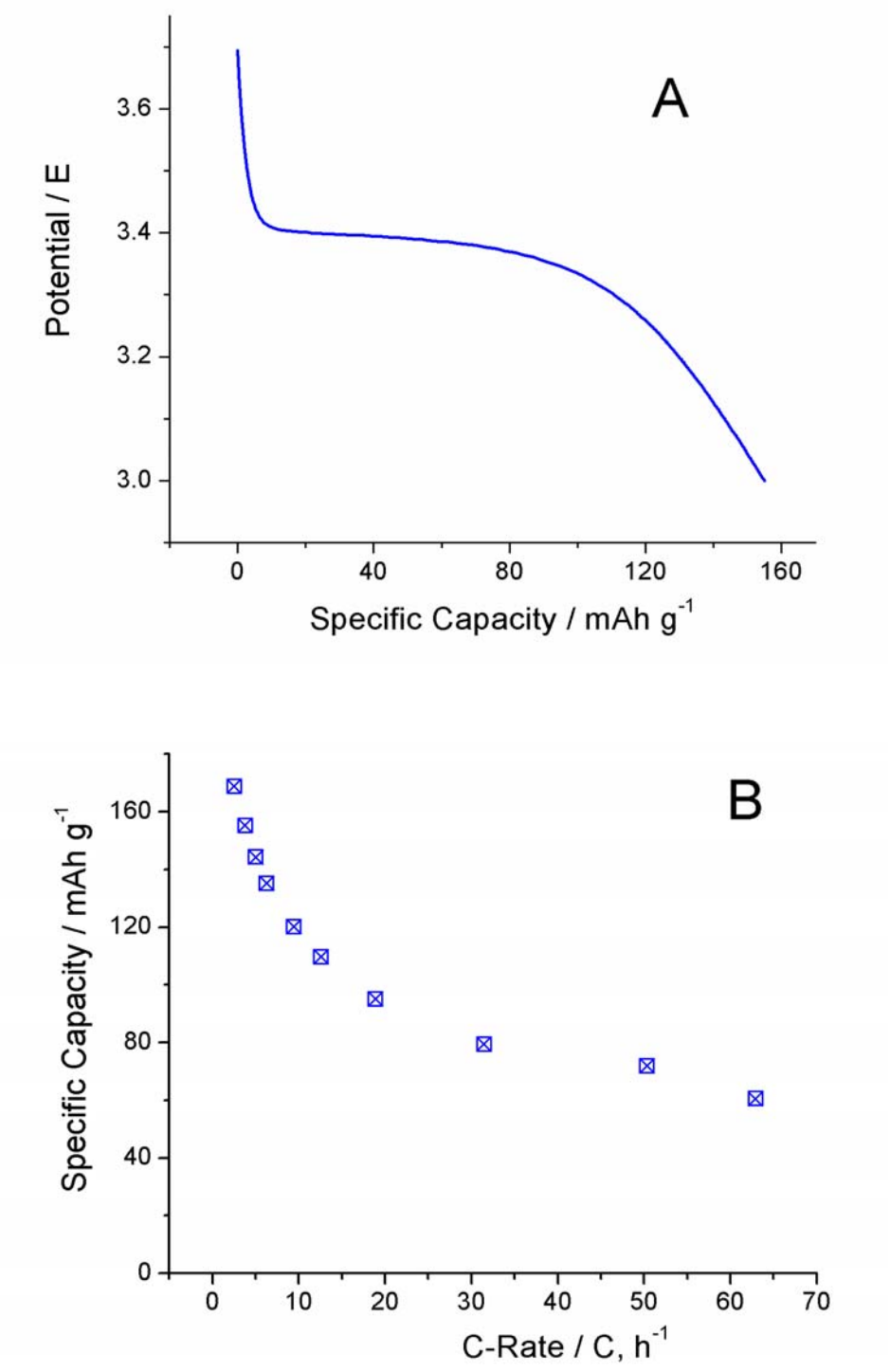

Figure 4-6: Constant current experiments. A) Constant-current (3 C) discharge of $LiFePO_4$/carbon nanocomposite electrode. B) Specific capacity versus C-rate for the nanocomposite $LiFePO_4$/carbon electrode prepared using a template with 50 nm-diameter pores.

Chapter Summary

We have described here a new type of template-prepared nanostructured $LiFePO_4$ electrode. LiFePO4 was developed as an alternative cathode material to LiCoO2, the industry standard. LiFePO4 is an energetic material with advantages of both cost and safety. However, this material is inherently electronically insulating. This material is also susceptible to the concentration polarization with larger micron-diameter particles.

Our nanocomposite electrode consists of nanofibers of the $LiFePO_4$ electrode material mixed with an electronically conductive carbon matrix. It is created by a modified template-synthesis procedure, where the polymeric template is pyrolzed. This carbon matrix coats the $LiFePO_4$ nanostructures and provides an improved electron pathway. Therefore, both rate-limiting effects of electron-transfer and ion-transport are delayed. This unique nanocomposite morphology allows these electrodes to deliver high capacity, even when discharged at extreme rates necessary for many pulse-power applications. This nanocomposite is a specific example of nanotechnology overcoming the limits of conventional technology. We are currently working toward developing a commercially viable route for preparing such nanocomposite electrodes.

CHAPTER 5
MAGNESIUM-ION INTERCALATION INTO TEMPLATE-SYNTHESIZED NANOSCALE ELECTRODES IN THE ABSENCE OF CARBON

Introduction

Li-ion batteries have powered the mobile electronic industry. Though these energy-storage devices have enjoyed tremendous commercial success, they remain the subject of international research. This is primarily due to the consumer driven demands of an increasingly portable world, specifically, the desire for increased pulse-power and decreased size. The Li-ion intercalation reaction (mechanism by which the host-electrodes store charge) is shown previously. Lithium-ions were chosen because of their low reduction potential (-3.05 vs. NHE) and their small dimensions facilitate both the intercalation process and the solid-state diffusion process.

We have had great success synthesizing and characterizing Li-intercalation into template-synthesized nanostructured electrodes. *Template-synthesis* is a general nanofabrication method pioneered in the Martin group. Employing this method, we have shown that with no addition of inactive ancillary components (carbon or polymeric binder), template-synthesized nanostructured electrodes are capable of reversibly storing and delivering a dramatically greater portion of the electrode's theoretical capacity (mAh g^{-1}) than similarly constructed microstructured electrodes. These nanostructured electrodes are capable of this, due to their small solid-state diffusion distance and large surface-area per gram. These traits serve to delay the effects of concentration polarization and sluggish electron-kinetics, respectively.

Dramatically fewer researchers have explored the field of polyvalent-ion intercalation.[90-92] The charge-storage mechanism for this device is similar to that of the Li-ion battery; however, whereas the Li-ion intercalation reaction has 1 electron equivalent per Li-ion each Mg-ion has 2 electrons. Simply stated, by doubling the quantity of electrons available, one can store an amount of specific energy that is not stoichiometrically possible via the Li-ion intercalation process. However, the diffusivity of these ions is further hindered by its polyvalent nature and larger dimensions. Therefore, a structure that has proven to be able to delay the limiting effects of such phenomena may be able to successfully intercalate such ions. Template-synthesized V_2O_5 nanostructured electrodes have, in fact, this ability.[25] Here we detail these studies and demonstrate the ability to reversibly (de)intercalate Mg^{2+} into/out of the host (template-synthesized V_2O_5 nanostructures) by Equation 5-1.

$$x\,Mg^{2+} + 2x\,e^- + V_2O_5 \underset{\text{charge}}{\overset{\text{discharge}}{\rightleftharpoons}} Mg_xV_2O_5 \qquad 5\text{-}1$$

Other advantages of Mg-based technology are that concerns still exist with the safety and stability of lithiated carbon as well as the expense of the constituents of the battery.

Electrode Synthesis

As stated, these electrodes were created by the template-synthesis method. This process is similar to those described previously; however, the notable exception is that the current collector is Indium Tin-Oxide (ITO)-glass. Another research group has demonstrated the usefulness of the substitution.[91] This is a piece of glass that has a thin layer of conductive Indium Tin-Oxide deposited onto it. Therefore, one of the surfaces of

the glass is electronically conductive. Electrodes were synthesized on both ITO-glass substrates as well as platinum.

A commercially available (Poretics) polycarbonate filter was used as the template. This membrane has nominally-cylindrical track-etched pores (~ 50 nm in diameter) that run its entire length of 6 microns. There are 6 x 10^8 of these pores per cm^2 of template area. In an inert environment (Ar-filled gloebox) a 3 cm^2 section of template is placed atop a section of electrically conducting ITO-glass. A 1 μL volume of TIVO (triisopropoxide vanadium) was placed atop the template membrane. The precursor's low viscosity allows it to flood the pores of the filter. This assembly is then moved to a low water environment (antechamber of glovebox). In the presence of the atmospheric water, the TIVO precursor hydrolyzes. At this point, the assembly is heat to 80 ^oC for 2 h in air to ensure complete hydrolysis and conversion to the gel-phase. Any top surface layer is then removed with a damp cotton swab.

The assembly is then placed into oxygen plasma (20 W; 10 Pa; 2 hours) to etch away the organic template. The resulting nanowires extend from the ITO-glass (or platinum) communal current collector and mirror the geometry (length, diameter, and number density) of the pores of the membrane. The electrode is then heated to 400 ^oC in flowing O_2 for 10 hours to form crystalline V_2O_5 nanowires.

XRD Studies

X-ray diffraction is a convenient experiment to identify the crystalline phase of the electrode material. Like SEM, it is non-destructive. In a powder x-ray diffraction (XRD) experiment, a quantity of powder-form sample is exposed to X-rays at a sweeping angle. These incident X-rays deflect off the sample onto a detector at a pattern relative to the

crystalline lattice structure of the powder. The arrangement of the atoms in a relationship to each other can be determined from the pattern and Bragg's law. It is displayed in terms of Miller indices (*hkl*), coordinates of parallel planes in a unit cell.

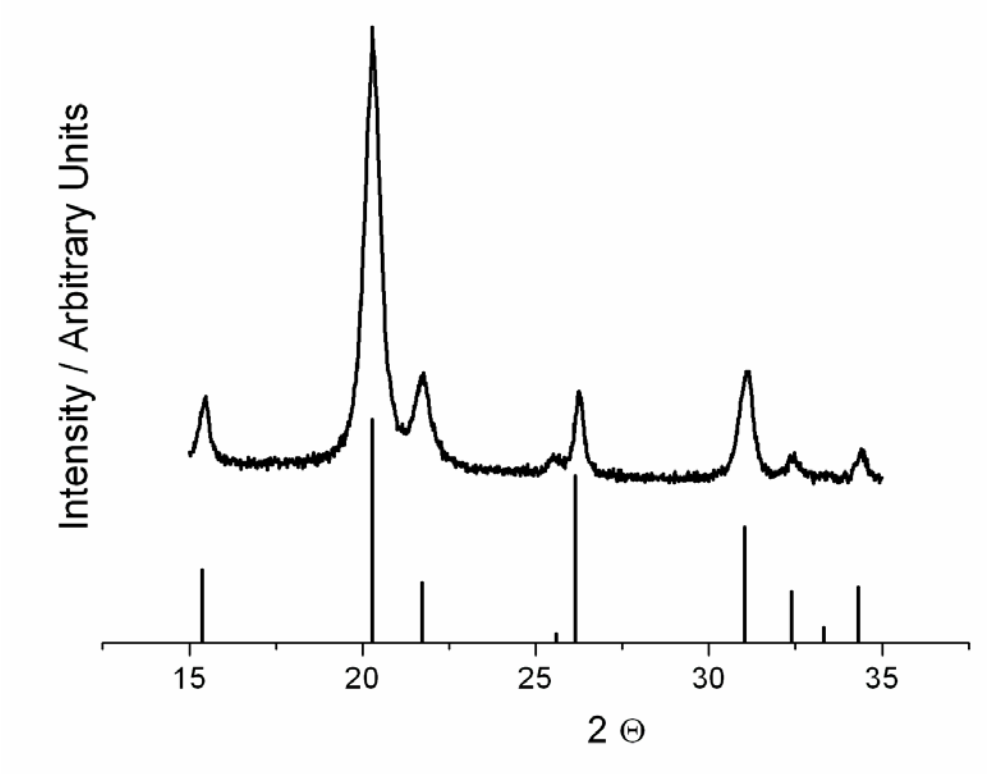

Figure 5-1: X-ray diffraction experiment. The sample is nanostructured V_2O_5 on Pt. Acquisition time =10 s. The discrete lines represent the accepted values for orthorhombic phase V_2O_5 (JCPDS 41-1426).

This continuous line is the response of a nanostructured V_2O_5 electrode. The discrete lines represent the internationally accepted pattern for orthorhombic V_2O_5 as per JCPDS card 41-1426, which replaced card 9-387. These two patterns are similar, with only the relative intensity of the peak at $2\Theta = 26.1$ (representing the (*110*) plane) being smaller than the standard. The 2Θ range was limited to 15 to 35, so as to not record the intense Pt peak at 39.8, which would dwarf the relative intensities of the V_2O_5 sample. An acquisition time of 10 s per step was used to increase resolution of the pattern.

The XRD pattern of a powder can also be used to estimate the crystallite size of the sample. This relationship is described in the following Equation 5-2 first described by Scherrer[93] and refined by Biscoe and Warren.[94]

$$t = \frac{0.89 * \lambda}{B * \cos\Theta_B} \qquad 5\text{-}2$$

The term t is the size of the crystallite. The term λ is the wavelength of the incident X-rays (Copper α = 1.54 Angstroms). The Θ_B is the Bragg's angle being analyzed. The term B represents the full-width half-max of the crystallographic peak in radians.

Here the data from the most intense 001 plane is compared. Using this equation, the nanostructured electrode has an average crystallite size of 20.1 nm; whereas, the microstructured electrode (data not shown) has an average crystallite size of 32.3 nm. So, qualitatively the particles of the micronstructured electrode are lager on a crystallographic plane than the nanostructure electrode. This also indicates that each wire may consist of a number of smaller crystallites.

Electrochemical Investigations

The electrode was characterized in a three-electrode half-cell configuration. The cell differs significantly from the ones discussed earlier. The V_2O_5 nanostructures on ITO-glass (or platinum) were the working electrode. Lithium must be excluded from the cell to ensure that all charge-storage is due to Mg^{2+}. Polished Mg ribbons were used as the reference and counter electrodes. The electrolyte is 1 M $Mg(ClO_4)_2$ in dry acetonitrile. This system been used by other researchers in this field.[91] This cell was assembled and characterized in the Ar-filled glovebox.

Ferrocene Pseduo-Reference

As stated previously, Li-ions must be excluded from the electrochemical system to ensure that the response is strictly from the Mg-ion intercalation. Therefore, the reference electrode in this experiment is Mg/Mg^{2+}. This reference reaction is not as common, especially in this particular electrolyte system. We use the well established ferrocence / ferrocenium redox couple as a pseduo-reference.

The first system has lithium ribbon as the counter and the reference electrode. Platinum metal is used as the working electrode. The electrolyte is 1 M $LiClO_4$ in EC:DEC (3:7). Ferrocence is also dissolved into the solution. A cyclic voltammogram is taken using this system. Figure 5-2 shows the potential of the reversible ferrocence redox reaction to be 3.25V vs. Li/Li^+.

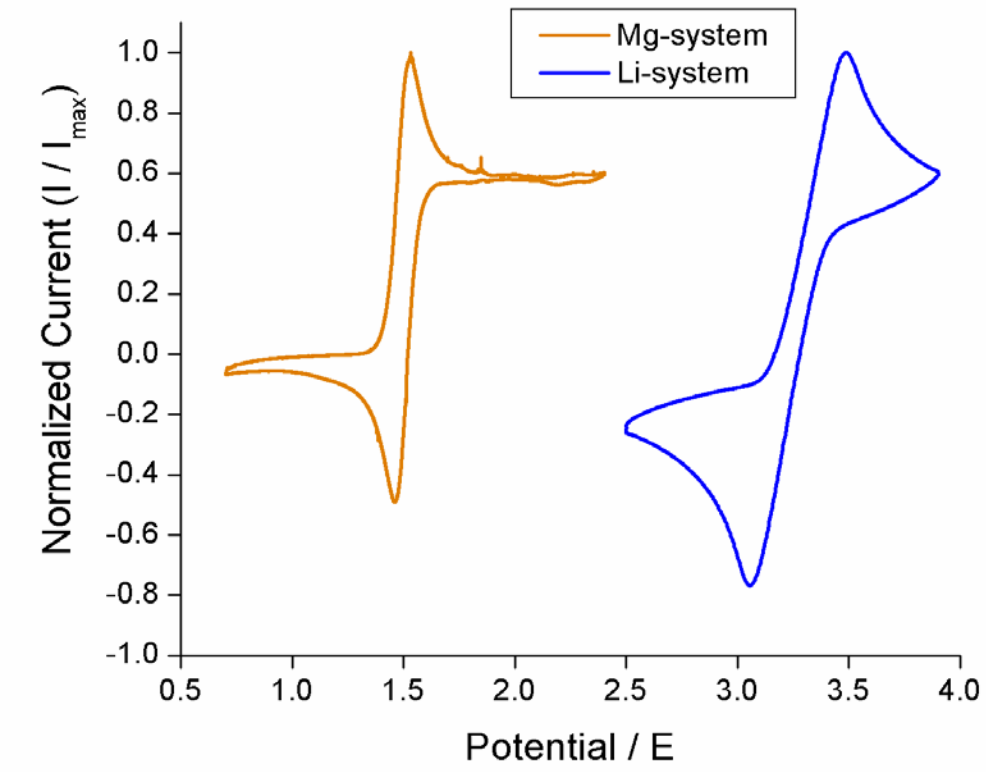

Figure 5-2: Cyclic voltammogram of ferrocence in Li-based and Mg-based systems (see text). Scan rate = 50 mV s^{-1}.

The comparative system has magnesium ribbon as the counter and the reference electrode. Platinum metal is again used as the working electrode. The electrolyte is 1 M $Mg(ClO_4)_2$ in dry acetonitrile. Ferrocence is also dissolved into the solution. A cyclic voltammogram is taken using this system. The potential of the reversible ferrocence redox reaction is 1.5 V vs. Mg/Mg^{2+}. The same redox reaction occurs in the Mg-based system at a potential that is 1.75 V negative of the potential at which is occurs in the Li-based system. Therefore, the Mg/Mg^{2+} reference is 1.75 V negative of the Li/Li^+ reference (*i.e.*, 0 V versus Mg/Mg^{2+} is +1.75 V versus. Li/Li^+).

Cyclic Voltammetry

ITO-glass current collector

The CV experiment (Figure 5-3) was performed at the scan rate of 0.1 mV s^{-1}. The electrolyte is the Mg-based system described above. There is a peak, indicating a charge-storage process, during both intercalation and deintercalation scans. The most notable characteristic is the large peak separation associated with these peaks. Interestingly, this low-potential peak does represent the deintercalation of Mg^{2+}, because if the experiment is terminated at 1.5 Volts, then the high-potential peak is not seen again in the next scan (i.e., it becomes an irreversible reaction). To date, we are uncertain as to the source of this phenomenon. It appears too large to be iR drop, an effect of arising from the uncompensated resistance between the reference and working electrodes. For such small currents, the resistance would need to be on the order of 100 kΩ. The conductivity of the solution was measured to be 25 S cm^{-1}. This translates to a R_{uncomp} of > 25 Ω in this system. (The distance between working and reference electrode would need to be 4 m for

this to be the source of the peak separation.) Also note that the R_{uncomp} was estimated by Electrochemical Impedance Spectroscopy to be approximately 10 Ω.

The effect is most probably related to either the vulnerability of the ITO layer during the thermal processing step or a resistive passivation layer. The poor thermal stability of ITO is undoubtedly an effect, because the mass of the ITO-glass post-heat treatment is significantly lower mass prior to the heat treatment. Other groups[91] were able to use ITO-glass as a substrate, because they apply the active electrode material post-processing (*i.e.*, it is not necessary for the current collector to be compatible with the fabrication process of the material synthesis, as it is in our case).

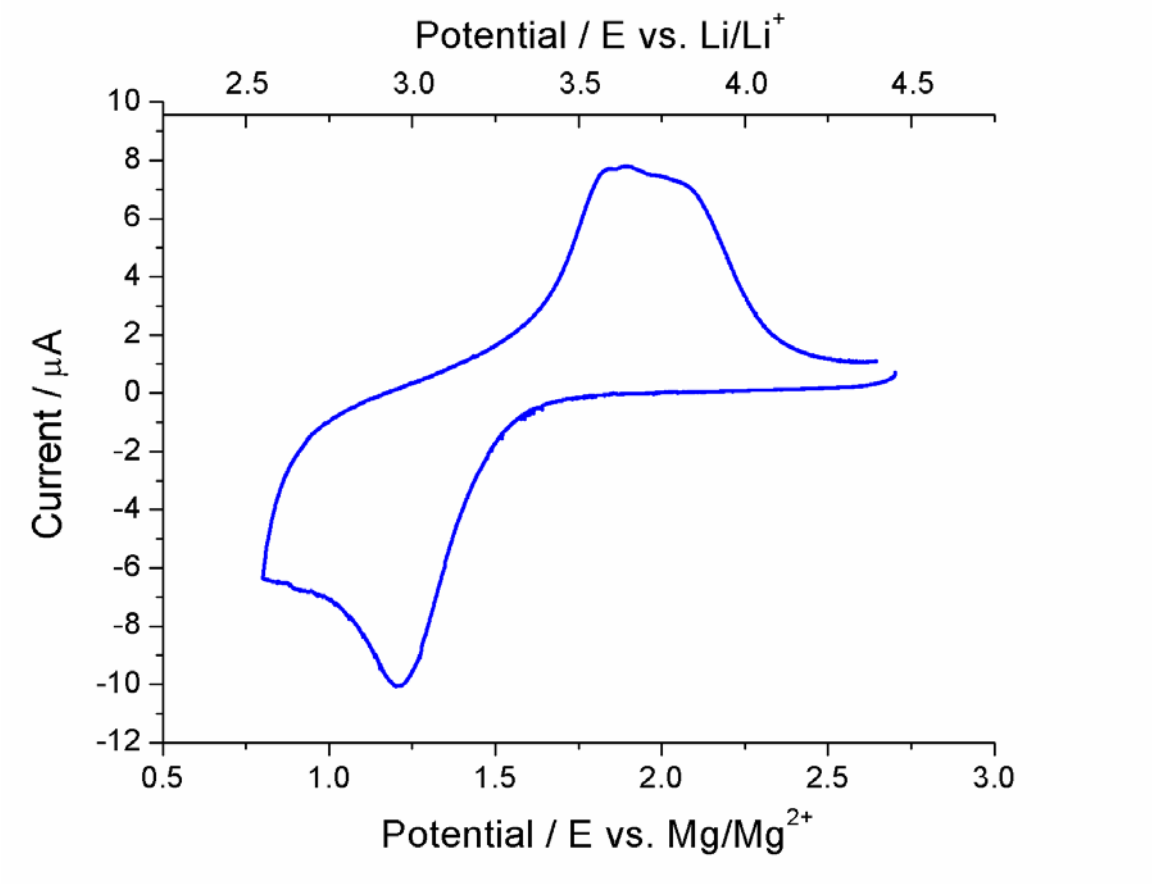

Figure 5-3: Cyclic voltammogram of ITO-glass/$Mg_xV_2O_5$ nanowire electrode. Scan rate = 0.1 mV s^{-1}. X2-axis is calculated from data shown in Figure 5-1.

Pt foil current collector

For comparison, we also used our standard Pt foil as a substrate. The results of this experiment are shown in Figure 5-4. The current response during the voltammetric sweep is much greater for approximately the same sample mass. This represents the inertness during the synthetic process seen with Pt as opposed to ITO-glass. However, the large peak separation still exists. This suggests that this peak-separation is not dominated by interactions between the current collector and the electrolyte system. It is possible that a Mg-insulating passivation layer forms on the surface of the electrode. Other groups have also proposed this theory[90]. Our electrodes created by template-synthesis may, in fact, be particularly susceptible to such limiting factors, due to the high surface area. This theory would explain the resistive nature of the current-response.

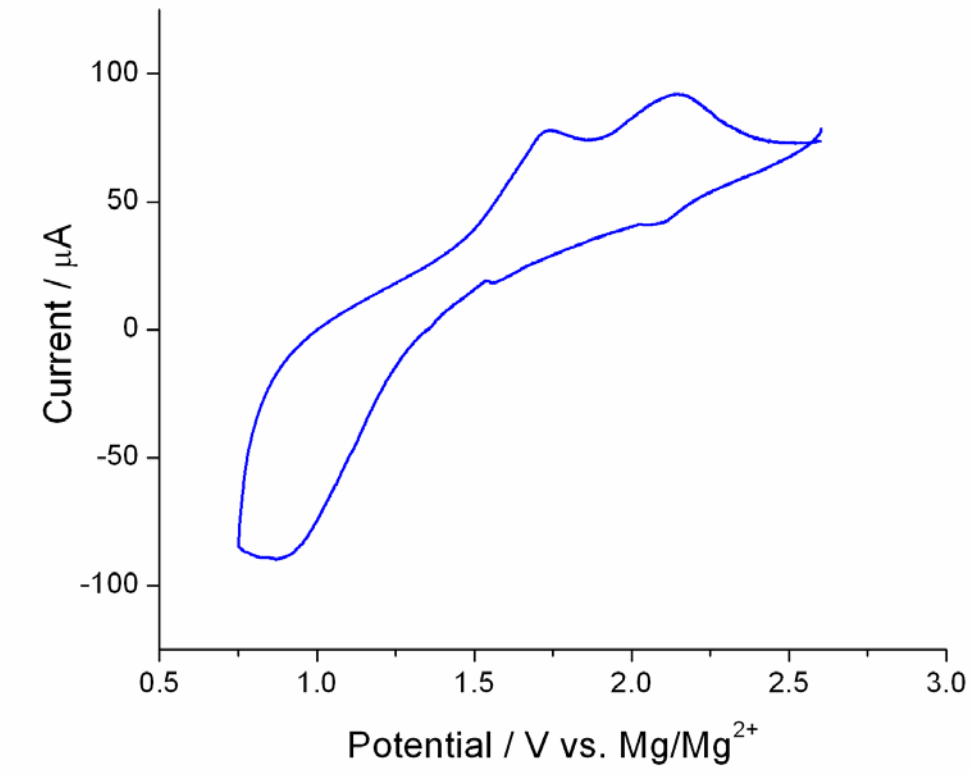

Figure 5-4: Cyclic voltammogram of Pt/$Mg_xV_2O_5$ nanowire electrode. Scan rate = 0.1 mV s^{-1}. The potential reference is Mg/Mg^{2+}.

Rate Capability

We also characterized this ITO-glass/V_2O_5 electrode using the galvanostatic method to charge and discharge the electrode. The potential limits used were 2.7 and 0.8 versus the Mg/Mg^{2+} reference.

While the ITO-glass/V_2O_5 electrode has advantages during the electrochemical characterization, this system has a distinct problem in template-synthesis. As stated earlier, the standard method of Li-ion battery construction processes the active material of the electrode separately from the current collector. However, in the template-based method the electrode material is processed from "cradle to grave" with the current collector. The chemical and thermal inertness of platinum makes it a good choice. During the final heating stage of the synthesis, the ITO-layer degrades. This is easily seen by noting that the mass of an ITO-glass is significantly less after a similar heating process than before. Therefore, in Figure 5-5 can analyze the rate capability data using the electroactive mass, as we did with the $LiFePO_4$.

We have taken data comparing rate-capabilities of nanostructured (50-nm template) microstructured (0.8 micron) and film electrodes. These data are presented in Figure 5-6. Each of these was analyzed for mass post-electrochemical characterization by dissolving the V_2O_5 electrode material in 2 M H_2SO_4 and analyzing for the V-ion by ICP-AES at 310 nm. Again, we observe an advantage in rate capabilities of the nanostructured electrode compared to the controls. However, there is markedly less specific capacity, when using the mass determined by ICP-AES.

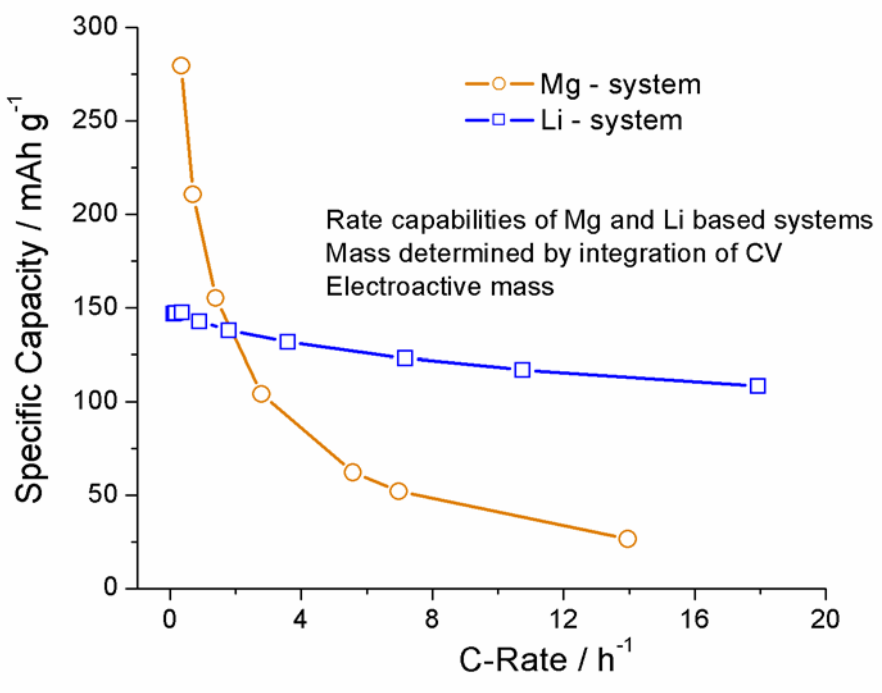

Figure 5-5: Comparison of rate capabilities of $Li_xV_2O_5$ and $Mg_xV_2O_5$. The mass for these calculations is the electroactive mass determined by integration of the respective cyclic voltammogram.

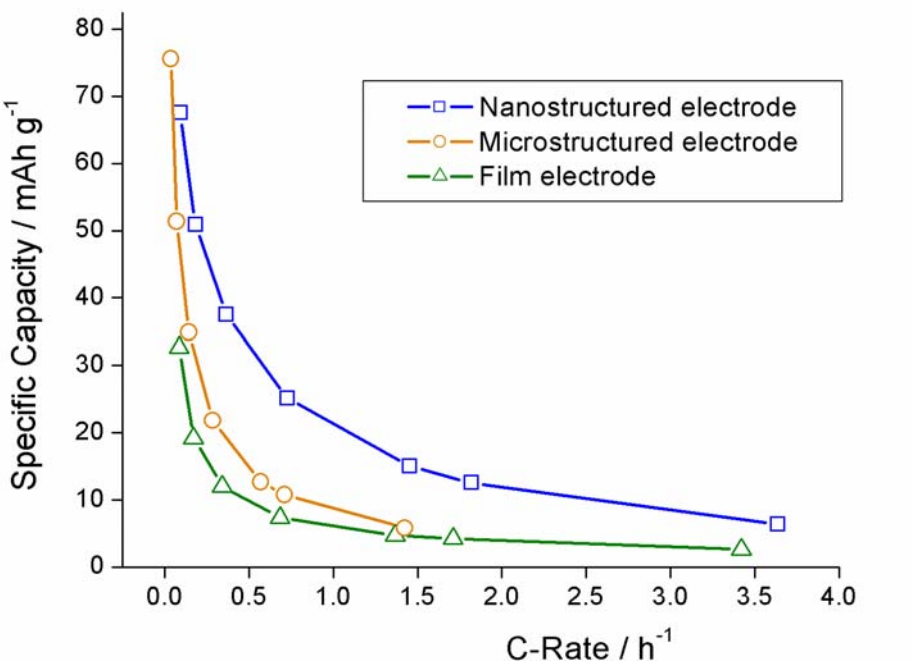

Figure 5-6: Comparison of rate capabilities of nano- and micro-structured $Mg_xV_2O_5$. The mass for these calculations is the mass determined by ICP-AES analysis of the V-ion from post-electrochemical dissolution.

Investigations of a Possible Mg-Sn Alloy

There is evidence in the literature that Mg and Sn form an alloy.[95] Previously, we and others have demonstrated the superior charge-storage properties associated with a reversible Sn-Li alloying process.[20] We propose that if the Mg-Sn could form a reversible alloy by electrochemistry, then it may be an alternative anode for a Mg-based system. This technology is based on two interesting reactions. First, a sol-gel route is used to synthesize SnO_2 nanowires. These wires are electrochemically converted to Sn, which reversibly alloys with Li, thus storing charge. Figure 5-7 is the typical electrochemical response in the Li-system, which serves as a control for the synthetic process. The first wave is the electrochemical conversion to Sn; whereas, the reversible waves are attributed to the Sn-Li alloying process.

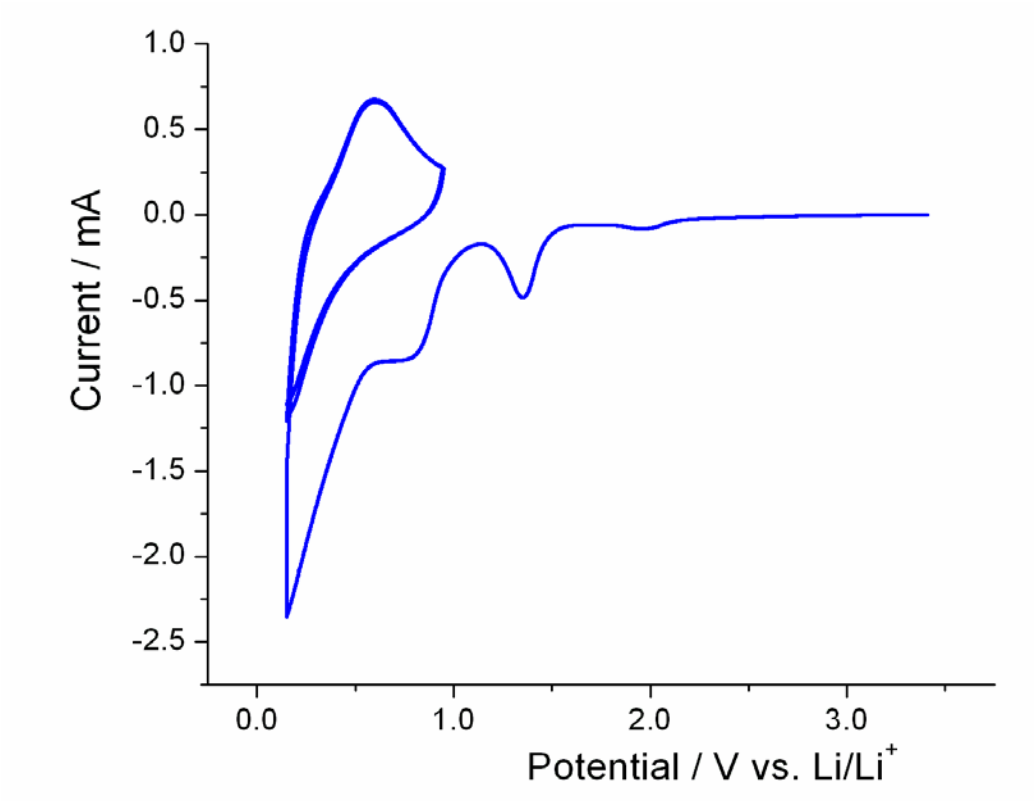

Figure 5-7: Cyclic voltammogram for Sn-based electrode in Li-system prepared using a template with 50 nm-diameter pores. Scan rate = 0.1 mV s^{-1}.

However, when the SnO_2 electrode is inserted into the Mg-based system, there is only a single reduction wave. We can attribute this to the conversion of SnO_2 to Sn, analogous to what was seen in the Li-system. As the potential is swept more negative, we fail to see the reversible waves of charge-storage. Therefore, we can conclude that where SnO_2 may successfully become Sn, Sn has trouble forming Mg_xSn by this electrochemical means. The apparent inability of this reaction eliminates it from consideration as an alternative anode system.

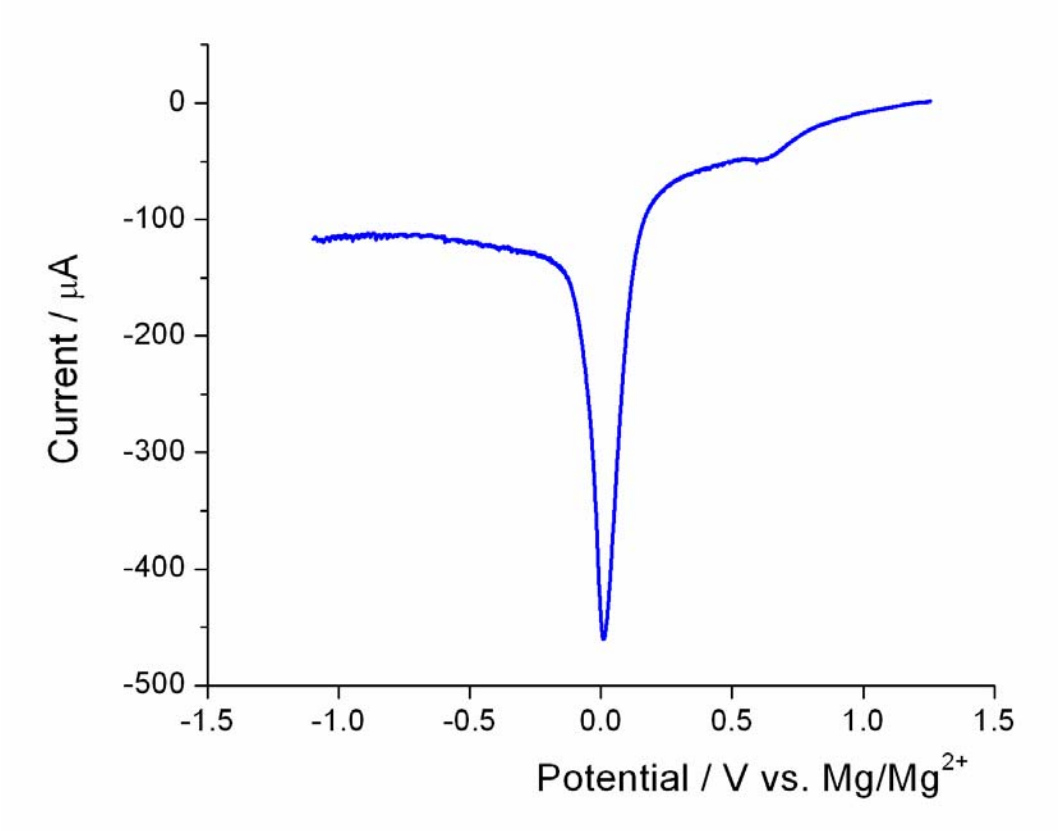

Figure 5-8: Cyclic voltammogram for Sn-based electrode in Mg-system prepared using a template with 50 nm-diameter pores. Scan rate = 0.1 mV s^{-1}.

Chapter Summary

We were able to form several conclusions from this preliminary series of experiments. Our primary goal of demonstrating reversible intercalation of Mg-ions into V_2O_5 nanowires without carbon or binder was achieved. We also showed that at a low discharge rate, more charge can be stored per gram in the Mg-based system than the Li-based system. This is from the rate capability experiment ITO-glass, using the electroactive mass obtained via voltammetric integration. Another observation is that at large discharge rates, the charge-per-gram stored by the Li-based system comes to exceed that stored by the Mg-based system. This suggests a decrease in diffusivity of the Mg-ion compared to the Li-ion. When diffusion profiles are given less time to propagate, this is more of a concern.

ITO-glass was determined to be a satisfactory current collector because of its available potential window, but it is incompatible with this synthetic process. Data suggest that this results in only islands of material that is electronically addressable. Also, a comparison between the ITO-glass and the Pt systems reveals some background specific to the platinum. This may be a result of excess capacitance associated with the exposed back of the metal. This would not be a factor with the ITO-glass, because the exposed back of that substrate is not conductive. It is notable though, that this effect appears to be unique to this system, as is not dominant in previous studies.

CHAPTER 6
CONCLUSIONS AND FUTURE DIRECTIONS

Conclusions

Li-ion batteries are the current power source for portable electronics. We are part of an intense, global effort to improve upon this existing design, in order to expand the applications of these batteries. We are specifically investigating the effects of nanomaterials on the design of Li-ion batteries. This dissertation details our use of nanostructured electrodes created by template-synthesis as tools in fundamental studies of these batteries.

Chapter 1 is an introduction to the field of Li-ion battery research and nanofabrication method of template-synthesis. This chapter lays a framework for the dissertation and explains the significance of our research.

In Chapter 2, we demonstrate the advantages of template-synthesis as it pertains to Li-ion batteries. The electrode precursor is deposited into the pores of a commercially available polycarbonate template membrane. The template serves to restrict particle growth as the precursor is hydrolysized to V_2O_5, a known Li-battery cathode material. These V_2O_5 wires extend from the surface of a current collector like bristles of a brush. The geometry of the pores of the template is imparted onto these wires – a nanoporous template yields nanostructured wires and microporous template yields microstructured wires. We demonstrated the ability to create structures of reproducible diameters by this template-synthesis method.

Three of these electrodes with different wire geometries were electrochemically charged and discharged by a constant-current. By creating particles of the shortest solid-state diffusion distance, we were able to demonstrate superior low-temperature rate-capabilities when compared to microstructured control electrodes. However, these superior discharge characteristics would be achieved with any competitive nanofabrication method. The ability of template-synthesis to create structures of reproducible solid-state diffusion distance and surface-area is what differentiates it from other nanofabrication methods. Analysis of these data identifies the decrease in solid-state diffusion coefficient of the Li-ion associated with the decrease in temperature to be the rate-limiting factor in Li-ion batteries. The conclusions presented in this chapter are a benchmark study in the field of low-temperature Li-ion battery research.

Chapter 3 is derivative of the previous study, as we demonstrate the measurement of solid-state diffusion coefficient of Li-ions (D_{Li+}) as a function of potential and temperature. This is accomplished using the potential intermittent titration technique (PITT). D_{Li+} decreases over the range of potentials with temperature. Using this value recorded at several temperatures, we are able to calculate activation energy for the diffusive process via the Arrehenius relationship. We also report the results of cyclic voltammetric experiments where ΔE_{pk} is seen to be dependent on temperature, but independent of electrode-geometry (solid-state diffusion distance and electrode-particle area per template-area. The key to this analysis is the ability of template-synthesis to create structures of determinable diameter, length and number density.

In Chapter 4, we have described a new type of template-prepared nanostructured $LiFePO_4$ electrode. $LiFePO_4$ is a promising alternative cathode material, but, to date, its

use is limited by its inherently poor electron-conductivity. The electrode described in this chapter is a composite consisting of nanofibers of the $LiFePO_4$ material mixed with an electronically conductive carbon matrix. This composite is created by a modified template-synthesis procedure, where the polymer template membrane is pyrolyzed. This nanocomposite electrode provides an intimate-contact mechanism between carbon and $LiFePO_4$ nanostructures. This encompassing carbon matrix provides an improved electron-pathway, while the nanostructured geometry minimizes Li-ion diffusion distance. Therefore, the composite assists on both rate-limiting factors. This unique nanocomposite morphology allows these electrodes to deliver high capacity, even when discharged at extreme rates necessary for many pulse-power applications.

In Chapter 5, we were able to demonstrate the reversible intercalation of a polyvalent-ion into a Li-ion battery electrode. From this preliminary series of experiments, we can form several conclusions. Our primary goal of demonstrating reversible intercalation of Mg-ions into V_2O_5 nanowires without carbon or binder was achieved. We also showed that at a low discharge rate, more charge can be stored per gram in the Mg-based system than the Li-based system. This is from the rate capability experiment ITO-glass, using the electroactive mass obtained via voltammetric integration. Another observation is that at large discharge rates, the charge-per-gram stored by the Li-based system comes to exceed that stored by the Mg-based system. This suggests a decrease in diffusivity of the Mg-ion compared to the Li-ion. When diffusion profiles are given less time to propagate, this is more of a concern.

ITO-glass was determined to be a satisfactory current collector because of its available potential window, but it is incompatible with this synthetic process. Data

suggest that this results in only islands of material that is electronically addressable. Also, a comparison between the ITO-glass and the Pt systems reveals some background specific to the platinum. This may be a result of excess capacitance associated with the exposed back of the metal. This would not be a factor with the ITO-glass, because the exposed back of that substrate is not conductive. It is notable though, that this effect appears to be unique to this system, as is not dominant in previous studies.

Future Directions

When given the forum to layout the future directions of a project, I first consider the goals of academic research. I perceive the goal of academic research in the pure sciences as the exploration of fundamental principles and the fostering of creativity. Approaching experiments and challenges by a strategy well founded in the scientific method ensures an understanding of underlying processes. It is the responsibility of the private sector to adapt the creative findings of academia to the marketplace. Graduate school is as much about the contribution of the field to the student as it is about the contribution of the student to the field. My journey through graduate school has instilled a tremendous respect for original thought.

With these goals in mind, I believe that the existence and interplay of the physical and chemical phenomena of this complex system can be resolved Electrochemical Impedance Spectroscopy (EIS). EIS imposes a small amplitude sinusoidal AC potential onto a DC potential. The response to this voltage perturbation is a current. The signal in (voltage) and signal out (current) are related by the impedance. This impedance has both a resistive and capacitive contribution. This response can be modeled as the response of an equivalent electric circuit constructed of different inductors, capacitors, resistors, and diffusive components in different connectivity and of different value. These electric

components represent true physical-chemical processes, such as charge-transfer resistance and double-layer capacitance. By modulating the frequency of the voltage perturbation, processes on different timescales can be probed. For instance, a typical experiment would investigate frequencies from the 100s of kHz to 1s of mHz. The geometries available from the template-synthesis of nanoscale electrodes studied by EIS should help to separate the collective current response into the contributions of faradaic and non-faradaic processes. Here a complex system requires a complex method of investigation.

Another topic where focused resources can be productive is expanding upon the preliminary studies outlined in Chapter 5. The results presented in that chapter lay a framework for a polyvalent-ion intercalation project. Since there are orders of magnitude difference in the number of researchers investigating these principles compared to Li-ion intercalation, it is a field ripe for progress. This could result in a new class of less expensive batteries. This new class of batteries could become a compromise of cost and performance, a niche of systems more powerful than those based on Ni (NiMH or Ni-Cd), while less expense than the Li-ion.

On a broader view, the field of Li-ion batteries works to constantly improve on the interplay of size, weight and power. Improvements are sectioned into materials and design. Research in the field of materials has been a focus of engineers since the Li-ion battery introduction in the early 1990's. After fifteen years of research, the standard commercial battery still uses the same (or very similar) components. If there is to be another great advance in the field, it will come in the design of the battery. These materials have sufficient intrinsic properties to function as Li-ion battery components.

The key to providing more power using a smaller, lighter device is to become more elegant in its design. The issues with the current materials are their expense and toxicity. Both of these issues are direct functions of quantity. Apparently, the consumer is perfectly content with the "hidden" cost of this type of battery. This cost is hidden, because it is integrated into the total price of a laptop or the contract from a cellular phone service provider. An explicit price such as in a replacement battery, it warrants a raise of the eyebrow (about $50 for a cellular phone and $200 for a high-performance laptop). Why are these batteries so expensive? A main contributor to this is cost of the raw materials. Conservation comes from better design. What is meant by better design? The use of smaller, better contacted particles.

Another fundamental tool in elegant design is a polymer electrolyte. Such an electrolyte allows the engineers more design flexibility. This should reduce the capital cost of these batteries. An electrochemically deposited polymeric electrolyte that has room-temperature Li-ion conductivity to rival that of the liquid electrolyte would be a major advance. Without a doubt there is a pot of gold at the end of this rainbow. A battery with a polymeric electrolyte is termed a *solid-state battery*. It is a difficult proposition though as the deposition process for each component of a solid-state battery has to be successively compatible. The components can be constructed of nanoparticles or "nano-machined" from deposited macrostructures by laser or plasma ablation. Indeed, the ultimate goal of this document is to inspire the next generation of graduate students to take hold of the methods and findings presented here and to direct them as they see fit.

LIST OF REFERENCES

(1) Nagaura, T. Tozawa, K. *Progress in Batteries and Solar Cells* **1990**, *9*, 209-217.

(2) Tarascon, J. M. Armand, M. *Nature* **2001**, *414*, 359-367.

(3) Tullo, A. H. *Chemical & Engineering News* **2002**, *80*, 25-26.

(4) Moshtev, R. Johnson, B. *Journal of Power Sources* **2000**, *91*, 86-91.

(5) Van Schalkwijk, W. A. Scrosati, B. In Eds.; Kluwer Academic / Plenum Publishers: New York, 2002,

(6) Martin, C. R.; Menon, V. P. Parthasarathy, R. V. *Polymer Preprints (American Chemical Society, Division of Polymer Chemistry)* **1994**, *35*, 229-30.

(7) Jirage, K. B.; Hulteen, J. C. Martin, C. R. *Science* **1997**, *278*, 655-658.

(8) Brumlik, C. J. Martin, C. R. *Journal of the American Chemical Society* **1991**, *113*, 3174-5.

(9) Wirtz, M. Martin, C. R. *Advanced Materials* **2003**, *15*, 455-458.

(10) Menon, V. P. Martin, C. R. *Analytical Chemistry* **1995**, *67*, 1920-8.

(11) Miller, S. A.; Young, V. Y. Martin, C. R. *Journal of the American Chemical Society* **2001**, *123*, 12335-12342.

(12) Che, G.; Lakshmi, B. B.; Fisher, E. R. Martin, C. R. *Nature* **1998**, *393*, 346-349.

(13) Che, G.; Lakshmi, B. B.; Martin, C. R.; Fisher, E. R. Ruoff, R. S. *Chemistry of Materials* **1998**, *10*, 260-267.

(14) Lakshmi, B. B.; Patrissi, C. J. Martin, C. R. *Chemistry of Materials* **1997**, *9*, 2544-2550.

(15) Lakshmi, B. B.; Dorhout, P. K. Martin, C. R. *Chemistry of Materials* **1997**, *9*, 857-862.

(16) Martin, C. R. *Accounts of Chemical Research* **1995**, *28*, 61-8.

(17) Che, G.; Jirage, K. B.; Fisher, E. R. Martin, C. R. *Journal of the Electrochemical Society* **1997**, *144*, 4296-4302.

(18) Kuwabata, S.; Idzu, T.; Martin, C. R. Yoneyama, H. *Journal of the Electrochemical Society* **1998**, *145*, 2707-2710.

(19) Li, N.; Martin, C. R. Scrosati, B. *Electrochemical and Solid-State Letters* **2000**, *3*, 316-318.

(20) Li, N. Martin, C. R. *Journal of the Electrochemical Society* **2001**, *148*, A164-A170.

(21) Nishizawa, M.; Mukai, K.; Kuwabata, S.; Martin, C. R. Yoneyama, H. *Journal of the Electrochemical Society* **1997**, *144*, 1923-1927.

(22) Patrissi, C. J. Martin, C. R. *Journal of the Electrochemical Society* **1999**, *146*, 3176-3180.

(23) Patrissi, C. J. Martin, C. R. *Journal of the Electrochemical Society* **2001**, *148*, A1247-A1253.

(24) Sides, C. R.; Li, N.; Patrissi, C. J.; Scrosati, B. Martin, C. R. *MRS Bulletin* **2002**, *27*, 604-607.

(25) Sides, C. R. Martin, C. R. *Advanced Materials* **2005**, *17*, 125-128.

(26) Sides, C. R.; Croce, F.; Young, V.; Martin, C. R. Scrosati, B. *Electrochemical and Solid-State Letters* **2005**, *8*, A484-A487.

(27) GE Osmotics, I., 2003, 1220457, Revision B.

(28) Fleisher, R. L.; Price, P. B. Walker, R. M. *Nuclear Tracks in Solids*; University of California Press: Berkeley, 1975.

(29) Apel, P. *Radiation Measurements* **2001**, *34*, 559-566.

(30) Poretics, Product Guide, 1995.

(31) Martin, C. R.; Nishizawa, M.; Jirage, K. Kang, M. *Journal of Physical Chemistry B* **2001**, *105*, 1925-1934.

(32) Despic, A. Parkhutik, V. P. In *Modern Aspects in Electrochemistry*; Bockris, J. O., White, R. E. Conway, B. E., Eds.; Plenum Press: New York, 1989, 20, Chap. 6, 401-503.

(33) West, W. C.; Myung, N. V.; Whitacre, J. F. Ratnakumar, B. V. *Journal of Power Sources* **2004**, *126*, 203-206.

(34) Stein, A. Schroden, R. C. *Current Opinion in Solid State and Materials Science* **2001**, *5*, 553-564.

(35) Turner, M. E.; Trentler, T. J. Colvin, V. L. *Advanced Materials* **2001**, *13*, 180-183.

(36) Velev, O. D.; Tessier, P. M.; Lenhoff, A. M. Kaler, E. W. *Nature* **1999**, *401*, 548.

(37) Jiang, P.; Bertone, J. F. Colvin, V. L. *Science* **2001**, *291*, 453-457.

(38) Velev, O. D.; Lenhoff, A. M. Kaler, E. W. *Science* **2000**, *287*, 2240-2243.

(39) Hulteen, J. C. Van Duyne, R. P. *Journal of Vacuum Science and Technology A* **1995**, *13*, 1553-1558.

(40) Cepak, V. M.; Hulteen, J. C.; Che, G.; Jirage, K. B.; Lakshmi, B. B.; Fisher, E. R.; Martin, C. R. Yoneyama, H. *Chemistry of Materials* **1997**, *9*, 1065-1067.

(41) Russell, A.; Repka, K.; Dibble, T.; Ghoroghchian, J.; Smith, J. J.; Fleischmann, M. Pons, S. *Analytical Chemistry* **1986**, *58*, 2961-4.

(42) Karpinski, Z. J. Osteryoung, R. A. *Journal of Electroanalytical Chemistry* **1993**, *349*, 285-97.

(43) Drew, S. M.; Wightman, R. M. Amatore, C. A. *Journal of Electroanalytical Chemistry and Interfacial Electrochemistry* **1991**, *317*, 117-24.

(44) Hulteen, J. C.; Menon, V. P. Martin, C. R. *Journal of the Chemical Society, Faraday Transactions* **1996**, *92*, 4029-4032.

(45) Miller, S. A. Martin, C. R. *Journal of the American Chemical Society* **2004**, *126*, 6226-6227.

(46) Giddings, J. C. *Unified Separation Science*; John Wiley & Sons, Inc.: New York, 1991.

(47) Johnson, B. A. White, R. E. *Journal of Power Sources* **1998**, *70*, 48-54.

(48) Li, N.; Mitchell, D. T.; Lee, K.-P. Martin, C. R. *Journal of the Electrochemical Society* **2003**, *150*, A979-A984.

(49) Lytle, J. C.; Yan, H.; Ergang, N. S.; Smyrl, W. H. Stein, A. *Journal of Materials Chemistry* **2004**, *14*, 1616-1622.

(50) Fransson, L.; Eriksson, T.; Edstrom, K.; T., G. Thomas, J. G. *Journal of Power Sources* **2001**, *101*, 1-9.

(51) Linden, D. Reddy, T. B., Eds., *Handbook of Batteries*, 3rd ed; McGraw-Hill, New York, NY, 2002.

(52) Scrosati, B. *Nature* **1995**, *373*, 557-8.

(53) Thomas, J. *Nature Materials* **2003**, *2*, 705-706.

(54) Morcrette, M.; Rozier, P.; Dupont, L.; Mugnier, E.; Sannier, L.; Galy, J. Tarascon, J. M. *Nature Materials* **2003**, *2*, 755-761.

(55) Hammami, A.; Raymond, N. Armand, M. *Nature* **2003**, *424*, 635-636.

(56) Thackeray, M. *Nature Materials* **2002**, *1*, 81-82.

(57) Polzot, P.; Laruelle, S.; Grugeon, S.; Dupont, L. Tarascon, J. M. *Nature* **2000**, *407*, 496-499.

(58) Croce, F.; Appetecchi, G. B.; Persi, L. Scrosati, B. *Nature* **1998**, *394*, 456-458.

(59) Plichta, E. J.; Hendrickson, M.; Thompson, R.; Au, G.; Behl, W. K.; Smart, M. C.; Ratnakumar, B. V. Surampudi, S. *Journal of Power Sources* **2001**, *94*, 160-162.

(60) Nagasubramanian, G. *Journal of Applied Electrochemistry* **2001**, *31*, 99-104.

(61) Salomon, M.; Lin, H. P.; Plichta, E. Hendrickson, M. In *Advances in Lithium-Ion Batteries*; Van Klinken, W. Scrosati, B., Eds.; Kluwer Academic/Plenum Publishers: New York, 2002, Ch 11.

(62) Lin, H. P.; Chua, D.; Salomon, M.; Shiao, H. C.; Hendrickson, M.; Plichta, E. Slane, S. *Electrochemical and Solid-State Letters* **2001**, *4*, A71-A73.

(63) Huang, C. K.; Sakamoto, J. S.; Wolfenstine, J. Surampudi, S. *Journal of the Electrochemical Society* **2000**, *147*, 2893-2896.

(64) Ratnakumar, B. V.; Smart, M. C.; Kindler, A.; Frank, H.; Ewell, R. Surampudi, S. *Journal of Power Sources* **2003**, *119-121*, 906-910.

(65) Aurbach, D.; Markovsky, B.; Rodkin, A.; Cojocaru, M.; Levi, E. Kim, H.-J. *Electrochimica Acta* **2002**, *47*, 1899 - 1911.

(66) X-Ray Powder Data File, 1962.

(67) Smart, M. C.; Ratnakumar, B. V.; Surampudi, S.; Wang, Y.; Zhang, X.; Greenbaum, S. G.; Hightower, A.; Ahn, C. C. Fultz, B. *Journal of the Electrochemical Society* **1999**, *146*, 3963-3969.

(68) Delmas, C.; Cognac-Auradou, H.; Cocciantelli, J. M.; Menetrier, M. Doumerc, J. P. *Solid State Ionics* **1994**, *69*, 257-64.

(69) Martin, C. R. *Science* **1994**, *266*, 1961-6.

(70) Levi, M. D.; Levi, E. A. Aurbach, D. *Journal of Electroanalytical Chemistry* **1997**, *421*, 89-97.

(71) Lu, Z.; Levi, M. D.; Salitra, G.; Gofer, Y.; Levi, E. Aurbach, D. *Journal of Electroanalytical Chemistry* **2000**, *491*, 211-221.

(72) Wen, C. J.; Boukamp, B. A.; Huggins, R. A. Weppner, W. *Journal of the Electrochemical Society* **1979**, *126*, 2258-66.

(73) Bard, A. J. Faulkner, L. R. In *Electrochemical Methods: Fundamentals and Applications*; Bard, A. J. Faulkner, L. R., Eds.; John Wiley & Sons: New York, 1980,

(74) Lantelme, F.; Mantoux, A.; Groult, H. Lincot, D. *Journal of the Electrochemical Society* **2003**, *150*, A1202-A1208.

(75) McGraw, J. M.; Bahn, C. S.; Parilla, P. A.; Perkins, J. D.; Readey, D. W. Ginley, D. S. *Electrochimica Acta* **1999**, *45*, 187-196.

(76) Miyazaki, H.; Sakamura, H.; Kamei, M. Yasui, I. *Solid State Ionics* **1999**, *122*, 223-229.

(77) Vivier, V.; Farcy, J. Pereira-Ramos, J.-P. *Electrochimica Acta* **1998**, *44*, 831-839.

(78) Levi, M. D. Aurbach, D. *Electrochimica Acta* **1999**, *45*, 167-185.

(79) Bard, A. J. Faulkner, L. R. In *Electrochemical Methods: Fundamentals and Applications*; Bard, A. J. Faulkner, L. R., Eds.; John Wiley & Sons: New York, 1980,

(80) Deiss, E. *Electrochimica Acta* **2002**, *47*, 4027-4034.

(81) Eftekhari, A. *Electrochimica Acta* **2005**, *50*, 2541-2543.

(82) Padhi, A. K.; Nanjundaswamy, K. S.; Masquelier, C.; Okada, S. Goodenough, J. B. *Journal of the Electrochemical Society* **1997**, *144*, 1609-1613.

(83) Ravet, N.; Chouinard, Y.; Magnan, J. F.; Besner, S.; Gauthier, M. Armand, M. *Journal of Power Sources* **2001**, *97-98*, 503-507.

(84) Huang, H.; Yin, S.-C. Nazar, L. F. *Electrochemical and Solid-State Letters* **2001**, *4*, A170-A172.

(85) Arnold, G.; Garche, J.; Hemmer, R.; Strobele, S.; Vogler, C. Wohlfahrt-Mehrens, M. *Journal of Power Sources* **2003**, *119-121*, 247-251.

(86) Chung, S.-Y.; Bloking, J. T. Chiang, Y.-M. *Nature Materials* **2002**, *1*, 123-128.

(87) Croce, F.; Epifanio, A. D.; Hassoun, J.; Deptula, A.; Olczac, T. Scrosati, B. *Electrochemical and Solid-State Letters* **2002**, *5*, A47-A50.

(88) Doeff, M. M.; Hu, Y.; McLarnon, F. Kostecki, R. *Electrochemical and Solid-State Letters* **2003**, *6*, A207-A209.

(89) Takahashi, M.; Tobishima, S.-I.; Takei, K. Sakuri, Y. *Solid State Ionics* **2002**, *148*, 283-289.

(90) Aurbach, D.; Lu, Z.; Schechter, A.; Gofer, Y.; Gizbar, H.; Turgeman, R.; Cohen, Y.; Moshkovich, M. Levi, E. *Nature (London)* **2000**, *407*, 724-727.

(91) Imamura, D.; Miyayama, M.; Hibino, M. Kudo, T. *Journal of the Electrochemical Society* **2003**, *150*, A753-A758.

(92) Jiao, L.; Yuan, H.; Wang, Y.; Cao, J. Wang, Y. *Electrochemistry Communications* **2005**, *7*, 431-436.

(93) Scherrer, P. *Nachr. Ges. Wiss. Gottingen* **1918**, 96-100.

(94) Biscoe, J. Warren, B. E. *Journal of the American Ceramic Society* **1938**, *21*, 287-93.

(95) Van der Planken, J. *Journal of Materials Science* **1969**, *4*, 927-9.

BIOGRAPHICAL SKETCH

Charles “Rob” Sides is the second of the four children of Charles Ray and Martha Campbell Sides. He was born in North Carolina and spent the vast majority of his life just across the state line in Fort Mill, SC. He graduated salutatorian of the class of 1996 from Fort Mill High School. Go Yellow Jackets! Rob received an undergraduate degree in chemistry at Clemson University in 2000 and enrolled immediately in graduate school. Go Tigers! Upon graduation from University of Florida, he hopes to spend several years doing an honest day’s work making other people a lot of money. Go Gators!